Age- and Diabetes-Related Changes in the Matrix and Fracture Resistance of Bone

By

Amy Creecy

Dissertation

Submitted to the Faculty of the

Graduate School of Vanderbilt University

in partial fulfillment of the requirements

for the degree of

DOCTOR OF PHILOSOPHY

in

Biomedical Engineering

August 10, 2018

Nashville, TN

Approved:

Jeffry Nyman, Ph.D.
Jeffery Davidson, Ph.D.
Maureen Gannon, Ph.D.
David Merryman, Ph.D.
Michael Miga, Ph.D.
Julie Sterling, Ph.D.

ACKNOWLEDGEMENTS

This work was made possible through the support of grants from the Veteran's Affairs Office of Research, National Institute of Aging, and a training grant from the National Institute of Diabetes and Digestive and Kidney Diseases.

First, I would like to thank my research advisor, Dr. Jeffry Nyman, for his guidance and support. I have always respected his integrity and appreciated his enthusiasm for research. I would also like to thank my committee members, Dr. Maureen Gannon, Dr. David Merryman, Dr. Jeffery Davidson, Dr. Michael Miga, and Dr. Julie Sterling for their advice and input over the years. Their advice has made my research better. Lastly, I would like to thank Dr. Paul Voziyan for all his help and training.

I would also like to thank the many wonderful colleagues I have had over the years. Specifically, I would like to thank Sasidhar Uppuganti for his help and expertise and the many times he trained me on specific techniques. I would also like to thank Dr. Mustafa Unal and Dr. Mathilde Granke for their advice on how to progress to the next stage of research. Thanks to Alyssa Merkel for all the times she has helped with tissue collection or animal care. Lastly, I would like to thank the Vanderbilt Center for Bone Biology for the supportive, collaborative environment.

Finally, I would like to thank my family and friends for their emotional support throughout the years.

TABLE OF CONTENTS

LIST OF FIGURES

Figure Page

LIST OF TABLES

Table Page

CHAPTER 1 INTRODUCTION

1.1 Motivation

As people age and become more prone to fracture, fractures increase mortality and decrease quality of life, as many people lose their ability to live independently [1]. Furthermore, as people age and experience a fracture, their probability of survival decreases [2]. Hip fractures, which have the greatest effect on survival probability [2], are expected to increase to 4.5 million by 2050 [3]. In general, fractures are expected to increase from 2 million in 2005 to over 3 million by the year 2025 [1] and the number of individuals with a 10-year probability for fracture is expected to be above 200 million by 2025 [4], partly due to our aging population. The gold standard for determining fracture risk is the measurement of areal bone mineral density (aBMD) by dual-energy X-ray absorptiometry (DXA). However, there is evidence that with aging and diseases such as type 2 diabetes (T2D) fracture risk is higher than what would be expected by aBMD [5-8]. Thus, bone quality, as well as bone quantity, matters for fracture resistance. Bone quality can refer to changes on multiple length scales of bone's hierarchical structure, but generally refers to factors that affect the ability of bone to resist fracture that are independent of bone size or aBMD [9].

The extracellular matrix (ECM) of bone is part of the hierarchical nature of bone and contributes to fracture resistance [10, 11]. The ability of bone to yield and prevent crack propagation is dependent on the matrix. Alterations to the protein collagen, the main component of the ECM, have had an adverse effect on the yield properties of bone [12-14]. Additionally, enzymatic crosslinks between collagen molecules seem to provide some stability to the matrix [15]. However, an overabundance of non-enzymatic advanced glycation end-products (AGEs) crosslinks may reduce toughness [16-18]. These may have a brittling effect on the matrix by

preventing collagen fibril sliding. Furthermore, bound water affects fracture resistance as collagen needs to be hydrated to contribute to toughness [19]. Non-collagenous proteins may prevent fracture through providing sacrificial bonds and by preventing crack propagation [20].

The exact mechanisms of how T2D and aging affect bone quality are unknown. Changes to the extracellular matrix, such as increases in non-enzymatic AGE crosslinks and other post-translational modifications (PTMs) to bone matrix proteins may decrease the fracture resistance of bone [15]. The effect of T2D and aging on the matrix must be determined in order to effectively design therapeutics to treat the diabetic and age-related increase in fracture risk. Working towards these goals, I devised the following aims:

Specific Aim 1: Examine the effect of duration of diabetes on bone matrix. *Primary hypothesis: As duration of diabetes increases, the fracture resistance of bone will progressively worsen in response to an accumulation of deleterious changes to the matrix.*

Approach: The TallyHO preclinical model of T2D was studied at 16 weeks and 34 weeks and compared to control SWR/J mice. The structural and mechanical phenotype of the bones were determined by μCT and 3-pt bend testing. The matrix was analyzed for crosslinks and other changes using high performance liquid chromatography (HPLC) and Raman spectroscopy.

Specific Aim 2: Analyze the effect of aging on bone matrix. *Primary hypothesis: As age increases, bone material properties will decrease and this will accompany key changes in the organic matrix.*

Approach: The bones of male and female adult BALB/c mice at a young age and an advanced age were analyzed for structural and mechanical phenotype. Matrix characteristics were determined by HPLC, Raman spectroscopy, and ^{1}H-NMR.

Specific Aim 3: Identify age-related post-translational modifications of bone matrix proteins. *Primary hypothesis: Post-translational modifications of bone matrix proteins will occur with age and may contribute to fracture resistance loss.*

Approach: Protein extracts from young and old adult BALB/c mice were analyzed using mass spectrometry to determine changes to concentration of proteins and changes such as PTMs to bone matrix proteins.

1.2 Innovation

The proposed studies will enable new insight into how aging and T2D affect the extracellular matrix of bone and thereby lower fracture resistance. The project is based on observations that fracture risk is increased with both T2D and aging beyond what would be expected from aBMD values. It will determine how T2D and aging lower fracture resistance in preclinical models and will provide new knowledge as to which PTMs of bone matrix proteins change with age as fracture resistance declines. The proposed studies have the potential to determine the mechanism behind how T2D and aging alter the bone matrix and give new insight as to treatment options.

1.3 Dissertation Outline

This dissertation follows the following format:

Chapter 1 provides an introduction to the motivation and main question of this dissertation, the specific aims designed to answer this question, and an outline of the dissertation.

Chapter 2 provides background information necessary to understand how the matrix affects bone's fracture resistance. It further addresses current knowledge gaps.

Chapter 3 examines how duration of disease alters the fracture resistance of bone in a preclinical model of T2D. This chapter addresses Specific Aim 1, and presents my findings on the overall fracture resistance of bone its matrix characteristics for this model.

Chapter 4 analyzes the effect of age on bone matrix and fracture resistance in a preclinical model of aging. This chapter covers Specific Aim 2.

Chapter 5 presents my findings on how matrix proteins may be altered with age-related loss in fracture resistance. This chapter addresses Specific Aim 3.

Chapter 6 presents the overall conclusions of this dissertation and suggestions for how this work could be expanded upon in the future.

CHAPTER 2 BACKGROUND

The following chapter is adapted from Unal, M., Creecy, A., Nyman, JS. *The Role of Matrix Composition in the Mechanical Behavior of Bone*. Current Osteoporosis Reports, 2018. **16**(3). 205-215. [21].

Reprinted with permission of Springer.

2.1 Bone: Mechanics, Structure and Organization

Bone is a composite material formed primarily from type I collagen and carbonated hydroxyapatite [22]. It is a highly adaptable material, able to self-heal and to respond to changes in mechanical stresses [23]. For its weight, it demonstrates high load bearing [24]. The total load a bone can carry is dependent upon its size and structure. A larger bone will be able to withstand a larger force before fracture. In contrast, material properties such as modulus, strength and toughness are independent of the geometry of bone. These properties can be calculated by converting the load-displacement curve from a mechanical test into a stress-strain curve [25]. The material properties of bone in the elastic region of the stress-strain curve such as modulus (i.e., stiffness independent of size) are primarily determined by its degree of mineralization and microscopic porosity, while the material properties in the inelastic or plastic region such as toughness are mainly determined by collagen, as it provides ductility to bone [26, 27]. Ductility is the ability of a material to deform. Material properties are of interest as they contribute to fracture resistance, as does bone structure and microarchitecture, and are affected by aging and disease [9, 28].

The material properties of bone depend on the hierarchical organization of bone [11, 22]. On a macroscopic scale, bone is separated into two types: cortical bone and trabecular bone. Trabecular bone is located in the interior of the bone. It is more heavily present in the end

regions of the bone known as the metaphysis and epiphysis [23]. It consists of units of trabeculae, which form rod and plate structures. It is more porous than cortical bone and is where most of the remodeling and bone turnover occurs in bone. Consequently, trabecular bone is usually younger than cortical bone and has a lower degree of mineralization [24]. This contributes to trabecular bone having lower material properties than cortical bone [24]. Cortical bone is on the exterior of the bone and composes most of the diaphysis. The basic unit is the osteon or Haversian canal. Cortical bone is more densely packed than trabecular bone and is responsible for most of the load bearing in bone.

While different in macrostructure, the cortical bone and trabecular bone are composed of the same basic units. Thin sheets of mineralized collagen fibrils called lamellae form both osteons and trabeculae. In osteons, lamellae are wrapped in concentric circles of differing orientations around a central canal. In trabeculae, lamellae are more loosely organized to form rods and plates [11, 22]. Mineralized collagen fibrils consist of several parallel lines of collagen molecules aligned in a quarter-staggered fashion. The staggered structure allows for mineralization between collagen to occur [29]. The holes between individual collagen molecules and between layers allow for the placement of non-collagenous proteins as well. Individual collagen molecules form fibrils by self-assembly, which are then stabilized through enzymatic crosslinks [11].

Failure in bone occurs through a process of crack propagation. The material resists fatigue failure by its ability to resist either crack initiation or crack propagation [30, 31]. The composite nature of bone helps it resist crack propagation. Energy is dispersed whenever a new barrier is hit. The ability of a material to dissipate deformation energy without crack propagation is a measure of toughness [32]. This is the proposed function of cement lines, the outer barrier of

the osteon. Studies have shown that minor cracks (below 100 μm) are stopped at cement lines [30]. The lamellar structure is also important as crack propagation takes more energy when it encounters collagen at differing orientations [32].

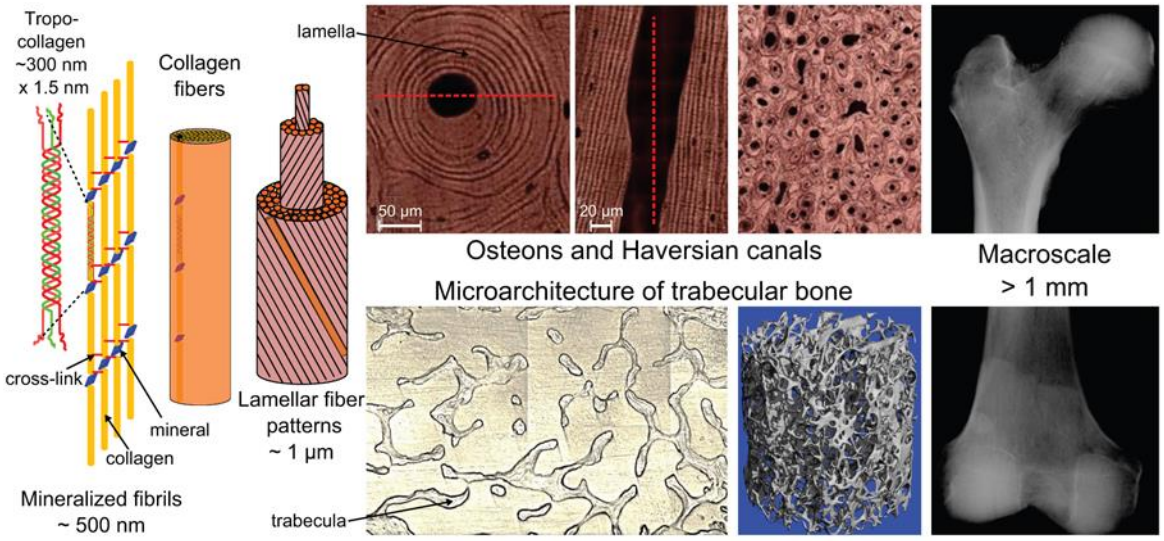

Figure 2.1 Hierarchical organization of trabecular and cortical bone from collagen triple helix to macroscopic structure of trabecular and cortical bone. Reprinted with permission of Springer [33].

2.2 The Role of Matrix in the Mechanical Behavior of Bone

The factors contributing to the age- and disease-related increase in fracture risk are multifactorial and include deleterious changes to the compositional characteristics of the bone matrix. Since there are currently no clinical tools for directly assessing these characteristics in patients, much of the knowledge regarding the role of matrix composition in the fracture resistance of bone comes from studies of cadaveric bone, discarded bone acquired at the time of surgery, and iliac crest biopsies as well as from rodent studies of aging and diseases that affect the bone (e.g., diabetes, osteogenesis imperfecta, loss of matrix-associated genes). In such studies, matrix properties were either correlated with the age-related decrease in material

properties of bone as determined by a variety of mechanical tests [10] or reported as difference in tissue-level compositional and mechanical properties between a control group and a osteoporotic group [34].

The measurement of areal bone mineral density (aBMD) from dual-energy X-ray absorptiometry (DXA) remains the gold-standard for deciding whether an individual has osteoporosis (i.e., a T-score ≤ -2.5). While the use of clinical risk factors (FRAX) and trabecular bone score (i.e., texture analysis of DXA images of the lumbar spine) improve the prediction of fracture risk over T-scores alone [35], fragility fractures still occur in seemingly low risk individuals [36]. As recently described in a review article [37], several advances in imaging technologies have been developed to overcome the limitations of the projected measurement of aBMD and potentially improve fracture risk assessment beyond statistical models based on epidemiological studies. To date, these technologies − from finite element analysis derived from quantitative computed tomography (QCT) images of the hip or spine to assessments of cortical structure and trabecular architecture at peripheral sites − have indicated that thinning of the cortices [38], increases in cortical porosity [39], and deterioration in trabecular architecture [40] all likely contribute to higher fracture risk.

Clinical studies involving the OsteoProbe®, a hand-held micro-indentation device, suggest that deleterious changes in the bone matrix also contribute to higher fracture risk. The device provides a measurement of the resistance of a patient's tibia mid-shaft (periosteal surface on the anterior-lateral side) to impact loading at a scale of ~350 μm. Called Bone Material Strength index (BMSi), this measurement is the depth of a spheroconical tip into bone divided by the depth of the same tip into a standard reference material. As discussed in a recent guidelines paper [41] and a review paper on the technique [42], the compositional factors influencing BMSi

are unknown. Nonetheless, several case-control studies have reported lower BMSi for patients with fragility fracture(s) compared to age-matched individuals without a history of low-energy fractures: combined vertebral (n=8), hip (n=10), and non-vertebral/non-hip fractures (n=45) vs. non-fracture cases (n=27) [43], combined vertebral (n=24), hip (n=25), and non-vertebral/non-hip fractures (n=17) vs. non-fracture cases (n=66) [44], and distal radius fractures (n=57) vs. control cases (n=93) [44]. However, BMSi was not associated with a history of fracture in one study (fragility not distinguished from high-energy fracture, n=117 vs. non-fracture, n=63) [45]. Also, the lower BMSi for hip fracture cases (n=41) compared to control cases (n=93) did not reach statistical significance (p=0.09) [46]. Three independent groups reported that post-menopausal with type 2 diabetes (T2D) had lower BMSi than age-matched women without the disease [47-49]. Since T2D is associated with higher fracture risk for a given T-score [50], the lower BMSi suggests diabetes affects matrix composition, though underlying cortical porosity could be a contributing factor. While much remains to be learned about how compositional characteristics affect BMSi, the quality of the bone matrix (or lack thereof) likely contributes to increases in fracture risk that occur with aging and certain diseases.

Key attributes of the mechanical behavior of bone include: i) being stronger in compression than in tension, while experiencing greater post-yield deformation in tension than in compression [51]; ii) having higher fracture toughness when a crack propagates perpendicular to the primary direction of osteons (transverse) than when it propagates parallel to osteonal direction (longitudinal) [52]; iii) becoming stiffer but more brittle (lack of plasticity) as the strain rate increases over orders of magnitude [53]; iv) exhibiting both microdamage accumulation and creep during fatigue loading (cyclic loading below the yield strength at low frequency over an extended period of time) [54]; and v) exhibiting viscous dampening during dynamic loading

(cyclic loading at variable frequency over a short period of time) [55]. All these attributes arise not only from the unique composition of the bone matrix (collagen, mineral, and water) but also from the unique arrangement of the primary constituents such as the shifting orientation of collagen fibrils, the varying degrees of mineralization (heterogeneity), and stabilizing interactions between water, hydrophilic residues of peptides, surfaces of mineral crystals, and possibly non-collagenous proteins (NCPs). Bone has numerous toughening mechanisms at multiple length scales (Fig. 2.2) such as sacrificial bonds between neighboring mineral crystals (dilatational bands), uncoiling of collagen I, fibril sliding, diffuse and microdamage accumulation, crack deflection at cement lines, fibril bridging of a crack, and un-cracked ligament bridging (tortuosity) [56]. The composition of the bone matrix contributes to each of these mechanisms making bone a remarkable material but also susceptible to multiple deleterious changes that increase fracture risk.

Herein, the role of each of the 3 primary compositional components (mineral, organic matrix, and water) in the mechanical behavior of bone is described. Of course, the three constituents are interdependent such that the formation of collagen I into fibrils affects mineralization, which in turn can affect the hydration status of the organic matrix.

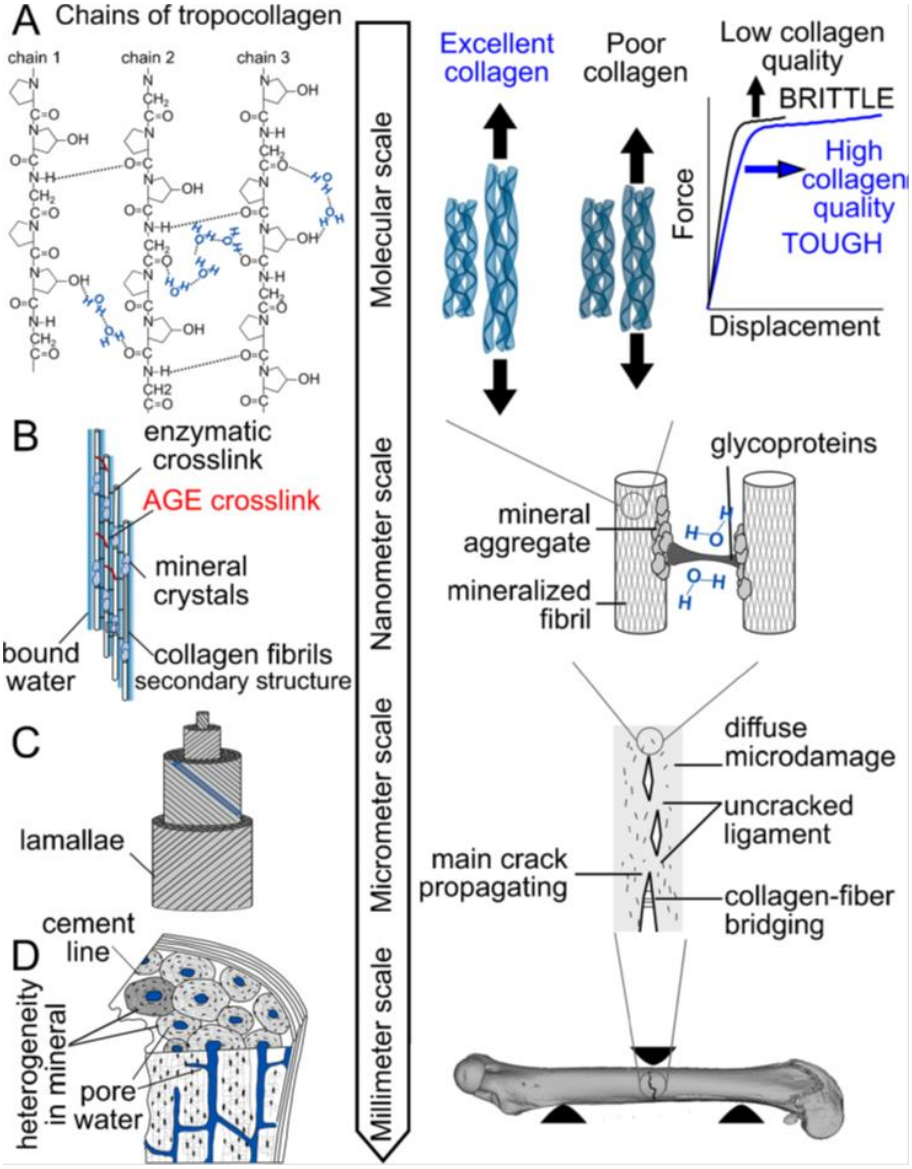

Figure 2.2 Toughening mechanisms in bone exist at multiple hierarchical levels of organization. A: PTMs affecting hydroxyl groups may alter the secondary structure of collagen I. B: PTMs to matrix-bound glycoproteins (right) and excessive non-enzymatic crosslinking (left) may favor formation of damage and collagen rupture at the nano-structural level. C: Overall changes in collagen structure and hydration at the nanometer scale reduce the ability of bone to prevent cracking, thereby lowering fracture toughness at the material-level. D: An increase in porosity (pore water) can also lower fracture resistance. Reprinted with permission of Springer [21].

2.2.1 Proper collagen formation and organization are required for post-yield toughness

The organic phase of bone is primarily a network of interlinked type I collagen. Specifically, tropocollagen (300 nm x 1.6 nm in diameter) is a triple helix consisting of two α-1 chains and one α-2 chain with a distinct motif $(Glycine\text{-}X\text{-}Y)_n$ in which X is often proline. Post-translational modifications (PTMs) of collagen I are important to the overall structure and stability and, in turn, the mechanical behavior of bone. Hydroxylation of proline is one type of PTM that forms hydroxyproline, which facilitates hydrogen bonding with both water and other amino acids within the collagen chain. Other PTMs such as glycosylation facilitate crosslink formation between neighboring collagen molecules [57]. With this enzymatic crosslinking, collagen molecules self-align into fibrils. Collagen organization is reviewed in-depth elsewhere [13], but in general, the staggered arrangement of tropocollagen into fibrils generates a periodicity known as a D-band. In atomistic simulations of hydrated microfibrils with a D of 67 nm (overlap and gap regions of 0.46D and 0.54D, respectively), the Young's modulus of collagen was determined to be ~300 MPa at small deformation and ~1.2 GP at large deformation (>10% strain) [58]. When mineral is introduced into the model, the tensile modulus increases as a function of increasing mineral content [59]. D spacing varies among fibrils, and there is experimental evidence that the distribution can shift towards higher values as toughness of bone increases upon *ex vivo* incubation of raloxifene, a small molecule that targets the estrogen receptor [60].

The collagen-rich matrix of bone confers toughness as the mineral phase is rather brittle (little post-yield deformation). As an example of the importance of collagen to bone toughness, irradiating bovine cortical bone at a high enough gamma dose (33 kGy) to damage the organic matrix (radiolysis) decreased work-to-fracture, post-yield strain, and fracture toughness [12],

parameters related to the ductility of bone. Multiple mouse models of osteogenesis imperfecta (OI), a genetic disease of improper collagen organization, have demonstrated a brittle bone phenotype [61]. As one example, the deletion of an enzyme (cyclophilin B) important to collagen folding resulted in reduced 3-hydroxylation and lower post-yield displacement, plastic energy and elastic energy-to-fracture as measured in 4-point bend testing of the femur [62]. Cortical area, ultimate load, and aBMD were lower as well, indicating this model has multiple skeletal defects. Furthermore, accompanying altered fibril structure, there was an increase in the enzymatic crosslinks hydroxylysinonorleucine (immature) and lysylpyridinoline (mature) per collagen molecule, with the loss of cyclophilon B [62]. Proper formation of the tropocollagen and then proper PTMs and subsequent crosslinking are required for bone to deform after yield or the onset of damage.

2.2.2 Collagen fibril orientation influences strength and fracture toughness

Moving up the hierarchical arrangement of the organic matrix to the micron-scale, the orientation of collagen fibrils changes from one lamellae to the next (Figure 2.2). This altering orientation gives rise to oscillating modulus values across lamellae as observed by scanning acoustic microscopy measurements of cortical bone sections [63, 64]. Raman spectroscopy (RS) mapping of the lamellae (Amide I) indicated that the oscillating elasticity at the tissue-level is due to alternating fibril orientation as opposed to alternating mineralization [63]. The varying fibril orientations across lamellae increases the energy that must be expended to propagate a crack [32]. In a study combining mechanical tests of cortical micro-beams (focus ion beam followed by loading with tip of an atomic force microscope) and computational mechanics, fibril orientation correlated with calculated bone strength [65]. As an example of the importance of fibril organization to bone toughness, the brittle bone phenotype of mice lacking activating

transcription factor 4 (ATF4) was not necessarily due to differences in tissue mineral density but rather to an apparent difference in fibril orientation between ATF4 knock-out and wild-type littermates [66]. Specifically, the change in the Amide I peak relative to the prominent phosphate peak upon rotating the femur mid-shaft 90 degrees relative to the polarization axis of the laser was dissimilar between the genotypes. Furthermore, in a transgenic mouse model of steroid-induced osteoporosis (n=5), there was an increase in the randomness of fibril orientation and an increase in fibril strain for a given tissue strain as well as reduced mineralization, compared to the wild-type mice (n=5), culminating in lower tensile breaking stress of anterior cortices (femur) [67]. The effect of fibril orientation on mechanical properties is not necessarily independent of mineralization as the long axis of HA crystals align with the long axis of collagen fibrils.

2.2.3 Mature enzymatic collagen crosslinks stabilize the matrix providing strength to bone

Collagen crosslinks add stability to the organic matrix, preventing micro-fibrils from sliding past one another. Enzymatic crosslinks are formed by lysyl oxidase and lysyl hydroxylase. In a mouse model of lathyrism (lysyl oxidase inhibition by a toxin), there was a positive correlation i) between fracture toughness (femur diaphysis) and the ratio of mature to immature enzymatic crosslinks (R^2=0.208, $p<0.05$) and ii) between bending strength (tibia diaphysis) and mature pyridinoline crosslinks (R^2=0.159, $p<0.05$) [68]. Furthermore, the lower bending strength and lower fracture toughness for the mice administered the toxin compared to the controls occurred without a difference in tissue mineral density. In a study comparing adolescent bone (n=7) to elderly bone (n=3), the ratio of mature to immature enzymatic crosslinks increased in humans, but the post-yield toughness decreased (distal fibula) [69]. The discrepancy between the mouse and human study is likely due to the difference in experimental design. Disrupting enzymatic crosslinking as in McNerny et al. likely lead to changes in collagen

structure, thereby decreasing the fracture resistance of bone [68], but in normal physiology, these enzymatic crosslinks mature, increasing the mature to immature ratio, with skeletal maturation. Along with the increase in mineralization that also occurs with skeletal maturation, adult bone with higher non-enzymatic collagen crosslinks also loses the initial high post-yield deformation capacity of adolescent bone. In aging rats with little remodeling, the loss in bone toughness accompanied increases in mature crosslink concentrations but also an increase in tissue mineral density and a decrease in matrix-bound water [70].

2.2.4 Non-enzymatic collagen crosslinking can lower bone toughness

While enzymatic crosslinks may confer stability to the organic matrix, increases in non-enzymatic crosslinks are thought to have an embrittling effect on the matrix. Non-enzymatic collagen crosslinks, a type of advanced glycation end-product (AGE), are usually quantified by either high performance liquid chromatography (HPLC) to measure pentosidine or a fluorescence assay to measure total fluorescent AGEs (fAGEs), though a recent study identified a FTIR measure of non-enzymatic crosslinking in bone [71]. Pentosidine can be viewed as a marker for total fAGEs, but there are limitations to when it correlates with fAGEs, which is a non-specific measurement [72]. AGEs accumulate in the bone matrix with age, and as AGEs increase, the toughness of cortical bone decreases [10]. In a study that incubated bovine cortical bone in a high concentration of ribose, pentosidine increased while post-yield strain and flexural toughness decreased [73]. Interestingly, differential scanning calorimetry determined that the glycated samples had a higher thermal stability as indicated by a higher thermal denaturation onset temperature (T_{onset}), and scanning electron microscopy images of the tensile side of the beam specimens showed a smoother fracture surface suggesting reduced toughening mechanisms [73]. Decreases in microcrack density and increases in crack length with glycation have been

observed in another ribose study involving human cortical bone [74]. When cancellous bone was incubated in ribose, tissue-level stiffness as measured by nanoindentation did not alter despite an increase in pentosidine [75] further supporting that AGE accumulation does not affect elastic properties but rather plastic properties. In a transgenic mouse model of early-onset, severe type 1 diabetes, OVE26 mice (n=6), pentosidine was higher while fracture toughness parameters was lower compared to the non-diabetic FVB mice (n=6) [76]. There are also other abundant AGEs in bone including carboxymethyllysine, which is an adduct, not a crosslink. Overall though, there is a paucity of information on whether such AGEs plus non-fluorescent AGEs (e.g., glucosepane) affect the mechanical behavior of bone. Moreover, there is no in vivo evidence, to date, that blocking AGE accumulation rescues the loss in bone toughness with aging and the onset of diabetes.

2.2.5 Non-collagenous proteins contribute a toughening mechanism at the nano-scale

While collagen I is the most abundant protein in the organic matrix, non-collagenous proteins (NCPs) likely contribute to fracture resistance of bone. NCPs such as osteopontin influence mineralization, and when carboxylated, they become trapped in the matrix. These proteins create sacrificial bonds that can dissipate energy and provide a toughening mechanism to bone at the nano-scale level of organization [77]. Using atomic force microscopy and confocal laser microscopy imaging of bone specimens subjected to fatigue loading, the identification of dilatational bands were associated with NCPs [78]. The role of NCPs in the fracture resistance of bone has been primarily based on knock-out models [10]. More recently, in a mouse model of accelerated aging, the α-klotho$^{-/-}$ mouse (n=4), there was less stiffening in dynamic nanoindentation tests (i.e., less of an increase in storage modulus with an increase in frequency of laoding), compared to wild-type mice (n=4) [79]. The authors suggested that the known

reduction in osteocalcin in this model caused a loss of dilatational bands to form under dynamic loading. For mice deficient in both osteocalcin and osteopontin (n=8), fracture toughness (femur diaphysis) was lower compared to control femurs (n=8) [78], but the structural strength (radius diaphysis) was higher because of a higher cortical area that occurred in the double knock-outs [80]. Thus, global deletion of NCPs can have multiple effects beyond tissue composition, and so unravelling their role in fracture resistance is challenging. More studies involving human bone are needed to determine their contribution to bone fragility relative to other established toughening mechanisms that are affected by age and disease.

2.2.6 Subjected to imperfections to its structure, bone mineral confers strength

The mineral phase of bone is mainly composed of calcium phosphate in the form of nano-sized crystals of hydroxyapatite (HA). Differing from synthetic HA, bone mineral incorporates carbonate (5-8%) over time substituting phosphate (Type-B) and hydroxyl groups (Type-A) within the crystal lattice [81]. With other trace cations (e.g., Mg^{2+}, K^{1+}, Na^{1+}) and trace anions (e.g., F^{1-}, CI^{1-}) substituting for calcium, phosphate, or hydroxyl groups over time as well and with citrate and water filling vacancies in the lattice [82], the crystal structure of bone mineral is an imperfect plate (5 nm x 70 nm x > 200 nm) rather than the prismatic shape of an HA crystal [83]. Thus, bone mineral is carbonated HA with varying crystallinity and varying substitutions within the lattice.

Mineral primarily contributes to the strength and elastic modulus of bone such that these mechanical properties increase as ash fraction [84] or degree of mineralization [85] increase. Using wide-angle X-ray scattering/small-angle X-ray scattering (WAXS/SAXS) techniques coupled with in situ compressive loading of bone, recent studies further established that mineral mainly carries compressive load in bone [86, 87]. In addition to mineral quantity, its distribution

spatially and its quality (i.e., mineral maturity/crystallinity and carbonate substitutions) likely influences the mechanical behavior of bone, though less is known about the role of mineral quality in the mechanical behavior of bone.

2.2.7 Increases in mineralization can promote strength but too much hinders fracture resistance

Various techniques exist to quantify degree of mineralization including quantitative microradiography (qMR), quantitative backscattered electron imaging (qBEI), micro-computed tomography (μCT), Fourier transform infrared (FTIR), and RS [88]. Unlike qBEI-derived mineralization (Ca-Peak) or μCT-tissue mineral density (mgHA/cm^3), mineral-to-matrix ratio (MMR) from FTIR or RS provides the amount of mineral per amount of organic matrix [89]. Several rodent studies have reported direct correlations between MMR and bone strength (aging) [90] and between MMR and tissue tissue-level modulus (vitamin D deficiency) [91]. In rodents, Ca^{2+} content and tissue-level modulus and hardness concomitantly increase through skeletal maturity (6-7 months) but do not vary much with aging (between 7 months and 17 months) [92]. Tissue mineral density has been observed to increase in male rats between 12 months and 24 months without any change in bending strength [70] suggesting other factors influence strength of bone. Thus, increasing mineralization of maturing bone confers an increase in elastic properties including modulus at the tissue-level and strength at the apparent level.

A decrease in the degree of mineralization with osteoporosis is typically the result of elevated bone turnover [93], and associations between various measurements of mineralization and fracture risk can be found in previous review [34]. In a recently published study involving embedded and sectioned iliac crest biopsies from age- and aBMD-matched post-menopausal subjects with (n=60) and without history of fracture (n=60), Vennin et al. [94] found that the median value of tissue-level modulus and hardness (nanoindentation) of only the cortical bone

was lower for the fracture than for the non-fracture cases. Interestingly, there were no significant correlations between the nanoindentation properties and MMR (FTIR). In another recent biopsy study, patients on long-term bisphosphonates (BPs), a common treatment for osteoporosis which represses osteoclast activity, who experienced an atypical sub-trochanteric fracture (n=17) had higher MMR (FTIR and RS but not qBEI-derived mineralization) and higher tissue-level hardness (nanoindentation) than patients on long-term BPs with typical femoral neck fractures (n=10) or BP-naïve patents with typical fracture (n=11) or without fracture (n=12) [95]. In mature human bone undergoing normal remodeling, the contribution of local mineralization to apparent-level modulus and strength is less important as micro-structure (e.g., cortical porosity) dictates strength, but in certain cases (e.g., suppressed remodeling), loss of heterogeneity can become a dominant factor in which high mineralization relative to the organic matrix reduces fracture resistance.

Based on genetic mouse and iliac biopsy studies, degree of mineralization (qBEI) is known to increase in OI [96] likely due to increased packing density of crystals, not an increase in crystal size [97]. As reported in a recent study involving pediatric cortical bone from mild to severe OI, tissue mineral density (μCT) and MMR (RS) was higher while tissue-level modulus (nanoindentation) was lower in OI individuals [98] indicating a disruption in the structure-function relationship between elastic behavior and mineralization. In a traditional genetic mouse model of OI (oim mice that produce only the α1 chain), the higher degree of mineralization, compared to control bone, also accompanied a reduced tissue-level modulus (nanoindentation) [99] as well as a decrease in crack initiation toughness [100]. In the mouse model of OI involving deletion of prolyl 3-hydroylase 1, important for PTMs to proline, there was both an increase in bone mineralization (qBEI) [101] and abnormalities in the collagen fibril

ultrastructure [102]. Thus, the apparent hypermineralization in OI likely contributes to the brittle bone disease but so does defect in the collagen structure.

2.2.8 Mineralization heterogeneity contributes to a toughening mechanism

Mineralization heterogeneity refers to the spatial variation in the degree of mineralization throughout bone at the micron length scale and is typically assessed as the full width at the half maximum (FWHM) of the distribution of mineralization levels (e.g., by qBEI, FTIR imaging, or qMR). Studies of human bone samples observed both higher [103, 104] and lower [105, 106] mineralization heterogeneity for fragility fracture cases compared to control cases. Based on computational mechanics [107], the presence of mineralization heterogeneity at the microscale level increases the energy to propagate a crack, thereby providing bone's ability to resist crack propagation (cement line density also increased fracture toughness). However, increasing mineralization heterogeneity arises from an increase in remodeling and the accompanying increase in porosity can lower fracture toughness [108]. A recent fatigue study of trabecular bone involving sequential labeling of damage also indicated that compositional heterogeneity favored propagation of microdamage within center of trabeculae, not at regions of high stress (surface of trabeculae) [109]. Therefore, there is likely both an optimal heterogeneity in mineralization (as well as fibril orientation/structure) and an optimal spatial distribution of varying mineralization (as well as varying fibril orientation) that effectively promotes fracture resistance.

2.2.9 How crystallinity/mineral maturity contributes to mechanical behavior of bone is not known

Crystallinity is an overall indicator of crystal size and crystal lattice perfection (i.e., the degree of order of the ions within the crystal lattice) of mineral [110]. Mineral maturity, on the other hand, refers to the transformation of unstable non-apatitic substance into more crystalized

stable mineral, reflecting the age of bone mineral [111]. In a genetic mouse model of matrix metalloproteinase deletion (MMP-2), Bi et al. [112] reported that crystallinity (RS) was directly proportional to bending modulus (R^2= 0.64, $p<0.05$, n=36) and strength (R^2= 0.40, $p<0.05$, n=36). In a study involving human cadaveric cortical bone specimens, Yerramshetty et al. [113] found that crystallinity (RS) was directly proportional to elastic modulus (R^2= 0.16, p=0.001, n=64) and yield strength (R^2= 0.07, p=0.039, n=64) when all data was pooled. Of course, these associations do not demonstrate that an increase in crystallinity directly increases material strength of bone as other factors of the bone matrix can influence the mechanical behavior. For human bone (117 bone biopsies from 40 females and 77 males between 0 and 90 years old), Hanschin et al. found that crystallinity (X-ray diffraction) was observed to increase up to 25 years of age while it did not vary in individuals between 30 and 80 years old [114], an age range in which fracture resistance declines. Thus, crystallinity is likely not a major contributor to the age-related decrease in the mechanical properties of bone, but it could be a biomarker of diseased bone.

For example, crystallinity (RS) was found to be lower with a corresponding reduction in indentation modulus for sample from OI subjects (n=7) than for age-matched controls (n=3) [98]. In an iliac bone biopsy study involving long-term treatment of postmenopausal osteoporosis with the BP alendronate (6-10 years) and matching for the degree of mineralization across the groups, the treated group (n=6) had significantly lower crystallinity compared to the BP-naïve group (n=5) [115]. Moreover, crystallinity (FTIR) was negatively associated with tissue-level modulus and hardness in only the treated group (R^2=0.18 and R^2=0.29, $p<0.001$, respectively, n=6) when including the amount of mineral and collagen maturity (FTIR) as covariates. There is no data to date showing whether there is an optimal crystal size associated

with adequate bone strength while maintaining bone ductility. However, one hypothesis is that heterogeneity in crystal perfection (i.e., wide distribution in crystal sizes and substitutions) favors adequate bone strength [116].

2.2.10 Carbonate substitution increases with aging and may negatively affect fracture resistance

Carbonates substitution within the bone mineral lattice is thought to create internal strains in the matrix and increase the irregularity of the atomic arrangement of HA (i.e., Ca^{2+}, PO_4^{3-}, and OH^-) [111]. Thus, such substitutions may limit crystal growth by increasing the required energy for the process [117], consequently altering the length and thickness of the bone mineral crystal. Type B carbonate substitutions (CO_3/PO_4 by RS) have been found to correlate with bone mechanical properties. For example, this ratio inversely correlated with bending modulus and yield strength (R^2=0.33 and R^2=0.23, $p<0.05$, n= 13) of rat femurs tested in three-point bending [90] and inversely correlated with crack growth toughness of human cortical bone acquired from donors (n=62) spanning 21-101 years of age [118]. Again, establishing the causal role of carbonate substitutions in the mechanical behavior of bone is rather difficult. One possibility is that carbonate substitution may control bone crystal size such that high carbonate concentration results in smaller crystals [117]. Increasing substitutions then would limit the number of interactions between mineral and collagen I, thereby increasing tissue-level modulus (mineral is stiffer than collagen) while decreasing toughness (less energy dissipated from mineral-collagen separation).

2.2.11 Matrix-bound water promotes while pore water hinders mechanical properties of bone.

Water is an abundant component of bone and exists in three different compartments [19]: i) structural solid-like water as a part of the mineral lattice or integrated into the tropocollagen ultrastructure; ii) pore water (also referred to as mobile, unbound, or free water) within the

Haversian canals, canaliculi, and lacunae, and iii) bound water arising from hydrogen bonding (collagen) and electrostatic attractions (mineral) with various degrees of affinity, ranging from loosely to tightly bound states. Dehydration of bone causes an increase in stiffness at multiple length scales but an overall decrease in toughness [19]. In effect, matrix-bound water provides plasticity to the organic matrix allowing the collagen to extend beyond the yield point of bone. When water is removed, collagen contracts increasing the apparent stiffness of bone.

With the application of ^{1}H nuclear magnetic resonance (NMR) relaxomatry [119] and its translation to clinical magnetic resonance imaging (MRI) with ultra-short time-to-echo techniques [120], the independent role of different water compartments in the mechanical behavior of hydrated bone has begun to be investigated. Both pore water (negative) and bound water (positive) independently explain the variance in mechanical properties of bone [119-122]. Unal et al. recently implemented high wavenumber RS system to assess bound water in bone at the molecular level with the ability of probing both collagen- and mineral-bound water simultaneously [123]. In a follow-up study using this new technique, collagen-bound water measurement from hydrated bovine cortical bone significantly correlated with toughness (R^2=0.52, $p<0.001$, n=30), post- yield toughness (R^2=0.44, $p<0.001$, n=30) and bending strength (R^2=0.26, $p<0.001$, n=30) [14].

While pore water is essentially a surrogate measure of cortical porosity because of strong correlation between these two parameters [119, 124], the important factors affecting bound water with respect to mechanical behavior of bone is less clear. Matrix-bound water is likely important to the post-yield behavior of bone via its interrelationship with the organic matrix. As shown in a recent study, enzymatic treatment of human cortical bone surfaces to remove glycosaminoglycans (GAGs) caused a significant decrease in the tissue-level toughness (nano-

scratch testing) only when water was present [125]. In another recent study, bound water of human cortical bone increased following high dose of radiation exposure and following rotating fatigue testing [126]. A RS-derived Amide I sub-peak ratio also increased following these manipulations suggesting that gamma radiation-induced matrix damage increased the number of hydrogen bonding sites to which water could interact. It is still unclear how bound water decreases with aging but could involve a loss in matrix-bound glycoproteins and proteoglycans and/or unfavorable modifications in collagen I.

2.3 Current Rodent Models for Diabetes

There are multiple rodent models for T2D which can be separated into spontaneous and diet-induced models. The spontaneous T2D models develop diabetes due to genetic factors; however, the knockout of certain genes may affect the skeletal phenotype independent of effects seen due to diabetes [127]. Several studies have been done using rat models, particularly the Zucker Diabetic Fatty rat (ZDF) and the Zucker Diabetic Sprague Dawley rat (ZDSD). The ZDF rat has a leptin receptor deficiency which may separate effects on bone and experimentally this model has lower BMD [127, 128], not typically seen in T2D. ZDSD is more consistent with the skeletal structural phenotype [127], but the bone's material properties have been shown to not be significantly different [129, 130]. This does not reflect T2D phenotype in humans, and thus investigations should be conducted into the skeletal phenotypes of other rodent models. Recent mouse models such as the KK/A^y mouse have been utilized in studies on diabetic nephropathy [127, 131], but not much information exists on the skeletal characteristics. Using dual-energy X-ray absorptiometry, one study for KK/A^y showed a decreased in BMD [16], which is not consistent with the human phenotype. However, more studies are needed to verify this and to

determine if diet combined with its genetic predisposition will cause the model to more accurately mirror the human phenotype.

There are limitations with the mouse models for diabetes. Often, in order for diabetes to occur, genetic mutations were generated in mice, but these mutations are not known to exist in the human condition of the disease. For example, in the case of ob/ob and the db/db mice, the leptin hormone and the leptin receptor are defective, causing obesity [127, 132]. While these mice become diabetic, leptin signaling can directly affect bone [133-135], so observed differences in the material of properties between wild-type and mutant can exist independent of diabetic effects. The TallyHO mouse has been studied for T2D, but its early age of diabetes onset limits it to juvenile or early onset T2D studies [136]. However, while ob/ob and db/db are monogenic models, the TallyHO mouse is a polygenic model of T2D. Some of the models such as the New Zealand Obese mouse have a tendency to develop autoimmune disorders [127], which may lead to inaccurate results. Furthermore, there is a knowledge gap as there is often not much information on the skeletal phenotypes of the different rodent models.

2.4 Current Rodent Models for Aging

Rodents have been used in multiple studies on aging. Many of the studies used ovariectomized rodents in order to study estrogen-related bone loss [137]. However, as it became known that aging is an independent factor for fracture risk, studies began to examine the bones of aging rodents in both males and females of commonly available laboratory strains [137]. Previous work has shown that like humans, rats and mice have higher cortical porosity towards the ends of long bones and lower trabecular bone volume [70, 138-142]. Work with rats has shown lower toughness and material strength in aged rat bone [70, 143]. Unlike in humans, rodents have higher tissue mineral density or aBMD with age [137, 138, 142]. Apart from

commonly used laboratory strains, another rodent used to study aging is an accelerated aging model, the α-klotho$^{-/-}$ mouse. This knock-out mouse has multiple features of aging, including infertility, arteriosclerosis, and osteoporosis [144] and has been used to study aging in mouse bone [79].

When looking at studies using aging rodents, it is important to note that rodents lack the intracortical remodeling system that humans have [137, 145]. While some modeling may occur on the endosteal and periosteal surfaces, overall, there is less turnover in the bones of mice than in humans. This may explain the higher aBMD observed with age in rodents. Additionally, while there has been some work on tissue-level material properties in rats, there is much less available for mice. Two studies have examined strength in mice [142, 146], but the majority of the studies have examined structural mechanical properties. Lastly, there is a need for information on how the matrix is affected with age in mice.

CHAPTER 3 LOW BONE TOUGHNESS IN THE TALLYHO MODEL OF JUVENILE TYPE 2 DIABETES DOES NOT WORSEN WITH AGE

Work in this chapter is published as Creecy, A, Uppuganti, S, Unal, M, Bunn, RC, Voziyan, P, Nyman, JS, *Low bone toughness in the TallyHO model of juvenile type 2 diabetes does not worsen with age*. Bone, 2018 **110**: 204-214 [147]

Reprinted with permission of Elsevier

3.1 Introduction

Fracture risk is higher among individuals with diabetes compared to those without diabetes for a given T-score as determined by dual energy X-ray absorptiometry (DXA) [50, 148]. Multiple epidemiological studies have also found that the relative risk of fracture is higher among type 2 diabetics than age-matched non-diabetics [5, 6, 149-151]. This increase in fracture risk is most pronounced at the hip, and a meta-analysis by Janghorbani et al. estimated a 1.7 times greater risk of hip fracture for adults with type 2 diabetes (T2D) [149]. While risk factors unrelated to bone increase fracture incidence in T2D, elevated fracture risk is still observed when adjusting for diabetes-associated increase in the propensity to fall or in decreased muscle tone [149, 150, 152]. This elevated fracture risk is somewhat counterintuitive because a larger BMI and hyperinsulinemia in type 2 diabetics would generally favor a higher bone mass and strength, though the relation between obesity and femoral neck strength is complex [153]. The lack of an apparent loss in bone mineral density (BMD) with T2D suggests that the disease is negatively affecting bone quality [154].

Incidence of T2D is rising. According to the CDC, an estimated 6.5% of people in the United States had diabetes in 2015 up from 5.5% in 2005 [155]. The increasing prevalence of T2D does not just occur among adults [156], as the population of obese children has increased

[157, 158]. While this increase in obesity incidence may be leveling off in recent years, the continued rise in severe obesity could drive an increase in complications associated with juvenile-onset T2D [159]. Furthermore, as duration of diabetes increases, fracture risk appears to increase [6]. Thus, the increasing prevalence of T2D among juveniles may result in even higher relative risk of fracture later in life than current estimates. While there has yet to be a study examining this in juvenile-onset T2D, type 1 diabetes has been associated with increased fracture risk throughout lifespan [160].

There are multiple pathways through which T2D can lower bone quality and increase fracture risk [154, 161], but T2D is not necessarily causing a deterioration in cortical structure or trabecular architecture, at least not directly. Several cross-sectional studies involving high resolution, peripheral quantitative computed tomography (HR-pQCT) imaging of post-menopausal women did not find lower cortical thickness, lower estimated failure load in compression, lower trabecular thickness, or lower trabecular bone volume fraction for subjects with T2D compared to non-diabetic controls [47, 49, 162]. In one recent HR-pQCT study involving men and women (Framingham cohort), the cross-sectional area of the tibia mid-shaft, not the distal radius, was significantly lower (by 2.4%) for those with T2D compared to non-diabetics [163]. There were no significant differences in the trabecular architecture, trabecular volumetric BMD, or estimated compressive failure load between the groups at these peripheral sites, though cortical thickness was lower in T2D individuals with prior fracture [163]. With respect to micro-structure, cortical porosity (Ct.Po) has been observed to be higher in the distal radius [162, 164, 165] and tibia mid-shaft [165] for those with T2D, especially if the T2D patient had suffered a fracture [163, 166, 167], but an elevated Ct.Po with T2D has not always been observed [47-49]. With respect to material properties of bone, studies using a microindentation

tool, designed to assess the resistance of cortical bone at the tibia mid-shaft to impact loading, have found lower bone material strength index (BMSi) in post-menopausal patients with T2D compared to age-matched non-diabetic women [47-49]. At the matrix level of the hierarchical organization of bone, an increase in advanced glycation end-products (AGEs) caused by elevated glucose levels could also result in more brittle bones [15, 168].

Various rodent models have been used for investigating diabetic bone disease, but as previously reviewed [127], the effect of T2D on fracture resistance has only been reported for a few mouse models and done so with several limitations. For example, in a MKR transgenic mouse model of early onset T2D (hyperglycemia by 6-8 weeks) which has a mutation of insulin-like growth factor receptor 1 in skeletal muscle, the bones of MKR mice are structurally weaker than non-diabetic controls (FVB/N strain). Unlike humans with T2D, these mice have slender bones, are lean, and their insulin resistance is due to specific gene mutations, namely the loss of insulin and insulin-like growth factor 1 (IGF-1) receptors in skeletal muscle [169]. However, such gene mutations are rarely the clinical cause of T2D. Overcoming this limitation, the KK-A^y mouse is a polygenic model developing hyperglycemia spontaneously by 8 weeks [170]. When compared to non-diabetic male ddY mice, male KK-A^y mice had lower areal BMD at the proximal femur, not at the mid-shaft, by 18 weeks of age [171]. However, when using non-diabetic C57BL/6 for controls, Xu et al. observed lower volumetric BMD and lower structural strength in bending of the tibia mid-shaft for the diabetic KK-A^y mice [172]. Yet another study comparing male KK-A^y to male C57BL/6 mice observed higher areal BMD of the whole femur, lower volumetric BMD of trabecular bone in the distal femur, and higher volumetric BMD of cortical bone in the distal femur [173]. To the best of our knowledge, there is no study reporting on the fracture resistance phenotype of KK-A^y/a with respect to a/a littermate controls. Another

commercially available, polygenic, spontaneous mouse model for T2D is the TallyHO strain. This mouse develops hyperglycemia before skeletal maturity [174] and is obese compared to its recommended control strain, SWR/J [136, 175]. As previously reported by Devlin et al., the femur diaphysis is structurally stronger in bending but brittle (lower post-yield displacement) for the diabetic TallyHO compared to non-diabetic SWR mice at 17 weeks of age [136].

To determine whether the TallyHO mouse can be a model of diabetic bone disease that represents what is known about the disease in humans (i.e., shows increase in fracture risk with increase in duration of diabetes), we hypothesize that fracture resistance decreases as the duration of diabetes increases beyond skeletal maturity. We analyzed bones from both TallyHO mice and SWR/J controls at 16 weeks (short duration) and 34 weeks of age (long duration) using multiple techniques in order to establish whether bone parameters associated with greater bone fragility in humans changed. Specifically, we determined whether i) an increase in cortical porosity, ii) a deterioration in trabecular architecture, iii) an accumulation of matrix AGEs, and iv) alterations in the structure of collagen I reflective of crosslinking also accompany a T2D-related decrease in the mechanical properties of the bone in this mouse model.

3.2 Materials and Methods:

3.2.1 Animal care and tissue collection

TallyHO/Jng (n=30) and SWR/J (n=30), male mice were purchased from Jackson Laboratory (Bar Harbor, ME). Female mice were not included because female TallyHO mice do not develop overt diabetes [174]. Animals were fed standard chow 5L0D with 13% kcal from fat (LabDiet, St Louis, MO) up until 16 weeks of age. Subsequently, all animals were switched to a 12450B purified diet with 10% kcal from fat (Research Diet, Inc., News Brunswick, NJ). Weekly, animals were weighed and their non-fasting glucose levels measured using a OneTouch

UltraMini glucometer (LifeScan Inc., Milpitas, CA). Glycated hemoglobin (HbA1c) was measured for a sub-set of mice at 34 weeks of age using a Bayer DCA 2000 system by the VUMC Metabolic Phenotyping Core. Immediately prior to sacrifice, blood was collected by cardiac exsanguination while animals were under ketamine/xylazine anesthesia. Animals were either euthanized at 16 weeks of age or at 34 weeks of age. Due to 6 premature deaths from fungal nephritis (unexpected), 10 additional TallyHO mice were ordered. Mice were then housed in sterile cages. All animal protocols were approved by the local Institutional Animal Care and Use Committee. One SWR/J mouse was excluded from the study (34-week group) because lymphoma was observed at necropsy. Femurs and L6 vertebrae were frozen in phosphate buffer solution (PBS) for micro-computed tomography analysis (μCT) and biomechanical testing. The posterior side of the right femur from each mouse was micro-notched at the mid-shaft using first a low speed diamond embedded saw, and then a razorblade coated with a diamond solution.

3.2.2 Micro-computed tomography analysis

Both femurs and the L6 vertebra (VB) were imaged with high-resolution μCT scanner (μCT50; Scanco Medical AG, Brüttisellen, Switzerland). The regions of interest (ROIs) for the left femurs included the mid-shaft (1.86 mm) at the point of loading (described in subsequent section) and distal metaphysis (3.72 mm) extending approximately 25% below the growth plate. The scan parameters were: 70 kVp/114 μA, 0.5 Al filter, beam hardening (BH) correction, 1160 samples per 500 projections per 180° rotation, 600 ms integration time, and 6 μm isotropic voxel size. For L6 VBs, the ROI was the bone between the cartilaginous end-plates. Scan parameters were: 55 kVp/200 μA, 0.5 mm Al filter, beam-hardening correction, 500 samples per 500 projections per 180° rotation, 1200 ms integration time, and 12 μm isotropic voxel size. The mid-shaft of each notched, right femur was imaged with another μCT scanner (μCT40; Scanco

Medical AG, Brüttisellen, Switzerland). The scan parameters were: 70 kVp/114 μA, 0.5 mm Al filter, beam-hardening correction, 2048 samples per 1000 projections per 180° rotation, 300 ms integration time, 6 μm isotropic voxel size. Images were analyzed and contoured as described previously [66]. Thresholds varied among bone type: i) for the intact left femur diaphysis, global threshold was 912.6 mgHA/cm^3, ii) for the cortical compartment, an inverted threshold setting of 816.0 mgHA/cm^3 was also used to determine porosity (Ct.Po), iii) for the trabecular bone of the left femur metaphysis, global threshold was 393.2 mgHA/cm^3, iv) for the notched right femur, it was 863.1 mgHA/cm^3, and v) for trabecular bone in the vertebral body, it was 514.0 mgHA/cm3 [66]. A sigma of 0.2 and support of 1 (Gaussian filter) were used with all thresholds to suppress image noise.

3.2.3 Mechanical testing

3.2.3.1 Three-point bend testing of left femurs

Hydrated left femurs were loaded to failure in a three-point (3pt) bending at a displacement rate of 3 mm/min using a servo-hydraulic material testing system (DynaMight 8841, Instron, Norwood, MA) fitted with a 100 N load cell (Honeywell, OH, Model no. 060-C863-02). All femurs were placed on the lower supports with a span of 8 mm such that the anterior side was down and the medial side was forward. Using a custom Matlab script (Mathworks, Natick, MA), the force vs. displacement curve (sampled at 50 Hz during 3pt bending) was processed to determine structural properties (stiffness or slope, peak force, yield force, post-yield displacement, work-to-failure) [66], and then material properties (bending strength, peak moment, toughness, modulus, etc.) were estimated using μCT-derived structural parameters as previously described [176].

3.2.3.2 Fracture toughness testing

Notched right femurs were also tested in 3pt bending (DynaMight 8841, Instron, Norwood, MA) using the 100 N load cell while hydrated with PBS, but the span was adjusted to four times the mean outer anterior–posterior diameter (i.e., in the direction of loading) rounded to the nearest mm. The loading rate of these femurs was 0.06 mm/min. All tests were recorded using a high resolution DSLR camera (Canon EOS 7D) fitted with a macro lens to qualitatively monitor the crack propagation and to discard outliers if any. Again, force vs. displacement curves were processed using custom Matlab script to calculate the critical stress intensity factor, $K_{c,initial}$, using the peak force during the load-to-failure test and the initial notch angle (θ was determined using μCT images) as previously described [177]. Cracking toughness was measured by dividing the work-to-failure (W_f) by Ct.Ar and adjusted for the given span [66].

3.2.3.3 Axial compression testing

Each hydrated L6 VB was loaded to failure at 3 mm/min between two custom compression platens with a moment relief [66]. VB strength was defined as the peak force. Axial stress was determined by the peak force divided by the cross-sectional area of the VB. Cross-sectional area was estimated by dividing the segmented bone volume of the VB (transverse processes transected) by the axial length of the ROI.

3.2.4 Raman spectroscopy

Raman spectra were collected from right femurs after fracture toughness testing by focusing a 830 nm laser several millimeters away from broken surface. Using a confocal Raman microscope (Invia, Renishaw, Hoffman Estates, IL), an average of 10 consecutive spectra per bone (each collected for 5 s duration) was acquired through a 20X objective (NA=0.40). From the averaged Raman spectrum per bone sample, the background fluorescence was subtracted

using a 4th order polynomial curve. Subsequently, spectra were smoothed using a 4th order Savitzky-Golay filter (LabSpec software, Horiba Jobin Yvon, Edison, NJ) to the signal to noise ratio. Peak ratios of ν_1PO_4/Amide I, ν_1PO_4/Amide III, ν_1PO_4/Proline, and CO_3/ν_1PO_4 [178] as well as Amide I sub-peak ratios 1670/1640, 1670/1690, and 1670/1610 were calculated as previously described [179]. The crystallinity was calculated as the inverse of the width of the ν_1PO_4 peak at half maximum.

3.2.5 High Performance Liquid Chromatography (HPLC) and fAGE

The proximal and distal half of broken left femurs were flushed, weighed separately (wet mass) and separately demineralized in 20% EDTA at 4 °C. After demineralization, the samples were dehydrated for 24 hours at room temperature under a vacuum. Samples were then hydrolyzed with 6 N HCl at 110 °C for 20 hours. Hydrochloric acid was removed using a SpeedVac Concentrator System (ThermoFisher). Samples were filtered through 0.2 µm syringe filters (Fisher) and then split so as to have ≈1 mg of dry weight of bone for each assay. The proximal half was used for crosslink analysis. The crosslinks pyridinoline (PYD) and pentosidine (PE) were measured with a high performance liquid chromatography (HPLC) system (Beckman Coulter System Gold 126, Brea, CA) involving a silica-based, reversed phase C18 column (Waters Spherisorb® 5µm ODS2, Milford, MA) column and fluorescence detector (Waters 2475 Multi λ Fluorescence Detector) as we previously described [178]. Collagen was determined based on hydroxyproline measurements using a HPLC assay with a Waters PicoTag column (Waters, Milford, MA) and a UV detector (Beckman Coulter 168 Detector, Brea, CA) as previously described [178]. Crosslinks were calculated based on a standard curve using standards of known concentrations (PYD: Quidel®, TECOmedical group, Switzerland and PE: International Maillard Reaction Society).

The hydrolyzed samples from the distal half of the femur were suspended in 350 µL of 0.1 M H_2SO_4. Samples were compared to a standard of quinine sulfate suspended in 0.1 M H_2SO_4 as previously described [16]. 150 µL was pipetted in duplicate for each sample and standard into a black-bottom 96 well plate. Fluorescence was measured with an excitation wavelength of 370 nm and an emission wavelength of 440 nm. Fluorescent advanced glycation end-products (fAGEs) were calculated based on the standard curve and normalized to an estimated measurement of collagen based on the ratio of mol of collagen to wet mass of the proximal half.

3.2.6 Serum analysis

Serum was separated by centrifugation in serum collection tubes. Insulin was measured using a radioimmunoassay (RIA) from Millipore and was performed by the VUMC Hormone Assay and Analytical Services Core. P1NP and TRAcP-5b were measured in serum using Rat/Mouse ELISAs (Immunodiagnostic Systems, Inc., Fountain Hills, AZ) [180] according to the manufacturer's protocols.

3.2.7 Statistical Analysis

Instead of two-way analysis of variance, which assumes normality and homoscedasticity, general linear models (GLMs) with bootstrapping (500 replicates) were analyzed (STATA, College Station, TX) to determine whether each bone property depended on mouse strain, age, and their interaction (inter.), appropriate post-hoc comparisons were done using Mann-Whitney tests (Matlab, MathWorks, Natick, MA) with a Holm-Sidak correction for 2 multiple comparisons (e.g., TallyHO vs. SWR/J within 16 weeks and TallyHO vs. SWR/J within 34 weeks when strain was a significant factor). Subsequently, body weight, calculated as an average over 10 weeks to 16 weeks or over 24 weeks to 34 weeks of age, was included as a covariate in

the STATA GLMs to determine if body weight was the driving factor for strain differences in bone properties. These analyses of covariance were separated out by age group to limit the number of factors being analyzed at once. For each group, correlations between average blood glucose levels and bone properties were determined using linear regression analysis with bootstrapping (500 replicates). Averaged blood glucose was calculated from 8 weeks to 16 weeks for mice at 16 weeks of age and from 8 weeks to 33 weeks for mice at 34 weeks of age. Longitudinal body weight and glucose comparisons between strains were done at individual time points using Mann-Whitney.

3.3. Results:

3.3.1 TallyHO mice weighed significantly more than control mice and exhibited variable hyperglycemia

TallyHO mice had a higher body weight than SWR/J mice as early as 5 weeks of age (Figure 3.1A), and so the body weight, calculated by taking the average over the last 6 weeks or 10 weeks of life, was significantly higher for TallyHO than for SWR/J mice at both ages (Table 3.1). Diabetes, as defined by persistent non-fasting glucose levels above 250 mg/dL, a common threshold in rodent studies [181], occurred for most TallyHO mice around 10 weeks of age (Figure 3.1B). One TallyHO mouse (green symbols in Figure 3.1B) was excluded from the study due to inconsistent hyperglycemia. Eight TallyHO mice experienced significant weight loss and were euthanized before the end of the study. These premature deaths were likely due to complications

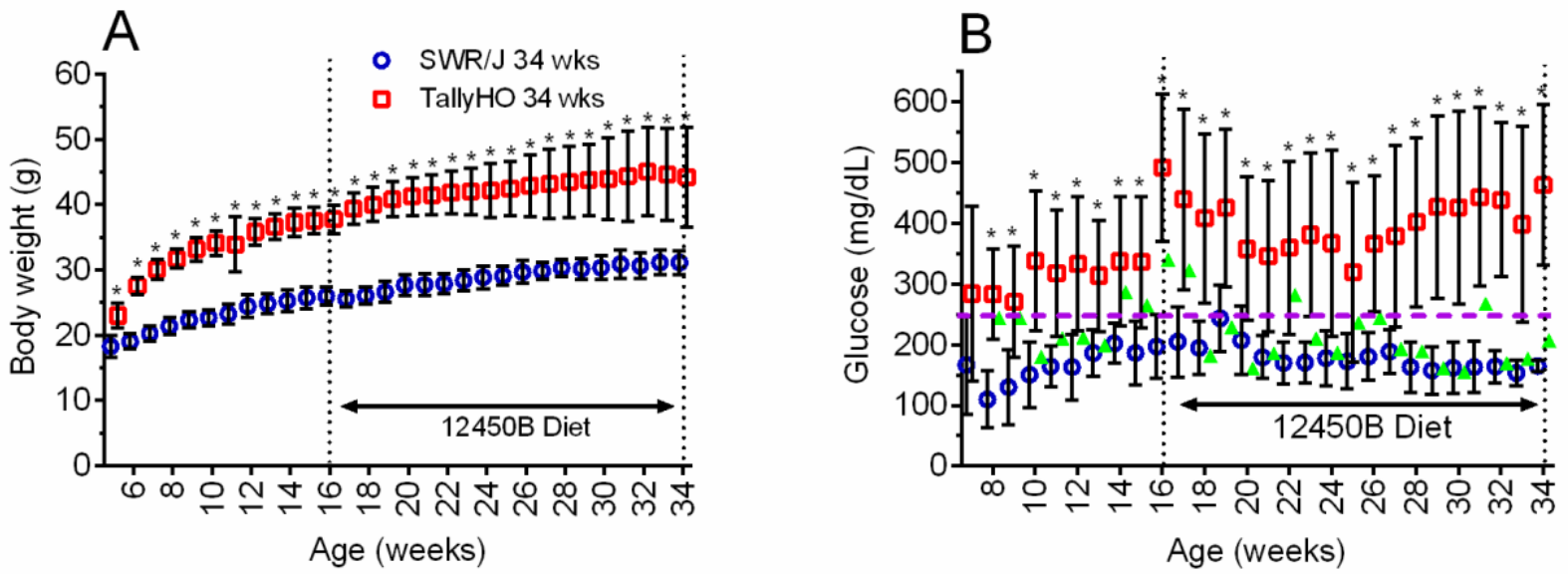

Figure 3.1 Age-related changes (mean ± SD) in body weight (A) and non-fasting blood glucose levels (B). TallyHO mice (n=13) were obese compared to SWR/J controls (n=16) starting at 5 weeks of age. Glucose levels in TallyHO mice were significantly higher than control mice at an early age but achieved persistent diabetic status (consecutive weekly levels > 250 mg/dL; purple dashed line) at 10 weeks of age. One TallyHO mouse (green triangle) was not consistently diabetic and was excluded from the study. Reprinted with permission of Elsevier [147].

Table 3.1 Selected characteristics (mean ± SD) of diabetic TallyHO mice and non-diabetic SWR/J mice.

		16 weeks			34 weeks			GLM p-values		
Property	Unit	SWR/J (n≥7)	TallyHO (n≥7)		SWR/J (n≥11)	TallyHO (n≥10)		Strain	Age	Interaction
Averaged body weight	g	24.6 ± 0.9	34.9 ± 2.4	#	30.2 ± 1.5 a	43.7 ± 5.6	#,b	**<0.0001**	**<0.0001**	0.096
HbA1c	%				3.9 ± 0.2	5.2 ± 1.3	#		N/A	
Insulin	ng/mL	0.278 ± 0.239	0.836 ± 0.565		0.129 ± 0.085	1.80 ± 1.21	#	**0.013**	0.109	**0.011**
P1NP	ng/mL	23.9 ± 6.5	12.3 ± 2.9	#	22.3 ± 5.2	10.8 ± 5.7	#	**<0.0001**	0.577	0.976
TRAcP-5b	U/L	11.58 ± 3.41	8.95 ± 3.16		6.33 ± 2.20 a	7.08 ± 1.21		0.174	**0.001**	0.090

#: adjusted p-value less than 0.05 for strain comparison within age group. a & b: adjusted p-value less than 0.05 for age comparison within strain. Reprinted with permission with Elsevier [147].

of overt, uncontrolled diabetes (>500 mg/dL) and occurred between 20 and 32 weeks of age. Glucose levels were higher in TallyHO mice compared to SWR/J mice, as expected, but the degree of hyperglycemia in TallyHO mice did not progressively increase with age (Figures 3.1B and 3.2A). Given the variability in non-fasting glucose measurements, HbA1c was measured for a 10-12 mice per group at 34 weeks. HbA1c was 33.3% higher in the TallyHO mice compared to SWR/J controls (Table 3.1), and this measure of glycated hemoglobin correlated with non-fasting glucose levels in TallyHO mice (Figure 3.2B).

3.3.2 Mechanical properties of bone from TallyHO mice did not progressively worsen with age

To determine whether fracture resistance at the material level (i.e., independent of bone structure) decreased with the duration of T2D, we assessed multiple mechanical properties of cortical bone. For intact femur diaphysis, bending strength, or the estimated peak stress endured by the intact femur diaphysis, was higher for diabetic mice at 16 weeks of age (Figure 3.3A), but not at 34 weeks of age. Toughness was lower for the TallyHO mice compared to non-diabetic controls, but it did not progressively worsen with age as anticipated (Figure 3.3B). Similarly, post-yield deflection was lower in the diabetic TallyHO compared to the control SWR/J mice, irrespective of age (Table 3.2). Body weight was a contributing factor to only bending strength and only at 34 weeks, but this did not change the lack of a T2D-related difference at this age (Table 3.7).

When testing the notched right femurs for the ability of bone to resist crack initiation, $K_{c,initial}$ trended towards being lower in diabetic mice (Figure 3.3C), but this reduction was not statistically significant. Cracking toughness, or the energy dissipated during crack propagation, was not different between diabetic and control mice. However, cracking toughness was

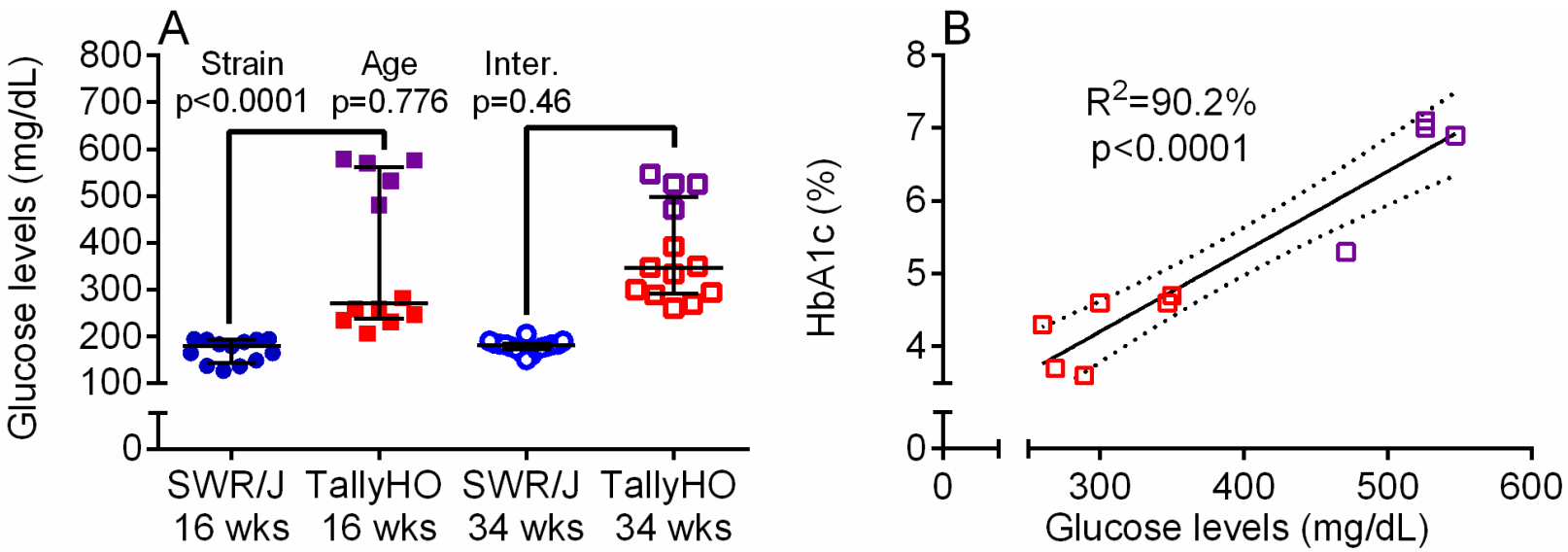

Figure 3.2 Blood glucose levels as an average between 8 weeks and 16 weeks for 16-week-old (wks) and between 8 weeks and 33 weeks for 34 wks (median ± interquartile range with GLM p-values) (A) and HbA1c vs. glucose levels (B). TallyHO mice had significantly higher glucose levels at both 16 weeks and 34 weeks, and these levels did not increase with age partly due to high variability among each age group. HbA1c values correlated strongly with average blood glucose levels. The data points from animals with blood glucose levels consistently higher than 450 mg/dL are shown in purple. Brackets indicate significant differences between strain within age group, and letters indicate significant differences between age groups within strain. Reprinted with permission of Elsevier [147].

Table 3.2 Biomechanical properties (mean ± SD) as determined from three-point bending tests of the left femur mid-shaft.

		16 weeks		34 weeks			GLM p-values		
Property	Unit	SWR/J (n≥13)	TallyHO (n≥12)	SWR/J (n≥15)	TallyHO (n≥13)		Strain	Age	Interaction
Modulus	GPa	12.4 ± 0.8	12.8 ± 1.5	13.1 ± 1.1	13.1 ± 1.3		0.432	0.062	0.522
PYD	mm	0.391 ± 0.081	0.275 ± 0.123	# 0.292 ± 0.072	a 0.187 ± 0.065	#	**0.006**	**0.001**	0.833
Yield Force	N	16.6 ± 1.4	19.1 ± 1.7	# 21.1 ± 2.3	a 23.2 ± 2.4	b	**<0.0001**	**<0.0001**	0.711
Peak Force	N	17.9 ± 1.4	20.5 ± 1.7	# 24.4 ± 1.9	a 27.3 ± 2.6	#,b	**<0.0001**	**<0.0001**	0.819
Stiffness	N/mm	112 ± 9	115 ± 10	154 ± 12	a 172 ± 18	#,b	0.417	**<0.0001**	**0.026**
Work-to-failure	N·mm	8.07 ± 0.97	7.33 ± 2.01	8.77 ± 1.54	7.12 ± 1.68		0.248	0.168	0.320

#: adjusted p-value less than 0.05 for strain comparison within age group. a & b: adjusted p-value less than 0.05 for age comparison within strain. Reprinted with permission of Elsevier [147].

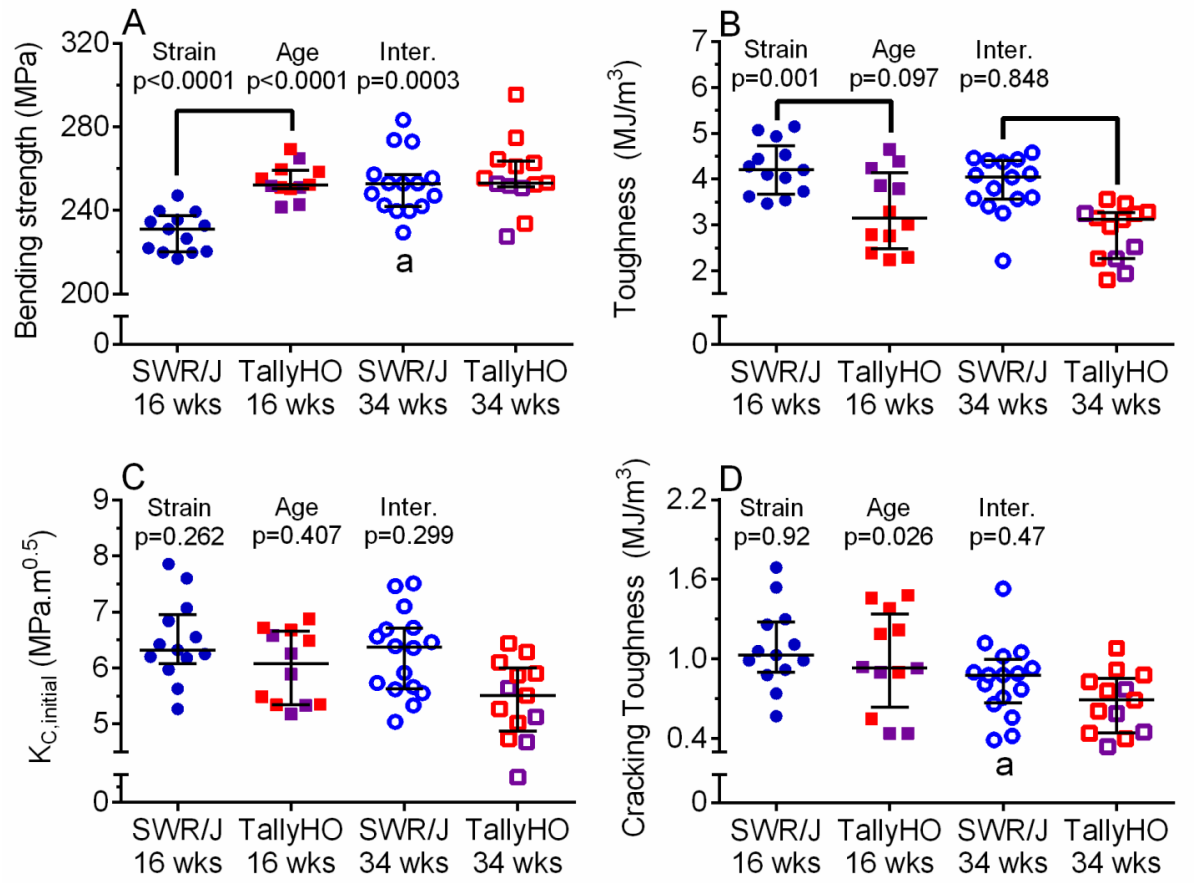

Figure 3.3 Estimated material properties from bending tests (median ± interquartile range with GLM p-values). Compared to control mice, bending strength of the femur diaphysis (A) was higher for diabetic mice initially at 16 weeks, but was no longer different at 34 weeks of age. Toughness (B) was lower for diabetic mice at both ages, but did not further decrease with the duration of diabetes. $K_{c,initial}$ (C) did not significantly vary with age or strain, though showed a tendency to be less for diabetic mice. Cracking toughness (D) did not differ between the strains, but was less for control mice at 34 weeks than for control mice at 16 weeks. The data points from animals with blood glucose levels consistently higher than 450 mg/dL are shown in purple. Brackets indicate significant differences between strain within age group, and letters indicate significant differences between age groups within strain. Reprinted with permission of Elsevier [147].

significantly lower at 34 weeks compared to 16 weeks in non-diabetic mice but not in diabetic TallyHO mice (Figure 3.3D). Body weight was not a significant contributor to either fracture toughness parameter, while strain became a significant explanatory variable ($p=0.038$) of cracking toughness at 34 weeks when body weight ($p=0.178$) was included as a covariate (Table 3.7).

3.3.3 The TallyHO femurs were structurally stronger than SWR/J femurs but this greater strength was not independent of body weight

With respect to fracture resistance at the whole-bone level (i.e., dependent on bone structure), the peak force endured by the femur was higher for TallyHO than for SWR/J mice. This is likely due to the cross-sectional area of the femur diaphysis (Ct.Ar) and the cortical thickness (Ct.Th) being larger for diabetic mice than non-diabetic mice at both ages (Figure 3.4A and Figure 3.4B). However, minimum moment of inertia (I_{min}) was higher in diabetic mice only at 34 weeks of age (Figure 3.4C). The endosteal perimeter (Ec.Pm) was lower for TallyHO mice at 16 weeks, but this increased with age for TallyHO mice so as to not be lower at 34 weeks compared to the SWR/J mice. Cortical porosity was lower in diabetic mice than non-diabetic mice at both ages and did not change with duration of diabetes (Figure 3.5A). Body weight was a significant explanatory variable of I_{min}, Ct.Ar, and periosteal perimeter (Ps.Pm) (Table 3.9) for both age groups. However, body weight significantly contributed to cortical thickness only at 16 weeks and to Ec.Pm at 34 weeks. Body weight was also significant factor in the linear models explaining peak force, yield force, and stiffness at both ages. Furthermore, when body weight was included as a covariate, the T2D-related difference in the peak force and the yield force was no longer significant.

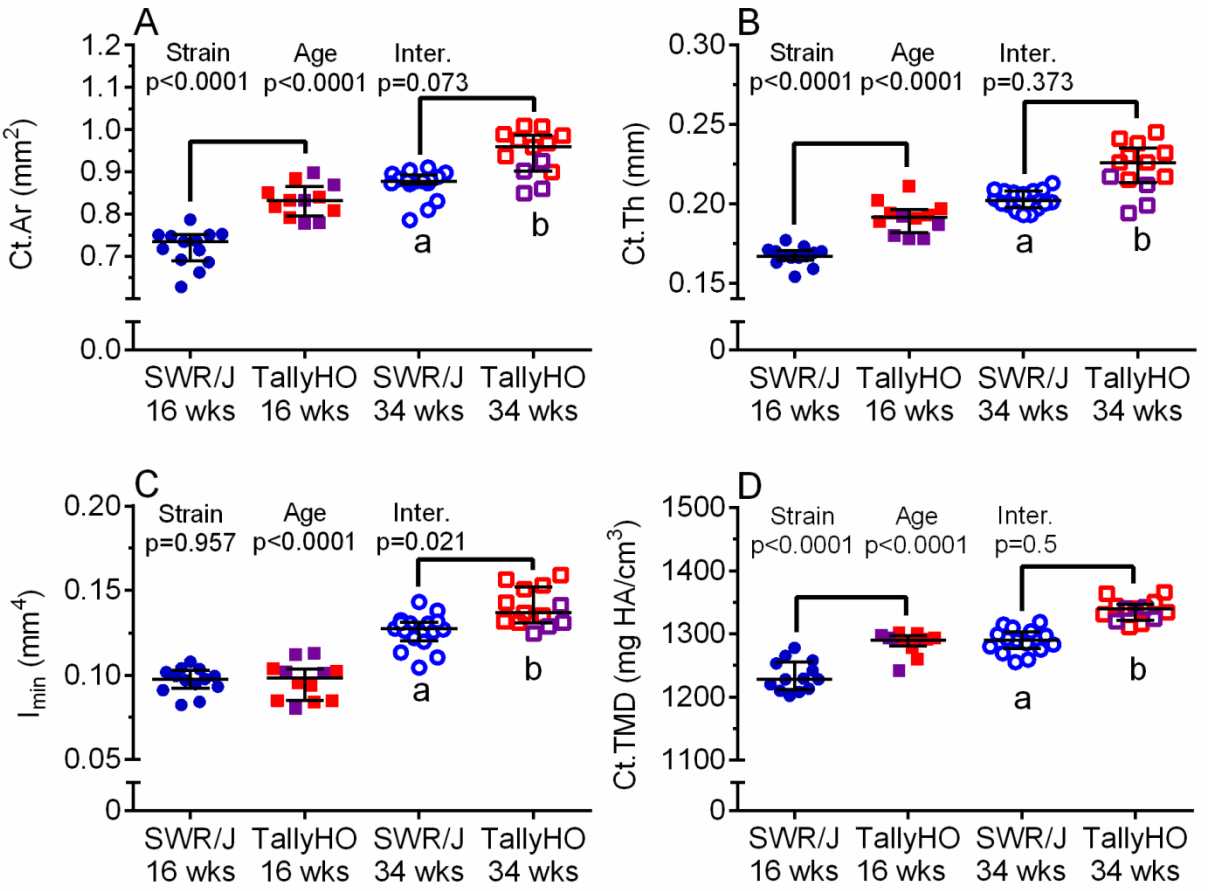

Figure 3.4 Structural properties and volumetric tissue mineral density of the femur diaphysis (median ± interquartile range with GLM p-values). Cortical area (A) and thickness (B) were higher for TallyHO mice than for the control mice at both ages, and these bone properties increased with age for both strains. Minimum moment of inertia (C) was not higher for diabetic mice until 34 weeks of age. TMD differences were similar to the strain- and age-related differences in cortical area and thickness (D). The data points from animals with blood glucose levels consistently higher than 450 mg/dL are shown in purple. Brackets indicate significant differences between strain within age group, and letters indicate significant differences between age groups within strain. Reprinted with permission of Elsevier [147].

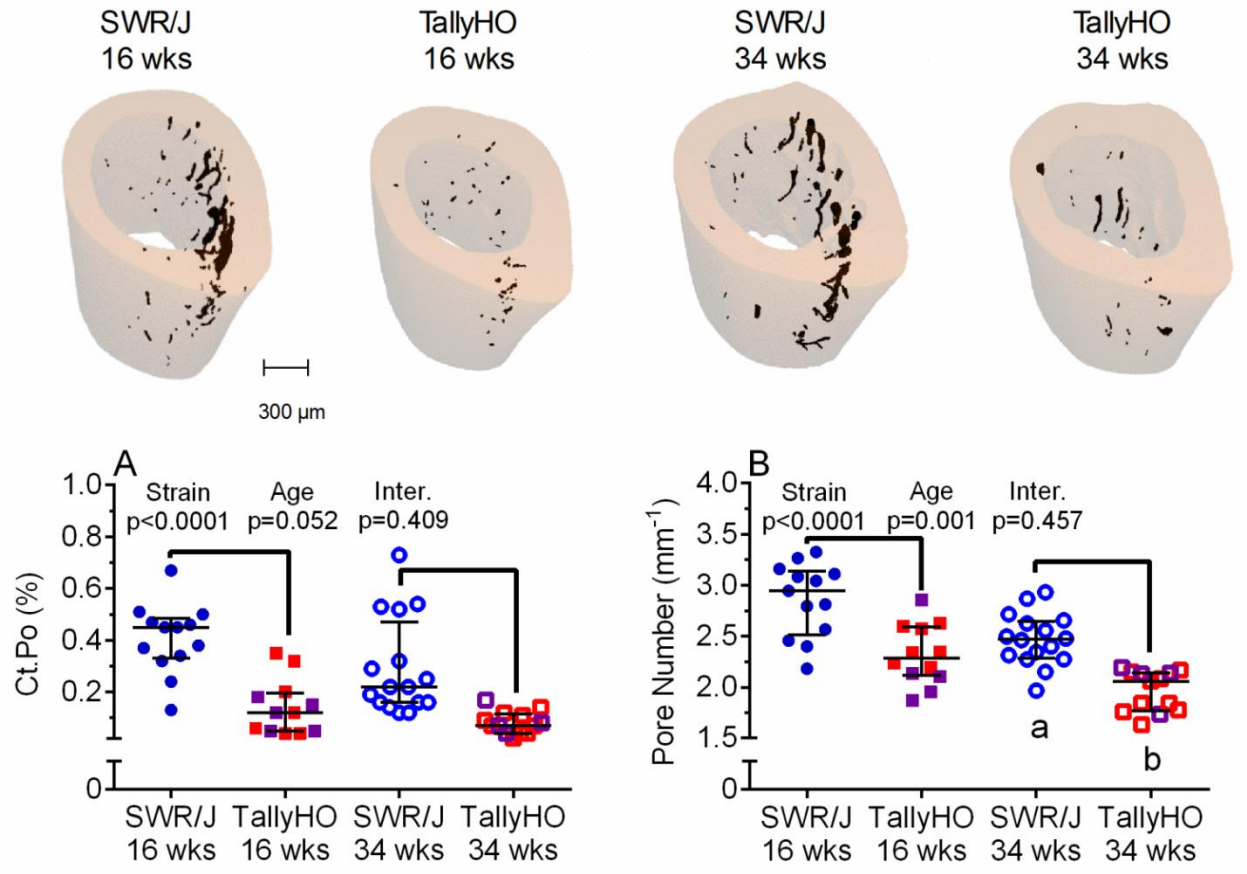

Figure 3.5 Cortical porosity (A) and pore number (B) for the femur diaphysis (median ± interquartile range with GLM p-values). Overall, cortical porosity was lower for diabetic mice compared to controls, but did not change with age for either diabetic or non-diabetic mice. Pore number was also lower for the TallyHO mice at both ages and decreased with aging for both strains. Representative 3D renderings of cortical bone depict the porosity distribution. The data points from animals with blood glucose levels higher than 450 mg/dL are shown in purple. Brackets indicate significant differences between strain within age group, and letters indicate significant differences between age groups within strain. Reprinted with permission of Elsevier [147].

3.3.4 Lower trabecular bone volume did not result in lower lumbar vertebra strength for the TallyHO mice compared to the control mice

In order to estimate the contribution of trabecular bone to whole-bone strength, compression tests of the L6 vertebra were performed. Neither strain nor age affected peak compressive force (Table 3.3). Despite the lack of difference in VB strength between the strains, trabecular bone volume fraction (BV/TV) of the vertebra was lower for the diabetic TallyHO compared to the non-diabetic mice at 34 weeks. As such, the apparent axial stress was higher for the TallyHO mice at both ages (Table 3.3). Similar strain-related differences in trabecular micro-architecture were observed in the distal femur metaphysis, though BV/TV was lower at 16 weeks for the TallyHO than for the SWR/J mice (Table 3.4). Body weight was a significant explanatory variable of BV/TV at 16 weeks of age for both the vertebra and femur, but strain remained a significant factor. Body weight affected only the strain-related difference in vertebral Tb.TMD at 16 weeks. It was not a significant contributor to peak force or any other compressive mechanical parameter (Table 3.8).

3.3.5 The bone matrix of diabetic TallyHO mice had altered secondary structure of collagen I and higher mineralization compared to control bone matrix

To identify a potential cause of the brittleness phenotype in TallyHO mice, various matrix characteristics were assessed. As measured by Raman spectroscopy, all 3 sub-peak ratios of the Amide I band that reflects the secondary structure of collagen I – 1670/1640, 1670/1610, and 1670/1690 (cm^{-1}) – were higher for diabetic than for the non-diabetic mice (Table 3.5).

Table 3.3 Selected properties (mean ± SD) from micro-computed tomography evaluations and compression tests of the 6th lumbar vertebra.

		16 weeks			34 weeks			GLM p-values		
Property	Unit	SWR/J (n≥13)	TallyHO (n≥12)		SWR/J (n≥16)	TallyHO (n≥13)		Strain	Age	Interaction
BV/TV	%	27.0 ± 2.2	25.0 ± 4.1		28.0 ± 2.0	23.0 ± 3.0	#	0.101	0.330	**0.044**
Tb.TMD	$mgHA/cm^3$	919 ± 9	968 ± 20	#	951 ± 5 a	995 ± 19	#,b	**<0.0001**	**<0.0001**	0.380
ConnD	mm^{-3}	226 ± 30	182 ± 20	#	197 ± 19 a	186 ± 42		**<0.0001**	**0.001**	**0.040**
SMI		0.315 ± 0.276	0.742 ± 0.342	#	0.294 ± 0.211	1.003 ± 0.236	#	**0.001**	0.866	0.080
Tb.N	mm^{-1}	4.79 ± 0.24	4.66 ± 0.22		4.89 ± 0.29	4.77 ± 0.50		0.158	0.335	0.925
Tb.Th	mm	0.054 ± 0.002	0.058 ± 0.005	#	0.055 ± 0.001	0.057 ± 0.004		**0.008**	**0.048**	0.268
Tb.Sp	mm	0.212 ± 0.013	0.211 ± 0.011		0.201 ± 0.013	0.206 ± 0.024		0.806	**0.014**	0.447
Axial stress	MPa	37.6 ± 4.9	44.8 ± 5.3	#	38.5 ± 8.3	44.0 ± 3.3	#	**<0.0001**	0.194	0.245
Peak force	N	29.3 ± 3.6	30.3 ± 4.1		28.0 ± 6.4	26.0 ± 2.8		0.553	0.404	0.207
Work-to-peak force	N·mm	6.25 ± 1.58	5.97 ± 2.60		5.41 ± 2.30	4.56 ± 1.87		0.732	0.237	0.620

#: adjusted p-value less than 0.05 for strain comparison within age group. a & b: adjusted p-value less than 0.05 for age comparison within strain. Reprinted with permission of Elsevier [147].

Table 3.4 Selected properties (mean ± SD) from micro-computed tomography evaluations of the left femur including caliper measurements of femur length.

		16 weeks			34 weeks			GLM p-values		
Property	Unit	SWR/J (n≥13)	TallyHO (n≥12)		SWR/J (n≥16)	TallyHO (n≥13)		Strain	Age	Interaction
Diaphysis										
Tt.Ar	mm^2	1.49 ± 0.05	1.45 ± 0.09		1.66 ± 0.09 a	1.71 ± 0.06 b		0.114	**<0.0001**	**0.016**
Ct.Po.Dn	mm^{-3}	2.16 ± 0.22	1.51 ± 0.20	#	1.57 ± 0.15 a	1.14 ± 0.14	#,b	**<0.0001**	**<0.0001**	**0.038**
Length	mm	14.1 ± 0.2	14.8 ± 0.2	#	14.8 ± 0.7 a	15.3 ± 0.3	#,b	**<0.0001**	**<0.0001**	0.295
Ps.Pm	mm	4.65 ± 0.08	4.64 ± 0.14		4.93 ± 0.13 a	5.02 ± 0.10 b		0.812	**<0.0001**	0.100
Ec.Pm	mm	3.23 ± 0.06	2.93 ± 0.21	#	3.33 ± 0.19	3.32 ± 0.15 b		**<0.0001**	**0.047**	**0.001**
Distal Metaphysis										
BV/TV	%	20.3 ± 2.8	10.0 ± 2.5	#	10.3 ± 2.6 a	5.6 ± 1.6	#,b	**<0.0001**	**<0.0001**	**<0.0001**
Tb.TMD	$mgHA/cm^3$	969 ± 11	981 ± 18		1027 ± 16 a	1038 ± 23 b		0.104	**<0.0001**	0.531
ConnD	mm^{-3}	347 ± 55	170 ± 67	#	122 ± 51 a	63 ± 22	#,b	**<0.0001**	**<0.0001**	**<0.0001**
SMI		1.08 ± 0.28	2.39 ± 0.35	#	2.01 ± 0.22 a	2.94 ± 0.24	#,b	**<0.0001**	**<0.0001**	**0.012**
Tb.N	mm^{-1}	5.31 ± 0.31	3.87 ± 0.24	#	3.37 ± 0.55 a	3.08 ± 0.47 b		**<0.0001**	**<0.0001**	**<0.0001**
Tb.Th	mm	0.046 ± 0.002	0.048 ± 0.005		0.048 ± 0.002	0.049 ± 0.008		0.206	**0.019**	0.897
Tb.Sp	mm	0.186 ± 0.012	0.256 ± 0.016	#	0.305 ± 0.058 a	0.329 ± 0.060 b		**<0.0001**	**<0.0001**	**0.039**

#: adjusted p-value less than 0.05 for strain comparison within age group. a & b: adjusted p-value less than 0.05 for age comparison within strain. Reprinted with permission of Elsevier [147].

Table 3.5 Bone matrix composition (mean ± SD) from Raman Spectroscopy and HPLC analysis of the femur

		16 weeks			34 weeks			GLM p-values		
Property	Unit	SWR/J (n≥12)	TallyHO (n≥12)		SWR/J (n≥15)	TallyHO (n≥13)		Strain	Age	Interaction
Raman	-									
ν_1PO_4/Amide I	-	28.6 ± 2.5	31.6 ± 4.0	#	30.7 ± 4.1	38.3 ± 3.7	#,b	**0.023**	0.109	**0.024**
ν_1PO_4/Amide III	-	26.1 ± 2.6	21.9 ± 4.9		18.2 ± 3.8 a	14.6 ± 4.5	#,b	**0.007**	**<0.0001**	0.781
ν_1PO_4/Pro	-	16.1 ± 0.8	17.6 ± 2.4	#	18.3 ± 3.0	23.5 ± 4.4	#,b	**0.041**	**0.005**	**0.028**
CO_3/ν_1PO_4	-	0.160 ± 0.003	0.152 ± 0.007	#	0.156 ± 0.006	0.146 ± 0.010	#	**0.001**	0.077	0.412
Crystallinity	-	0.054 ± 0.0	0.054 ± 0.001		0.056 ± 0.003 a	0.056 ± 0.001	b	0.174	**0.014**	0.880
1670/1640	-	1.55 ± 0.05	1.76 ± 0.18	#	1.65 ± 0.18	2.01 ± 0.33	#	**<0.0001**	**0.040**	0.198
1670/1690	-	1.78 ± 0.07	1.89 ± 0.06	#	2.13 ± 0.14 a	2.29 ± 0.20	#,b	**<0.0001**	**<0.0001**	0.400
1670/1610	-	2.89 ± 0.20	4.25 ± 1.84	#	3.36 ± 1.13	5.87 ± 2.52	#	**0.016**	0.103	0.209
HPLC	-									
PYD	mol/mol	0.123 ± 0.059	0.138 ± 0.069		0.215 ± 0.053 a	0.226 ± 0.048	b	0.547	**<0.0001**	0.894
Pentosidine	mmol/mol	203 ± 120	141 ± 49		135 ± 66	151 ± 98		0.087	0.082	0.111
Fluorescence										
fAGEs	ng/mg	92 ± 31	118 ± 44		127 ± 34 a	129 ± 33		0.095	**0.004**	0.217

#: adjusted p-value less than 0.05 for strain comparison within age group. a & b: adjusted p-value less than 0.05 for age comparison within strain. Reprinted with permission of Elsevier [147].

There was no significant difference in PYD, a mature enzymatic crosslink, between strains. Additionally, matrix pentosidine concentration was not altered with either diabetes or age (Table 3.5). fAGEs were not significantly different between the strains, and significantly increased with age in only SWR/J mice (Table 3.5). Raman spectroscopy confirmed the higher mineralization in cortical bone of TallyHO mice (Figure 3.4D) with multiple measurements of the mineral-to-matrix ratio (ν_1PO_4/Proline and ν_1PO_4/Amide I) being higher for the diabetic bone than for the non-diabetic bone at both 16 weeks and 34 weeks of age. However, ν_1PO_4/Amide III was only higher for the TallyHO mice than for the SWR/J mice at 34 weeks (Table 3.5). As for characteristics of the mineral phase, crystallinity increased with age for both strains (Table 3.5), but did not change with diabetes with respect to controls. CO_3/ν_1PO_4 was lower for diabetic mice at both ages, but did not further progress with age (Table 3.5). Body weight significantly explained ν_1PO_4/Proline and crystallinity at 16 weeks, but not at 34 weeks, and strain was still a significant factor. Interestingly, the strain-related difference in the Amide I sub-band peak ratios at 34 weeks was no longer significant when body weight was included as a covariate (Table 3.10).

3.3.6 Body weight and several bone structural parameters of the TallyHO mice negatively correlated with averaged blood glucose levels

Given the high variability in blood glucose levels within the TallyHO group, we tested for significant relationships between hyperglycemia and bone properties. First, averaged blood glucose levels negatively correlated with body weight for the TallyHO mice at 34 weeks (Figure 3.6A) indicating that mice with severe hyperglycemia either failed to gain weight or lost weight. Over the long duration of T2D, P1NP, a marker of bone formation, also negatively correlated

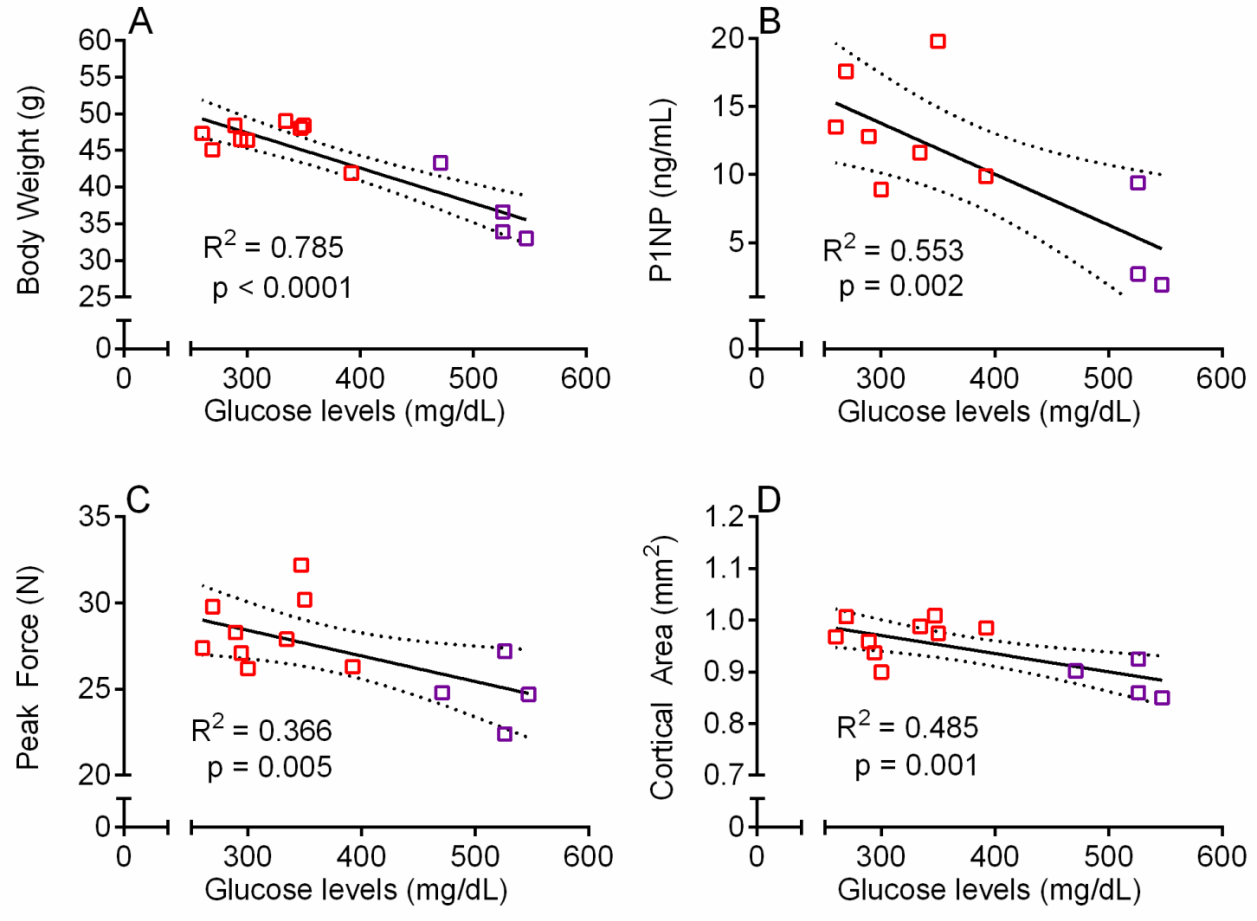

Figure 3.6 Linear regression of averaged blood glucose levels with body weight (A), P1NP (B), peak force (C) and cortical area (D) for TallyHO mice at 34 weeks of age. The data points from animals with blood glucose levels higher than 450 mg/dL are shown in purple. Reprinted with permission of Elsevier [147].

with blood glucose levels at 34 weeks (Figure 3.6B) suggesting that poorly controlled diabetes suppressed bone formation. P1NP was lower for TallyHO mice compared to SWR/J mice at both ages (Table 3.1). Although the TallyHO femur diaphysis was stronger, peak force (Figure 3.6C) and Ct.Ar (Figure 3.6D) decreased as hyperglycemia increased in these mice. At the material level, blood glucose levels correlated with toughness at 16 weeks in TallyHO mice such that those with high blood glucose levels unexpectedly had higher toughness (Table 3.12). On the other hand, glucose levels negatively correlated with cracking toughness at 16 weeks of age for TallyHO mice (Table 3.12). No such correlations were found among 34-week-old TallyHO mice. For the bone matrix properties, glucose negatively correlated with 1670/1640 ($r = -0.597$, $p = 0.009$) and 1670/1610 ($r = -0.555$, $p = 0.022$) ratios in TallyHO mice at 34 weeks, albeit the correlations were weak. Furthermore, when looking at the mineral phase, glucose levels correlated with crystallinity in TallyHO animals at 34 weeks. Surprisingly, pentosidine levels in the bone matrix did not correlate with blood glucose levels (Table3.15) nor did fAGEs levels at 34 weeks (Table 3.15).

3.4 Discussion:

There is a need for rodent models that mimic diabetic bone disease in humans because such animal models can be used in pre-clinical studies to prevent the diabetes-related decrease in fracture resistance. Moreover, by having an animal model in which BMD is not lower in the T2D rodents compared to non-diabetic rodents but instead the fracture resistance is progressively worse with diabetes duration, new pathogenic mechanisms leading to increased fracture risk could be identified as potential therapeutic targets as well as new matrix-sensitive tools for diagnosing high fracture risk could be assessed. While overall volumetric BMD was not lower in the diabetic TallyHO mice compared to their recommended non-diabetic strain, none of the

mechanical properties, whether determined at the whole-bone level or the material level, decreased as the duration of T2D progressed. Thus, this model of juvenile-onset T2D does not mimic the likely increase in fracture risk that occurs as the duration in type 2 diabetes increases among humans. Nonetheless, a subset of TallyHO who experience severe hyperglycemia may experience dysfunction in other organs (e.g., kidney) that contribute to a loss of fracture resistance.

The TallyHO mouse strain was developed from selectively breeding male mice that presented with hyperglycemia within a colony of Theiler Original mice. In the initial study describing the development of this mouse model of T2D [182], male mice at 26 weeks were overweight with an average body mass of 45 ± 2 g (mean ± SEM) and hyperglycemic with a non-fasting, plasma glucose levels of 544 ± 24 mg/dL (mean ± SEM). Compared to C57BL/6J mice (arbitrarily chosen), female TallyHO mice were also obese but were not hyperglycemic [182]. In a follow-up study by the Jackson Laboratory, the male TallyHO mice had significantly higher body weight by 4 weeks and were diabetic (plasma glucose levels above 250 mg/dL) by 10 weeks of age compared to male C57BL/6J mice [174]. These differences were similar to the present study comparing the body mass and glucose levels of the TallyHO mice to non-diabetic, male SWR/J mice. Because the SWR/J strain has greater genetic similarity to the TallyHO strain (86.8% homology), SWR/J mice are now recommended for use as the non-diabetic control by the Jackson Laboratory [183]. Nonetheless, the lack of a littermate control makes strain a possible contributor to the observed differences in bone between the non-diabetic and diabetic mice.

In this study, the phenotype of the diabetic TallyHO mice, when compared to the non-diabetic SWR/J mice at 16 weeks of age, was similar to the one previously described by Devlin

et al. at 17 weeks of age [136]. Specifically, in both studies, there was high variability in glucose levels among the TallyHO mice, and the onset of persistent hyperglycemia occurred by 10 weeks of age. With respect to the skeletal phenotype, cortical TMD and cortical thickness were higher in the TallyHO mice compared to the SWR/J mice in both studies. Devlin et al. also observed that the structural strength of femur diaphysis was higher for the diabetic mice, while post-yield displacement was lower. We additionally found that toughness (i.e., the ability of cortical bone to dissipate energy during fracture) did not change between 16 weeks and 34 weeks of age in both diabetic and non-diabetic mice. Furthermore, as with the Devlin study, we did not observe differences in fAGEs within bone between diabetic and non-diabetic mice. Notably, in a recent study analyzing hydrolysates from proximal femora of diabetic KK-A^y/a mice and non-diabetic a/a littermates at 20 weeks of age (12 weeks of hyperglycemia) [184], there were no significant difference in pentosidine concentration similar to our findings with the TallyHO mice.

The early onset of obesity and diabetes makes it difficult to determine whether or not there are differences in fracture resistance between the strains prior to hyperglycemia. Furthermore, as the SWR/J strain is not obese, certain differences between the strains may be due to obesity as suggested by the covariate analysis of bone structural properties (Tables 3.6-15). Notably, other T2D rodent models such as the ZDSD rat have strain-related differences in bone structure and strength before the onset of T2D [178]. Moreover, while the cortical bone of the femur from Zucker Diabetic Fatty rats ($ZDF^{fa/fa}$) was structurally weaker with lower areal BMD than those from the lean ZDF non-diabetic controls ($ZDF^{fa/+}$) at 33 weeks of age, no significant differences in material estimates of strength and toughness between the two groups were reported [130]. Effects of T2D on the fracture resistance of long bones at the material-level

in rodent models tends depend on the duration of hyperglycemia, though few studies investigated multiple time points during the progression of the disease [185].

With regards to the vertebrae, the peak force did not decrease with diabetes despite a lower trabecular bone volume at 34 weeks compared to age-matched non-diabetic mice. Unlike with Devlin et al. study [136], which reported differences in trabecular architecture within the lumbar vertebra, not VB strength, at 17 weeks of age between SWR/J and TallyHO mice, we did not find a difference in trabecular bone volume in the L6 VB at 16 weeks between these 2 strains of mice. At 34 weeks of age, the higher Tb.TMD (Table 3.3) could have compensated for the lower BV/TV and give added strength to the L6 VB of the TallyHO mice. However, while Tb.TMD increased with age for both mouse strains, peak force was not different between 16-week and 34-week old mice suggesting other factors within the lumbar vertebra (e.g., related to the matrix or the structure of the cortical shell) existed between the diabetic and non-diabetic mice. In the distal femur metaphysis, there was significantly lower BV/TV for the TallyHO mice at both ages (Table 3.4), and this is consistent with the previous study [136] and another study comparing male TallyHO to male C57BL/6J mice at 8 weeks of age [186]. T2D in humans does not appear to be a problem of poor trabecular architecture, at least not when assessed by HR-pQCT of peripheral sites [49, 163]. With regards to cortical micro-structure, porosity or pore number did not increase with duration of hyperglycemia as observed in ZDSD diabetic male rats [178] . There is however a limit to the size of pores that μCT analysis of mouse bones can resolve. Furthermore, unlike with human cortical bone, extensive remodeling of the cortex does not occur in mice, and so higher porosity in the diaphysis of mouse long bone is typically a reflection of elevated resorption near the endosteum (Figure 3.5). Possibly, with higher body weight, this resorption during diaphyseal expansion was lower for TallyHO mice.

Regardless of the cause (either strain-related or T2D-related), there are several possible explanations for the brittle bone phenotype of the TallyHO diabetic mice. The tissue mineral density (μCT) and the mineral-to-matrix ratio (Raman spectroscopy) were higher for TallyHO cortical bone than for SWR/J cortical bone. It has been suggested that there is a non-linear relationship between degree of mineralization and toughness such that hyper-mineralization is thought to confer low bone toughness [187-189]. In the present study though, as mineralization increased with age for both mouse strains, toughness did not significantly differ between the age groups. Cracking toughness (Figure 3.3D) and post-yield displacement (Table 3.2), other indicators of brittleness, did decrease with age, namely for the non-diabetic mice. Also, the age-related increase in Ct.TMD only resulted in a higher bending strength at 34 weeks compared to 16 weeks of age for the SWR/J mice.

An alternative explanation relates to the organic matrix. The Amide I sub-peak ratio 1670/1640 (intensity ratio at these wavenumbers) was higher in diabetic mice. Unal et al. previously showed that the Amide I sub-peak ratio 1670/1640 (cm^{-1}) was negatively correlated with toughness and post-yield toughness of bovine cortical bone and was sensitive to thermally induced denaturation and mechanical denaturation in bovine cortical bone (i.e., a marker of helical structure of collagen I) [179]. For the WBN/Kob rat model of T2D, Saito et al. [190] observed a decrease in immature enzymatic collagen crosslink concentration (before the onset of hyperglycemia) with the progression of diabetes, but no T2D-related changes in mature enzymatic pyridinoline (as observed in the present study). While we did not measure immature crosslinks, our Raman analysis also found that the Amide I sub-peak ratio 1670/1690 (cm^{-1}), known as the matrix maturity ratio, was also higher in bones of TallyHO mice. This change could reflect a difference in the enzymatic crosslinking profile. Thus, it is possible that the

increased brittleness of bone in TallyHO mice is due to an altered collagen structure in the bone matrix.

Finally, multiple mice experienced a loss in body weight as the duration of T2D increased. One TallyHO mouse in the 16-week group and three TallyHO mice in the 34-week group lost more than 10% of their peak body mass (other mice lost more than 20% of body mass and were euthanized before completion of the study), even though mice were fed a purified diet with a relatively low-fat content. The negative correlation between body weight and glucose levels (Figure 3.6A) suggests that this loss was related to uncontrolled hyperglycemia. Diabetic mice with the high glucose levels at 34 weeks of age also had reduced structural strength in bending (Figure 3.6C), reduced cortical area (Figure 3.6D), and reduced serum marker of bone formation (Table 3.1) suggesting additional complications potentially affecting the bone. Another limitation of the study is the lack of bone histomorphometry to confirm an inverse association between hyperglycemia and bone formation. Nonetheless, poor kidney function, a known complication of T2D, could alter bone turnover leading to structural deficits. Potentially, by counting on high variability in hyperglycemia from moderate to severe, the TallyHO model of T2D could be used to investigate the effect of glycemic control by standard (e.g., metformin) therapies and newer therapies (e.g., glifozins) on bone strength.

3.5 Conclusions

Overall, the fracture resistance of bone from TallyHO mice did not progressively worsen with the duration of T2D, and the low toughness of cortical bone for these diabetic mice compared to the non-diabetic SWR/J mice existed at skeletal maturity (16 weeks of age) and in adulthood (34 weeks of age). It is unclear whether strain or early-onset of elevated glucose levels or both contribute to the differences in toughness and organic matrix seen between the two

groups. While the TallyHO model mimics several features of type 2 diabetes in humans (glucose levels were variable and bone mass was not lower than normal), cortical porosity and trabecular number and thickness in long bones was lower compared to the non-diabetic mice when diabetic humans can have elevated cortical porosity with otherwise normal trabecular architecture. Moreover, AGEs did not accumulate in bone with diabetic progression as occurs in other tissues of diabetic humans. The lower trabecular bone volume fraction existing in this model juvenile-onset of T2D also did not confer lower lumbar vertebral body strength when comparing TallyHO to SWR/J mice at 34 weeks of age. The higher structural strength of femur mid-shaft for the diabetic mice was not independent of the difference in body weight between TallyHO and SWR/J mice. There is variability in individual blood glucose levels within the TallyHO group, and such levels negatively correlate with certain structural properties of the femur mid-shaft.

3.6 Acknowledgements

This work was funded in part by a training grant from NIDDK (DK101003) and by a grant from the National Institute of Arthritis and Musculoskeletal and Skin Diseases (AR067871). The VUMC Hormone and Analytical Core is supported by NIH grants DK059637 and DK020593. The content is solely the responsibility of the authors and does not necessarily represent the official views of the National Institutes of Health or other funding agencies.

Table 3.6 Selected global properties of mice with body weight as a covariate.

		16 weeks			34 weeks		
Property		Strain	BW	Interaction	Strain	BW	Interaction
HbA1c	p				**<0.0001**	0.465	**0.002**
	β				4.15	-0.23	-3.43
Insulin	p	0.965	0.518	NS	0.201	0.187	NS
	β	-0.05	0.65		0.35	0.43	
P1NP	p	**0.041**	0.520	NS	**<0.0001**	**0.004**	NS
	β	-1.09	0.33		-1.36	0.74	
TRACP-5b	p	0.805	0.863	NS	**0.031**	0.051	**0.039**
	β	-0.25	-0.16		9.03	3.98	-12.38

Table 3.7 Selected mechanical properties of the femur mid-shaft with body weight as a covariate.

		16 weeks			34 weeks		
Property		Strain	BW	Interaction	Strain	BW	Interaction
Bending Strength	p	0.093	0.572	NS	0.139	**0.047**	NS
	β	0.63	0.21		-0.55	0.78	
Toughness	p	0.846	0.389	NS	**0.003**	0.305	NS
	β	-0.10	-0.48		-0.95	0.34	
Cracking Toughness	p	0.480	0.623	NS	**0.038**	0.178	NS
	β	-0.48	0.35		-0.78	0.52	
$K_{c,initial}$	p	0.814	0.936	NS	0.760	0.862	NS
	β	-0.17	-0.06		-0.29	-0.16	
Modulus	p	0.360	0.418	NS	**0.013**	**0.023**	**0.010**
	β	0.76	-0.61		-7.32	-2.78	9.86
Rigidity	p	**0.017**	**<0.0001**	**0.003**	0.457	**0.012**	NS
	β	9.01	4.48	-13.17	-0.31	0.96	
PYD	p	0.670	0.175	NS	**0.019**	0.512	NS
	β	0.25	-0.80		-0.81	0.23	
Stiffness	p	**0.005**	**<0.0001**	**0.001**	0.485	**0.016**	NS
	β	9.28	4.58	-13.52	-0.31	0.95	
Yield Force	p	0.418	**0.025**	NS	0.248	**0.001**	NS
	β	-0.40	1.11		-0.29	0.82	
Peak Force	p	0.361	**0.023**	NS	0.229	**<0.0001**	NS
	β	-0.38	1.10		-0.35	1.05	
Work-to-failure	p	0.705	0.988	NS	**0.007**	0.118	NS
	β	-0.25	0.01		-0.99	0.60	

Table 3.8 Selected properties from micro-computed tomography (μCT) evaluations and compression tests of L6 vertebrae with body weight included as a covariate.

		16 weeks			34 weeks		
Property		Strain	BW	Interaction	Strain	BW	Interaction
BV/TV	p	**0.020**	**0.023**	NS	**0.026**	0.502	NS
	β	-1.77	1.55		-0.98	0.30	
Tb.TMD	p	0.655	**0.021**	NS	0.098	0.356	NS
	β	0.15	0.75		0.59	0.31	
ConnD	p	0.140	0.881	NS	0.373	0.457	NS
	β	-0.74	0.07		-0.60	0.48	
Tb.SMI	p	**0.001**	**0.012**	NS	**0.002**	0.755	NS
	β	1.77	-1.25		0.92	-0.09	
Tb.N	p	0.135	0.238	NS	0.272	0.394	NS
	β	-1.00	0.75		-0.55	0.46	
Tb.Th	p	0.267	**0.042**	NS	0.907	0.624	NS
	β	-0.79	1.33		0.07	0.29	
Tb.Sp	p	0.296	0.237	NS	0.293	0.398	NS
	β	0.69	-0.78		0.59	-0.50	
Axial stress	p	0.064	0.387	NS	0.072	0.483	NS
	β	1.13	-0.52		0.59	-0.21	
Peak Force	p	0.566	0.440	NS	0.628	0.952	NS
	β	-0.37	0.52		-0.18	-0.02	
Work-to-Peak Force	p	0.702	0.748	NS	0.983	0.645	NS
	β	-0.32	0.27		0.01	-0.24	

Table 3.9 Selected structural properties of femur mid-shaft and distal femur metaphysis with body weight included as a covariate

		16 weeks			34 weeks		
Property		Strain	BW	Interaction	Strain	BW	Interaction
Ct.Ar	p	**0.019**	**<0.0001**	**0.010**	0.290	**<0.0001**	NS
	β	4.79	2.98	-6.83	-0.26	1.05	
Ct.Th	p	0.759	**0.039**	NS	**0.006**	0.326	**0.010**
	β	0.10	0.78		-4.13	-0.71	5.50
I_{min}	p	0.141	**<0.0001**	**0.036**	**0.005**	**<0.0001**	**0.002**
	β	5.28	3.63	-8.77	5.15	2.93	-7.23
Ct.TMD	p	**<0.0001**	0.146	NS	**0.021**	0.122	NS
	β	1.26	-0.50		0.49	0.37	
Ct.Po	p	**<0.0001**	0.107	NS	**0.019**	0.376	NS
	β	-1.32	0.60		-0.83	0.25	
Ct.Po.N	p	0.110	0.540	NS	**0.010**	**<0.0001**	**0.001**
	β	-0.98	0.35		4.24	2.36	-7.14
Tt.Ar	p	0.093	**<0.0001**	**0.012**	**0.001**	**0.001**	**0.001**
	β	6.31	3.44	-9.92	7.90	3.67	-10.90
Ct.Po.Dn	p	0.086	0.629	NS	**0.046**	**0.029**	**0.010**
	β	-0.67	-0.18		2.75	1.33	-4.82
Length	p	**<0.0001**	**<0.0001**	**<0.0001**	0.221	0.889	NS
	β	7.41	2.45	-8.87	-0.65	-0.21	
Ps.Pm	p	**0.018**	**<0.0001**	**0.002**	**0.003**	**0.002**	**0.003**
	β	8.85	4.04	-12.8	7.83	3.78	-10.9
Ec.Pm	p	0.550	0.577	NS	**0.004**	**0.017**	**0.005**
	β	-0.38	-0.35		8.57	3.30	-11.6
BV/TV	p	**<0.0001**	**<0.0001**	NS	**<0.0001**	0.101	NS
	β	-1.56	0.70		-1.08	0.40	
Tb.TMD	p	0.725	0.388	NS	0.520	0.839	NS
	β	-0.30	0.73		0.21	0.08	
Conn.Dens	p	**<0.0001**	0.139	NS	**0.028**	0.951	NS
	β	-1.24	0.43		-0.61	0.01	
SMI	p	**<0.0001**	0.066	NS	**<0.0001**	0.614	NS
	β	1.44	-0.56		0.99	-0.10	
Tb.N	p	**<0.0001**	**0.005**	NS	0.096	0.194	NS
	β	-1.40	0.49		-0.76	0.55	
Tb.Th	p	0.104	**0.034**	NS	0.631	0.800	NS
	β	-1.34	1.68		0.26	-0.14	
Tb.Sp	p	**<0.0001**	**0.007**	NS	0.107	0.150	NS
	β	1.53	-0.64		0.79	-0.68	

Table 3.10 Selected compositional properties of the bone matrix from Raman spectroscopy and high performance liquid chromatography with body weight included as a covariate

		16 weeks			34 weeks		
Property		Strain	BW	Interaction	Strain	BW	Interaction
ν_1PO_4/Amide I	p	0.070	0.137	NS	0.386	0.052	NS
	β	1.51	-1.15		0.26	0.51	
ν_1PO_4/Amide III	p	0.926	0.405	NS	0.819	0.211	NS
	β	0.07	-0.60		0.11	-0.61	
ν_1PO_4/Pro	p	**0.014**	**0.026**	NS	0.643	0.298	NS
	β	1.98	-1.66		0.20	0.45	
CO_3/ν_1PO_4	p	0.177	0.669	NS	0.983	0.071	NS
	β	-0.88	0.31		0.01	-0.65	
Crystallinity	p	**0.001**	**0.008**	NS	0.779	0.638	NS
	β	1.63	-1.42		-0.12	0.21	
1670/1640	p	0.341	0.901	NS	0.811	**0.026**	NS
	β	0.74	-0.10		-0.08	0.76	
1670/1690	p	0.251	0.993	NS	0.395	**0.009**	NS
	β	0.66	-0.01		-0.32	0.88	
1670/1610	p	0.347	0.640	NS	0.621	**0.022**	NS
	β	0.92	-0.46		-0.17	0.84	
PYD per col	p	0.190	0.118	NS	0.493	0.198	NS
	β	-0.90	1.08		-0.30	0.48	
PE per col	p	0.015	0.018	0.014	0.476	0.669	NS
	β	14.71	6.15	-20.95	0.22	-0.14	
fAGEs per col	p	**0.034**	0.084	**0.027**	0.068	**0.027**	NS
	β	-9.09	-2.41	11.76	-0.65	0.78	

Table 3.11 Linear regressions of selected global properties of mice with averaged glucose levels

		16 weeks		34 weeks	
Property		SWR	TallyHO	SWR	TallyHO
Averaged body weight	p	0.252	**0.006**	0.158	**<0.0001**
	r	0.398	**-0.679**	0.388	**-0.886**
HbA1c	p			0.928	**<0.0001**
	r			0.047	**0.950**
Insulin	p	0.977	0.870	0.235	**0.030**
	r	0.079	-0.115	-0.395	**-0.615**
TRACP	p	0.869	**<0.0001**	0.623	0.130
	r	0.450	**0.934**	-0.211	0.447
P1NP	p	0.701	0.590	0.610	**0.002**
	r	-0.741	-0.445	-0.161	**-0.744**

Table 3.12 Linear regressions of selected mechanical properties of cortical bone with averaged glucose levels

		16 weeks		34 weeks	
Property		SWR	TallyHO	SWR	TallyHO
Bending Strength	p	0.639	0.333	0.388	0.076
	r	-0.120	-0.292	-0.270	-0.426
Toughness	p	0.054	**<0.0001**	0.874	0.339
	r	-0.490	**0.880**	0.042	-0.293
Cracking Toughness	p	0.721	**0.014**	0.418	0.085
	r	0.109	**-0.607**	0.294	-0.452
$K_{c,initial}$	p	0.983	0.966	0.919	0.966
	r	0.006	0.035	0.034	0.028
Modulus	p	0.063	0.706	0.937	0.369
	r	0.398	-0.120	-0.027	-0.255
PYD	p	0.275	**<0.0001**	0.794	0.424
	r	-0.327	**0.873**	0.068	-0.271
Stiffness	p	0.200	0.374	0.399	0.069
	r	0.384	0.292	0.250	-0.535
Yield Force	p	0.779	**0.047**	0.458	0.234
	r	-0.093	**-0.561**	0.275	-0.410
Peak Force	p	0.974	0.532	0.847	**0.005**
	r	-0.010	0.204	0.076	**-0.605**
Work to failure	p	0.127	**<0.0001**	0.689	0.128
	r	-0.454	**0.808**	0.114	-0.415

Table 3.13 Linear regressions of selected properties from the L6 vertebrae with averaged glucose levels

		16 weeks		34 weeks	
Property		SWR	TallyHO	SWR	TallyHO
BV/TV	p	0.567	**<0.0001**	0.232	0.355
	r	0.150	**-0.832**	0.281	-0.330
Tb.TMD	p	**0.005**	0.292	0.446	0.431
	r	**0.693**	-0.375	-0.201	-0.256
ConnDens	p	**<0.0001**	0.869	0.061	0.291
	r	**-0.640**	-0.056	0.349	-0.368
Tb.SMI	p	0.735	**<0.0001**	0.251	0.857
	r	-0.091	**0.888**	-0.222	0.068
Tb.N	p	0.543	**0.003**	**0.002**	0.124
	r	-0.199	**-0.634**	**0.609**	-0.407
Tb.Th	p	**<0.0001**	0.059	0.260	0.653
	r	**0.838**	-0.601	-0.312	-0.126
Tb.Sp	p	0.617	0.105	**0.001**	0.080
	r	0.175	0.469	**-0.666**	0.453
Axial stress	p	0.148	0.988	0.848	0.622
	r	0.392	-0.005	-0.054	0.140
Peak Force	p	0.087	0.114	0.932	0.678
	r	0.466	-0.454	-0.027	-0.123
Work-to-Peak Force	p	0.553	0.609	0.055	0.865
	r	0.157	0.170	-0.436	-0.071

Table 3.14 Linear regressions of selected structural properties of the femur mid-shaft with averaged glucose levels

		16 weeks		34 weeks	
Property		SWR	TallyHO	SWR	TallyHO
Ct.Ar	p	0.553	0.700	0.229	**0.001**
	r	0.193	-0.125	0.417	**-0.696**
Ct.Th	p	0.822	**<0.0001**	0.640	**0.002**
	r	0.073	**-0.781**	0.121	**-0.691**
I_{min}	p	0.915	0.317	0.530	0.116
	r	0.034	0.324	0.242	-0.391
Ct.TMD	p	0.890	0.618	0.725	0.706
	r	0.042	-0.190	-0.115	-0.115
Ct.Po	p	0.836	0.258	0.794	0.628
	r	0.062	-0.291	0.092	0.169
Ct.Po.N	p	0.942	0.171	0.577	0.235
	r	0.024	-0.425	-0.201	0.382
Tt.Ar	p	0.600	**0.011**	0.781	0.667
	r	0.181	**0.630**	0.115	-0.131
Ct.Po.Dn	p	0.757	0.218	0.236	**0.013**
	r	-0.109	-0.371	-0.399	**0.613**
Length	p	0.152	**0.013**	0.642	0.155
	r	0.433	**0.559**	0.073	0.410
Ps.Pm	p	0.442	**0.005**	0.657	0.487
	r	0.265	0.694	0.177	-0.227
Ec.Pm	p	0.910	**<0.0001**	0.974	0.420
	r	0.033	0.831	-0.014	0.328
Tb.BV/TV	p	0.595	**0.002**	0.052	**0.046**
	r	-0.193	**-0.698**	0.519	**-0.546**
Tb.TMD	p	0.055	0.208	0.538	0.779
	r	0.523	-0.371	0.185	0.070
Conn.Dens	p	0.392	**0.014**	0.075	0.684
	r	-0.302	**-0.557**	0.468	0.127
SMI	p	0.444	**0.002**	0.469	0.497
	r	0.263	**0.727**	-0.197	0.210
Tb.N	p	0.704	0.074	**0.012**	0.292
	r	-0.130	-0.492	**0.604**	-0.374
Tb.Th	p	0.970	0.160	0.066	0.702
	r	0.015	-0.453	0.451	0.116
Tb.Sp	p	0.642	0.094	**0.032**	0.206
	r	0.155	0.497	**-0.583**	0.438

Table 3.15 Linear regressions of compositional properties of femur mid-shaft with averaged glucose levels

		16 weeks		34 weeks	
Property		SWR	TallyHO	SWR	TallyHO
ν_1PO_4/Amide I	p	0.183	0.081	0.145	0.148
	r	0.359	0.588	0.339	-0.461
ν_1PO_4/Amide III	p	**0.016**	0.432	**0.011**	**0.035**
	r	**0.591**	0.238	**-0.676**	**0.535**
ν_1PO_4/Pro	p	0.849	0.133	**0.012**	0.280
	r	-0.056	0.477	**0.490**	-0.352
CO_3/ ν_1PO_4	p	0.592	0.745	**0.003**	**0.002**
	r	-0.181	-0.098	**-0.647**	**0.577**
Crystallinity	p	0.550	0.239	0.269	**0.044**
	r	-0.233	0.337	0.360	**-0.527**
1670/1640	p	0.540	0.712	0.058	**0.009**
	r	-0.178	0.111	0.444	**-0.597**
1670/1690	p	0.532	0.197	0.346	0.090
	r	-0.225	0.365	0.274	-0.511
1670/1610	p	0.221	0.727	0.057	**0.022**
	r	-0.343	0.110	0.352	**-0.555**
PYD per col	p	0.572	**0.012**	**0.002**	0.188
	r	-0.217	**-0.825**	**0.549**	-0.390
PE per col	p	0.080	0.373	0.368	0.829
	r	0.460	-0.283	-0.279	0.051
fAGEs per col	p	**0.007**	**<0.0001**	0.574	0.189
	r	-0.686	-0.843	0.192	0.371

CHAPTER 4 THE AGE-RELATED DECREASE IN THE MATERIAL PROPERTIES OF BALB/C MOUSE LONG BONES INVOLVES ALTERATIONS TO THE MATRIX

4.1 Introduction

With aging, there are deleterious changes to bone at multiple hierarchical levels of organization that lower the overall fracture resistance and hence elevate fracture risk. As examples, the cortices become thinner (macrostructure) reducing structural resistance to bending [39, 191, 192]; intracortical porosity [38, 193, 194] and fenestrations in trabeculae increase (microstructure) [195] such that the remaining tissue is subjected to higher-than-normal strain [40]; and advanced glycation end-products (AGEs) accumulate [196-198] within the organic matrix (ultrastructure) of cortical bone impeding the deformation of collagen fibrils [199]. Traditionally, osteoporosis is viewed as a problem of low bone mass causing reduced bone strength, but during aging, there is a well-known disproportionate increase in fracture risk relative to the decrease in areal bone mineral density (aBMD) that occurs after 50 years of age [7, 8]. As such, effective therapies that reduce the risk of a fragility fracture likely do more than prevent the loss aBMD, and to some extent, current anti-resorptive and anabolic therapies prevent or partially rescue deterioration in the macro and microstructure of bone [200-203]. None though were specifically developed to target age-related deficits in the bone matrix and to promote the material properties of bone. This is perhaps due to a lack of a well-validated preclinical model in which age-related changes in the matrix accompany a loss in fracture resistance.

All fractures do not occur through one single mechanism (e.g., a single overloading event) but rather fractures can arise through different biomechanical pathways [31]. For example, healthy bone can experience loads that exceed the yield limit of the tissue (i.e., the onset of

microdamage) but does not break. Remodeling removes the microdamage and replaces it with new tissue [204], thereby returning the bone tissue to its normal mechanical behavior. However, in the case of compromised bone, there can be a *brittle fracture*, a failure with little or no post-yield deformation (i.e., matrix has inadequate capacity for microdamage accumulation). An atypical fracture is perhaps the most striking example of a fracture that does not involve an overloading event but rather a loss in toughening mechanisms. To account for the variety of failure mechanisms across all types of materials, there are multiple material properties that characterize different attributes of fracture resistance. To date, the primary concern in pre-clinical studies has been whether a therapy increases bone strength, typically structural-dependent strength, even though numerous mechanical testing studies of cadaveric tissue have reported that in addition to material strength, impact energy, post-yield toughness, fatigue resistance, and fracture toughness at the apparent level (i.e., independent of macrostructure but not microstructure) decrease with age [119, 205-208].

Accompanying these age-related decrease in material properties are a number of changes to the microstructural and ultrastructural organization of bone [10]. With respect to the latter hierarchy, the organic matrix perhaps holds potential for new therapeutic targets to reduce the age-related increase in fracture risk. Hydrated type 1 collagen of course primarily contributes the toughness to bone (i.e., the mineral component of bone is brittle without collagen or water) [21], and numerous genes regulate the assembly of tropocollagen into highly organized, collagen fibrils embedded with mineral and non-collagenous proteins [13]. Moreover, collagen I undergoes multiple post-translations modifications (PTMs), some of which occur over the short-term as tropocollagen undergoes hydroxylation and glycosylation prior to maturing of the matrix via enzymatic crosslinking or over the long-term as chemical reactions between protein residues

(e.g., arginine) and glucose form AGEs. While enzymatic PTMs and crosslinks give stability to the matrix [68], AGEs, whether as crosslink and/or as an adduct, can have an embrittling effect on the matrix [73, 74].

Some of the age-related changes to human bone also happen to the bones of mice as they age. Namely, decreases in trabecular BV/TV occur at metaphyseal sites of the femur and tibia [138, 140-142] as well as within the lumbar vertebral body [141] with advanced aging (>20-mo. vs. 6-mo. or 12-mo.). Similar to humans [192, 209, 210], cortical thickness in long bones of C567BL/6J mice is known to decrease without an accompanying loss in cortical area or moment of inertia of the mid-shaft [138, 211]. Structural-dependent mechanical properties of the femur diaphysis actually increase with maturation, but then stay relatively stable with aging, with a few studies reporting lower stiffness and lower energy-to-fracture for old than for young adult mice, but no difference in ultimate force [142, 211]. For C57BL/6 mice, the estimated ultimate material strength of cortical bone (three-point bending tests of femur mid-shafts) was reported to peak between 34-wks and 52-weeks (male) and decline from the peak strength by 10-12% at 104-wks [211] or to decrease after 8-mo. (both male and female) [146]. For BALB/c mice, the age-related changes in material strength is less clear with yield and ultimate strength reported to not significantly change with aging after skeletal maturity when the radius was tested in three-point bending [142]. These mouse studies did not determine whether other material properties declined with advanced aging. Moreover, there is little information about how post-yield behavior and matrix-related characteristics of mouse bone change with aging.

While the quality of the bone matrix is generally believed to decline with aging, therapeutics for reducing fracture risk are primarily assessed for their ability to prevent or rescue bone loss in rodent models of sex hormone deficiency [212]. The objective of this study then was

to determine whether a mouse model of aging involves a loss in multiple material properties (strength, toughness, and fracture toughness) of cortical bone and ascertain whether there are age-related changes in the matrix of mouse cortical bone. We hypothesized that the ability of bone to dissipate energy and resist crack growth is lower for both male and female, 20-month-old BALB/c mice compared to young-adult (6-month-old), sex-matched BALB/c mice and that such changes coincide with age-related changes within the bone matrix (e.g., higher AGEs, higher type B carbonate substitutions, lower bound water, and lower resistance to cyclic reference point indentation).

4.2 Materials and Methods:

4.2.1 Study design and tissue collection

Male BALB/c mice at 19 months and 2 months of age were first acquired from the colony maintained by National Institute on Aging (NIA), and then later female BALB/c mice at 19 months and 5 months of age were acquired from the same colony. Mice were housed with no more than 5 mice per cage on a 12 hour light/dark cycle. Mice were fed a standard chow diet of 5L0D (LabDiet, St Louis, MO) ad libitum and were euthanized by cervical dislocation after cardiac exsanguination to collect blood serum while under deep anesthesia at 6 months (6-mo.) and 20 months (20-mo.). All procedures were approved by the Vanderbilt University IACUC. Femurs were immersed in phosphate buffered saline (PBS) and stored at -20 °C. Right femurs were subsequently notched at the mid-point of the diaphysis for later use in fracture toughness testing using a low speed diamond embedded saw and then the notch was sharpened using a razorblade coated in diamond solution. Tibiae, humeri, and radii were flash frozen in liquid nitrogen and stored at -80 °C.

4.2.2 Micro-computed tomography analysis

The notched region of each right femur (1.86 mm in length) was imaged using a µCT50 scanner (Scanco Medical AG, Brüttisellen, Switzerland) and the following scan parameters: X-ray tube voltage of 70 kVp drawing 114 µA, an isotropic voxel size of 6 µm, and an acquisition of 1000 projections per 360° rotation with an integration time of 600 ms. The mid-point (1.26 mm in length) of the left femur diaphysis was imaged using a µCT40 scanner (Scanco Medical AG, Brüttisellen, Switzerland): X-ray tube voltage of 70 kVp drawing 114 µA, an isotropic voxel size of 12 µm, and an acquisition of 1000 projections per 360° rotation with an integration time of 300 ms. The central point of curvature (1.09 mm in length) of each radius was imaged using a µCT50: X-ray tube voltage of 55 kVp drawing 200 µA, an isotropic voxel size of 4 µm, and an acquisition of 1000 projections per 360° rotation with an integration time of 1500 ms. For each scan, a 0.5 mm Al filter was used along with the manufacturer's specified beam hardening correction for the corresponding hydroxyapatite (HA) phantom calibration.

Following reconstruction, the notch angle was manually determined as previously described [66]. Upon fitting tight contours to the periosteal surface for slices above and below the notch, we used standard Scanco evaluation scripts to determine tissue mineral density of the cortex (Ct.TMD) and cortical porosity (Ct.Po) for a global threshold of 960.9 mgHA/cm^3 (image noise filter: sigma = 0.2 and support = 2) and a global, inverse threshold between -500 and 1298.5 mgHA/cm^3 (image noise filter: sigma = 0.3 and support = 1), respectively. To determine the structural properties and Ct.TMD of the mid-shafts, we also used standard Scanco evaluation scripts with the following segmentation parameters: i) a sigma=0.2, support=1, and global threshold of 666.8 mgHA/cm^3 (femur) and ii) sigma=0.2, support=1 and global threshold of 751.4 mgHA/cm^3 (femur). The Ct.Po of the intact left femur was also determined for a global

inverse threshold between -500 and 900.4 mgHA/cm^3 (image noise filter: sigma = 0.2 and support = 1).

4.2.3 Assessing material properties of cortical bone

Hydrated left femurs and right radii were loaded-to-failure at 3 mm/min in three-point (3pt) bending using a servo-hydraulic material testing system (Instron DynaMight 8841, Norwood, MA) with a 100 N load cell (Honeywell, OH, Model no. 060-C863-02). For each bone, the anterior side faced down (tension) while the medial side faced forward. The lower span for the bending tests of the femurs was adjusted to approximately maintain a span-to-anterior-posterior width ratio of 6.0 (varied between 6 mm and 8 mm in increments of 0.5 mm). The intact radii were all tested using a constant span of 8 mm. Force and displacement data was collected and used to calculate structural properties of peak moment and stiffness. Material properties were estimated using beam-theory equations with a custom Matlab script (Mathworks, Natick, MA) as previously described [176].

Notched right femurs were loaded in 3pt bending under hydration at 0.5 mm/min until failure. The posterior side was down and the span was adjusted to be 4 times the anterior-posterior width rounded to the nearest 0.5 mm. Crack propagation was recorded using a high resolution DSLR camera (Canon EOS 7D) attached with a macro lens. Load and displacement data was collected. $K_{c,initial}$ was calculated from yield force and cracking toughness was calculated as the work to fracture (W_f) normalized to Ct.Ar and adjusted for span as was previously described [176].

4.2.4 Assessing matrix composition

Raman spectra were collected from 10 sites randomly distributed within the mid-shaft of the left tibiae for males and the right tibiae for females using a 830 nm confocal Raman

microspectrocopy (Invia, Renishaw, Hoffman Estates, IL), providing ~1 cm^{-1} spectral resolution. Unfortunately, the right tibia from male mice was not available for Raman analysis, but we verified that there were no left-right differences in Raman properties for the female bones. An average of 10 consecutive spectra were collected per site with a 20X objective (NA=0.40) for a 5 s duration. Laser power was set at ~ 35 mW. Spectra were processed as previously described [147, 179]. Briefly, Raman raw spectra collected at ten points per bone specimen were averaged. Then, background fluorescence was removed from all averaged spectra by subtracting a 5^{th}-order polynomial function from the base of the raw spectra. Then, the averaged spectra were further smoothed to minimize noise using a proprietary de-noising (D-n) algorithm provided by the LabSpec 5 software (Horiba Jobin Yvon, Edison, NJ). From the averaged and de-noised spectrum per bone sample, we calculated the following Raman peak ratios: ν_1PO_4/Amide I, ν_1PO_4/Proline, ν_1PO_4/Amide III, and $CO_3/\ \nu_1PO_4$, and crystallinity (the inverse of the line-width of the ν_1PO_4 peak at half the height from baseline or half-maximum; 1/FWHM). To assess potential age-related differences in the secondary structure of collagen I, Amide I sub-peak ratios were calculated directly from the intensity ratios of the Amide I peak per sub-peak, the location of which was identified from the local minima of each second-derivative spectrum (Intensity at approximate wavenumber location): I_{1670}/I_{1640}, I_{1670}/I_{1610}, and I_{1670}/I_{1690} [213].

4.2.5 ^{1}H-NMR nuclear magnetic resonance relaxometry

Bound water was measured using our published ^{1}H NMR relaxometry technique [70, 121] on the broken right femurs following fracture toughness tests. After removing the marrow, the bone halves were placed within a low-proton radio-frequency (RF) coil along with a reference marker of water (20 μL). After placing the coil in a 4.7 T horizontal-bore magnet (Varian Medical Systems, Santa Clara, CA), Carr-Purcell-Meiboom-Gill (CPMG) measurements

with a total of 10,000 echoes were acquired at an echo spacing of 100 μs [176]. Each T2 spectrum was generated by fitting multiple exponential decay functions to the measurements, and the integrated area of bound water signal was converted to volume (based reference marker) and normalized to bone volume as measured using Archimedes' principle.

4.2.6 High Performance Liquid Chromatography (HPLC)

The proximal and distal ends of the left femur were removed and the remaining cortical bone was flushed prior to complete demineralization in 20% EDTA at 4°C. The radii were also flushed and demineralized in the same manner. Bones were subsequently dehydrated and then hydrolyzed in 6 N HCl with 4.5 mM alpha-amino-N-butyric acid (α-ABA) for 20 hours at 100 °C. Hydrolysates were filtered and split into approximately ~1 mg fractions. One fraction was used to measure the crosslinks pyridinoline (PYD), deoxypyridinoline (DPD), and pentosidine (PE) on a C-18 Spherisorb ODS2 column (Waters, Milford, MA) using a reverse-phase HPLC protocol previously described [178].

A second ~1 mg hydrolysate fraction was used to measure hydroxyproline. Hydrolysates were derivatized using phenoisothiocyanate (PITC) and measured on a PicoTag® column (Waters, Milford, MA) using a previously described protocol [178]. Hydroxyproline values were calculated from a standard curve normalizing to α-ABA. Crosslink values were normalized to a collagen content value estimated from hydroxyproline.

4.2.7 Statistical Analysis

Comparisons were made separately for males and females between 6 months of age and 20 months of age. Due to many variables not passing Shapiro-Wilk test for normality, Mann Whitney test was used to determine whether properties were significantly different between the age groups (GraphPad Prism v6, GraphPad Software, La Jolla, CA). For the multiple variable

regression, bootstrap general linear models (GLMs) were analyzed with 500 replications in STATA (StataCorp LLC., College Station, TX) with stepwise removal of non-significant interaction terms and then non-significant explanatory variables. Subsequently, bootstrap regressions were performed with one single variable.

4.3 Results:

4.3.1 Older Mice Had Higher Bone Area and Structurally Stronger Bones Compared to Younger Mice

Though there were no differences in body weight between the young and old female mice (Table 4.1), the moment of inertia (I_{min}) was higher at 20-mo. than at 6-mo. (Figure 4.1C). For males, body weight was significantly lower at 20-mo. compared to 6-mo. (Table 4.1), but as with females, I_{min} was higher at 20-mo. (Figure 4.1D). These structural differences in the mid-shaft were also reflected in increased Ct.Ar and Tt.Ar with aging (Table 4.1). Interestingly, while cortical thickness was higher in older female mice, it was lower in 20-mo. old male mice (Figure 4.1E). Similar age-related changes to structural properties occurred in the radius. I_{min} was higher for older than for younger mice, regardless of sex (Figure 4.1D), and cortical thickness was higher for older females but lower for older males (Figure 4.1F) compared to respective young adult mice.

Matching the age-related increase in I_{min}, the peak moment of the femur diaphysis was also higher in old females compared to young-adult females (Table 4.1). In contrast, there were no differences in peak moment between 20-mo. and 6-mo. for males, even though I_{min} was higher for older mice (Table 4.1). As for the radii, peak moment was higher at 20-mo. for both females and males (Table 4.1).

Cortical porosity can also influence structural strength, but for the intact femur mid-shaft, which was scanned at 12 μm voxel size (Figure 4.2C), cortical porosity (Ct.Po) was barely detectable, and so no age-related differences were detected. For the right femur scanned at 6 μm voxel size, evaluated above and below the notch, the female BALB/c mice had lower Ct.Po at 20-mo. (Figure 4.2D). Interestingly, both females and males had fewer pores at 20-mo. compared to 6-mo. in both femurs (Figure 4.2E and Figure 4.2F). Thus, the lack of a difference in structural strength between the age groups for male mice is likely due to an age-related change in material properties of the bone.

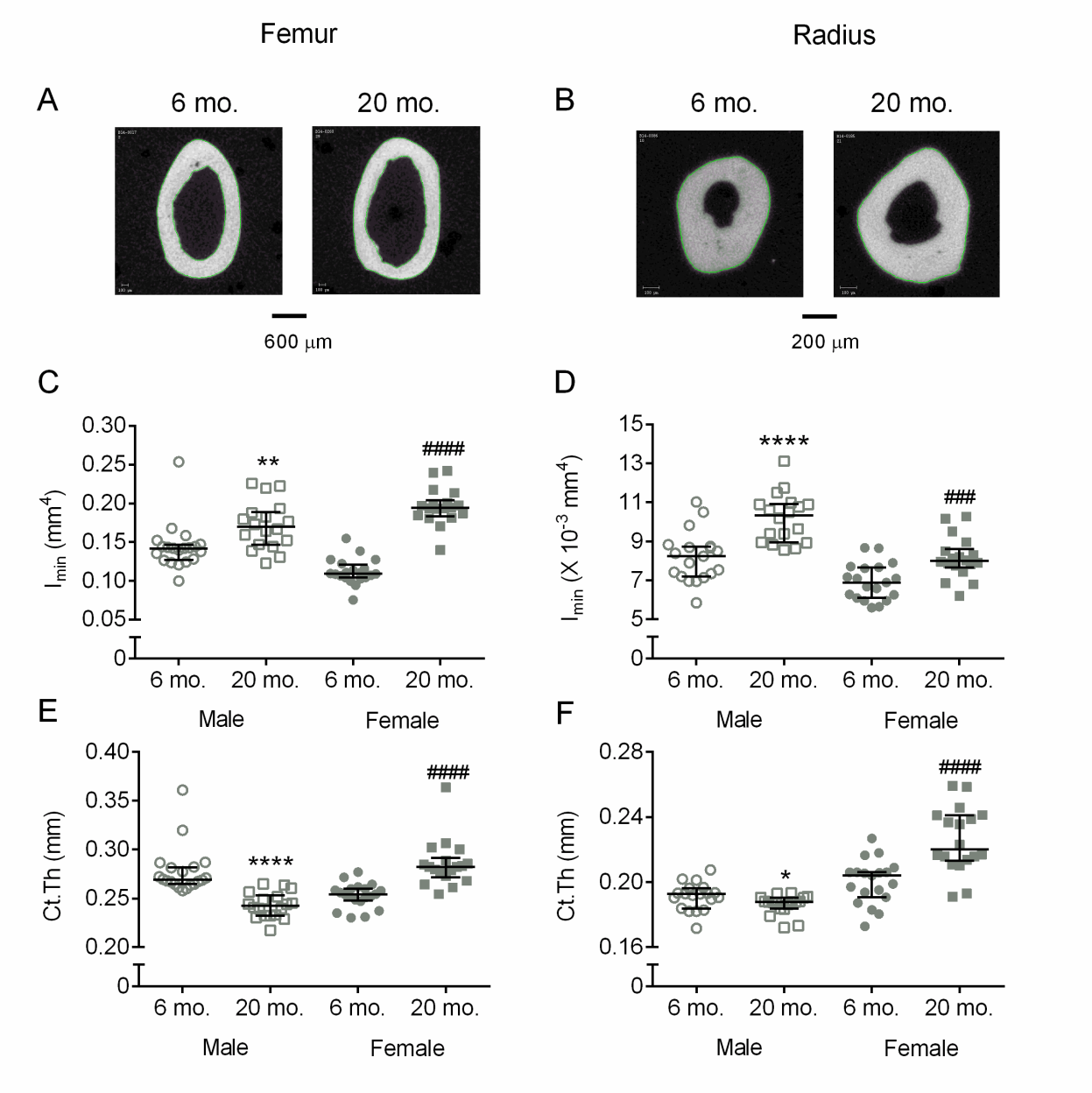

Figure 4.1 Structural parameters from μCT with representative images from male femurs (A) and radii (B). Imin was higher for older mice in both sexes for both the femur (C) and radius (D). Cortical thickness was higher for older females and lower for older males in both the femur (E) and radius (F). 6-mo mice are represented by circles and 20-mo. mice are represented by squares. Male mice are empty symbols and female mice are filled in symbols. Circles are 6-mo. and squares are 20-mo.

Table 4.1μCT and mechanical properties of cortical bone

		Male				Female				
		6-mo.		20-mo.		6-mo.		20-mo.		
Property	Unit	n ≥ 19		n ≥ 17		n ≥ 19		n ≥ 18		
Global										
Body weight	g	31.9	(31.7, 33.3)	30.5	(30.0, 31.6)	**	25.9	(25.0, 26.8)	26.8	(25.3, 29.5)
Femur										
Length	mm	14.7	(14.5, 15.0)	14.9	(14.7, 15.1)		14.8	(14.5, 15.1)	14.8	(14.7, 15.0)
Ct.Ar	mm^2	1.10	(1.08, 1.14)	1.08	(1.03, 1.14)		0.93	(0.90, 0.97)	1.10	(1.09, 1.15) ###
Tt.Ar	mm^2	1.81	(1.71, 1.87)	2.07	(1.92, 2.15)	****	1.51	(1.47, 1.57)	1.85	(1.83, 1.93) ###
Modulus	GPa	9.1	(7.2, 10.1)	10.6	(7.2, 11.6)		11.0	(10.2, 11.5)	11.3	(10.1, 11.9)
Post-yield toughness	N/mm^2	1.89	(1.53, 2.25)	1.04	(0.79, 1.29)	****	1.00	(0.77, 1.21)	0.29	(0.12 0.67) ###
PYD normalized	mm^{-1}	0.044	(0.034, 0.051)	0.024	(0.018, 0.027)	****	0.034	(0.026, 0.039)	0.015	(0.011, 0.021) ###
Peak Moment	N*mm	52.5	(50.3, 54.8)	55.4	(47.9, 58.3)		43.1	(40.5, 46.0)	60.1	(53.9, 61.3) ###
Stiffness	N/mm	162	(146, 193)	185	(153, 213)		197	(188, 202)	209	(188, 231) #
Work to fracture	N*mm	6.66	(6.20, 7.76)	4.63	(3.85, 5.40)	****	4.06	(3.71, 4.83)	3.73	(2.81, 4.16)
Radius										
Ct.TMD	$mgHA/cm^3$	1164	(1157, 1172)	1216	(1204, 1225)	****	1175	(1168, 1189)	1243	(1236, 1249) ###
Ct.Ar	mm^2	0.297	(0.291, 0.304)	0.310	(0.302, 0.319)	*	0.268	(0.260, 0.283)	0.304	(0.296, 0.316) ###
Tt.Ar	mm^2	0.371	(0.349, 0.381)	0.406	(0.386, 0.423)	****	0.327	(0.309, 0.341)	0.345	(0.342, 0.362) ##
Modulus	GPa	20.9	(18.7, 22.2)	20.4	(19.3, 21.6)		22.7	(21.4, 25.9)	22.9	(21.5, 25.5)
Post-yield toughness	N/mm^2	0.991	(0.816, 2.080)	0.606	(0.502, 0.788)	***	0.371	(0.308, 0.711)	0.348	(0.302, 0.675)
PYD normalized	mm^{-1}	0.045	(0.037, 0.106)	0.020	(0.018, 0.027)	***	0.015	(0.011, 0.035)	0.013	(0.012, 0.027)
Peak Moment	N*mm	8.55	(8.10, 9.26)	9.85	(9.39, 10.60)	****	8.24	(8.03, 8.57)	9.38	(8.98, 9.68) ##
Stiffness	N/mm	15.1	(14.1, 17.3)	20.2	(18.2, 20.7)	****	15.0	(14.3, 16.0)	17.7	(16.6, 19.0) ##
Work to fracture	N*mm	1.52	(1.37, 2.24)	1.23	(1.07, 1.28)	***	1.12	(0.90, 1.28)	1.15	(1.06, 1.44)

* indicate significant difference between 6-mo. and 20-mo. males, # indicate significant difference between 6-mo. and 20-mo. females

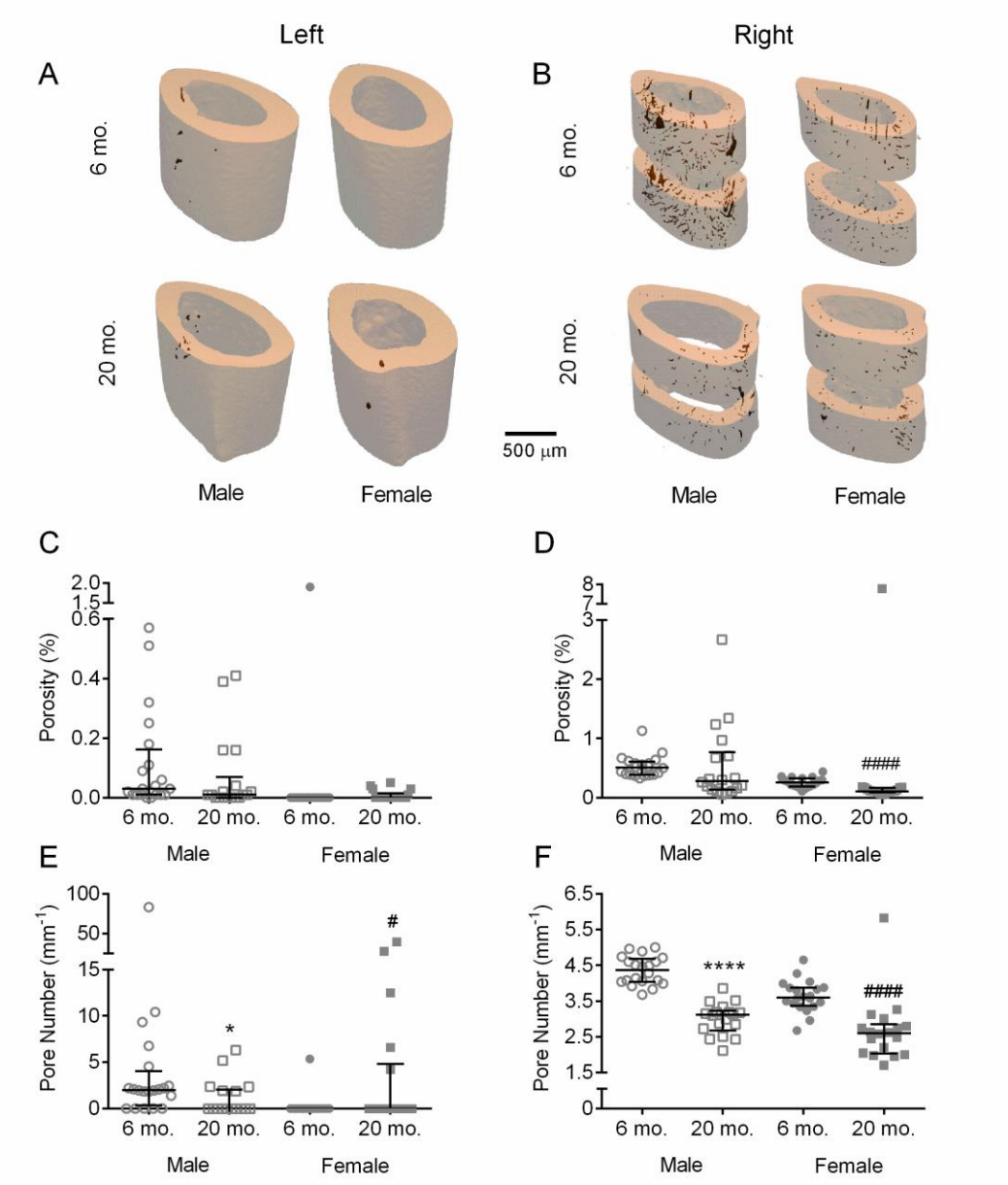

Figure 4.2 Porosity of the left and right femurs. Representative images from the left (A) and right femurs (B) show even distribution of pores. Porosity of the left (C) and right (D) femurs show minor changes in porosity, but pore number for both the left (E) and right (F) femurs was lower in older mice. 6-mo mice are represented by circles and 20-mo. mice are represented by squares. Male mice are empty symbols and female mice are filled in symbols. Circles are 6-mo. and squares are 20-mo.

4.3.2 In Addition to Lower Ultimate Strength, the Cortical Bone of Older Mice has Less Ability to Dissipate Energy (toughness) and Less Resistance to Crack Growth (fracture toughness)

When comparing material properties of cortical bone at the femur diaphysis, yield strength was indeed lower at 20-mo. compared to 6-mo. for male BALB/c mice but also for female mice (Figure 4.3C). However, for the diaphysis of the radii, there were no age-related differences in yield strength in either females or males (Figure 4.3D). The toughness of cortical bone was also lower at 20-mo. compared to 6-mo. (Figure 4.3E). On exception though, toughness did not differ between young-adult and aged mice when the female radii were tested in 3-pt (Figure 4.3F). Post-yield toughness and post-yield displacement followed the same trends as toughness with cortical bone becoming more brittle with age (Table 4.1). In fracture toughness tests on the right femur, the energy to initiate crack growth, $K_{c,initial}$, was lower at 20-mo. for both females and males (Figure 4.4C). Similarly, cracking toughness was lower at 20-mo. compared to 6-mo. for female and male BALB/c mice (Figure 4.4D).

4.3.3 Compositional Properties of the Bone Matrix Changed with Age in Both Females and Males

There were multiple age-related changes to the matrix. Ct.TMD of the femur mid-shaft, as measured by μCT, was higher at 20-mo. compared to 6-mo. in both females and males (Figure 4.5A). Similarly, mineral-to-matrix ratios (MMR) of the tibia mid-shaft, as measured by Raman spectroscopy, were all higher at 20-mo. for both sexes (Table 4.3). Multiple Amide I sub-peak ratios related to the second structure of collagen I significantly differed between the age groups.

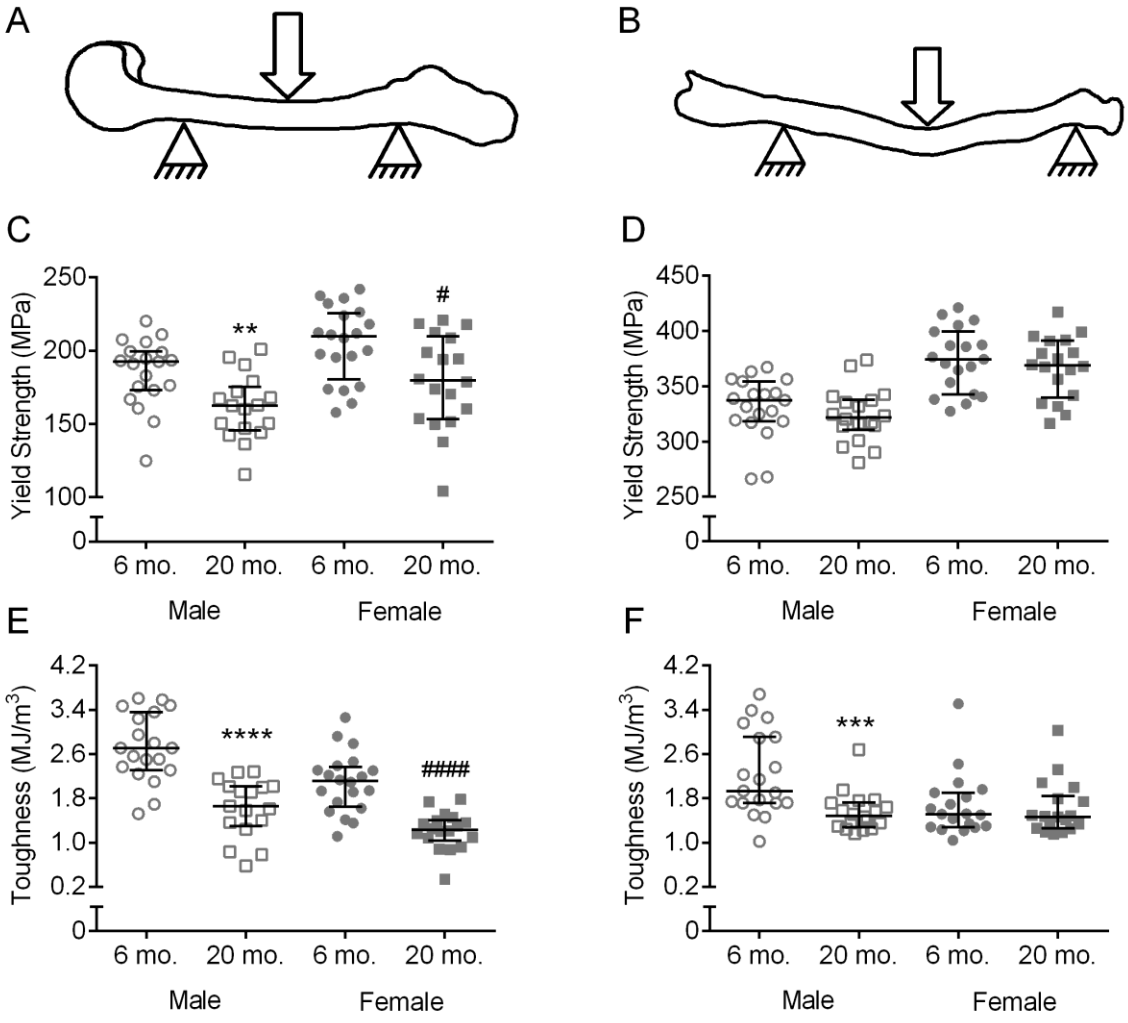

Figure 4.3 Material properties of the femur and radius. Cartoon schematics of 3-pt bending tests are shown for both the femur (A) and radius (B). Yield strength was lower for older mice in the femur (C) but not the radius (D) for both sexes. However, while toughness was lower in older mice for both sexes in the femur (E), it was only lower for older males in the radius (F). 6-mo mice are represented by circles and 20-mo. mice are represented by squares. Male mice are empty symbols and female mice are filled in symbols. Circles are 6-mo. and squares are 20-mo.

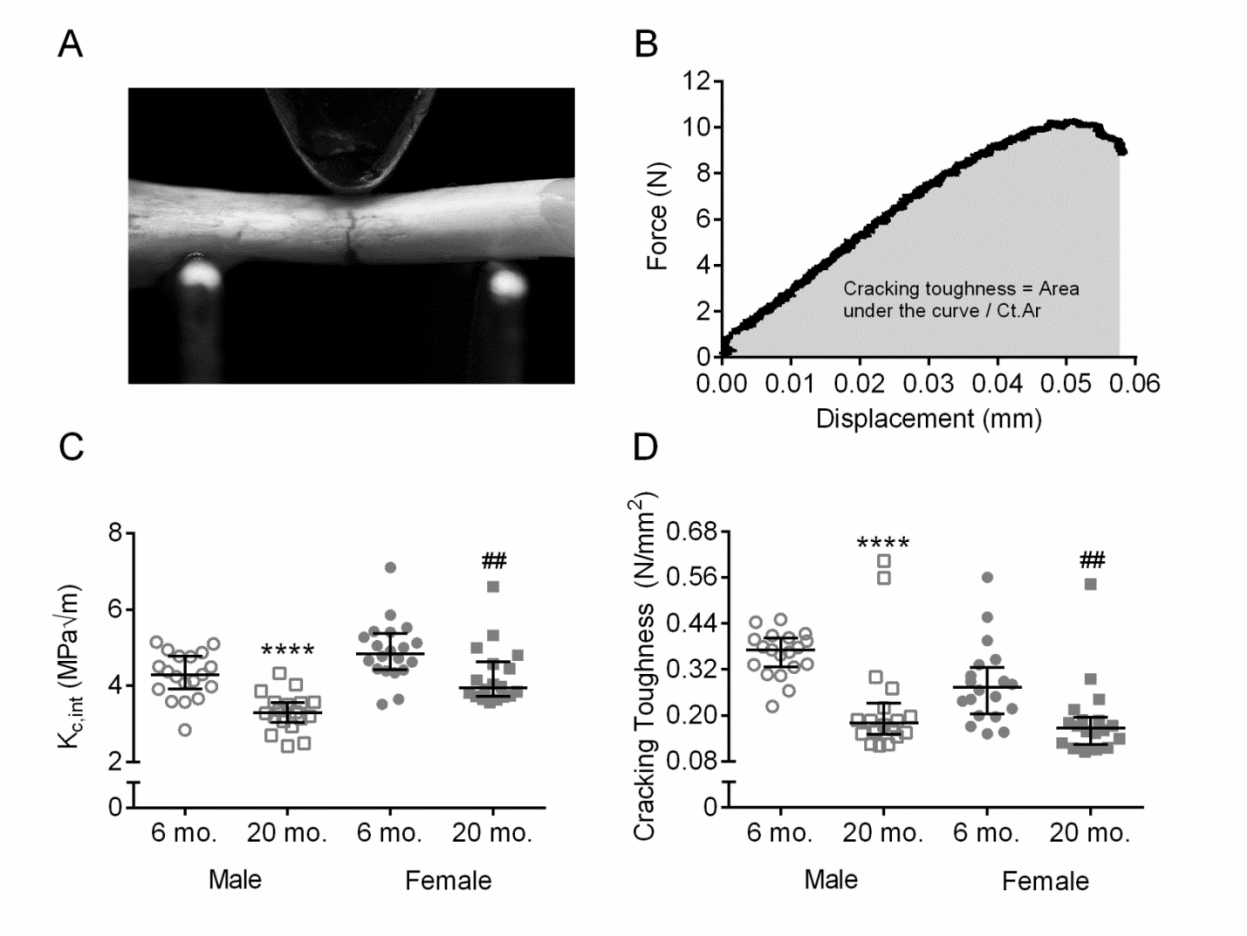

Figure 4.4 Fracture toughness of the right femurs. A representative image of a fracture toughness is shown in (A) and typical data generated from a test is shown in (B). $K_{c,initial}$(C) and cracking toughness (D) were lower for older mice in both sexes. 6-mo mice are represented by circles and 20-mo. mice are represented by squares. Male mice are empty symbols and female mice are filled in symbols. Circles are 6-mo. and squares are 20-mo.

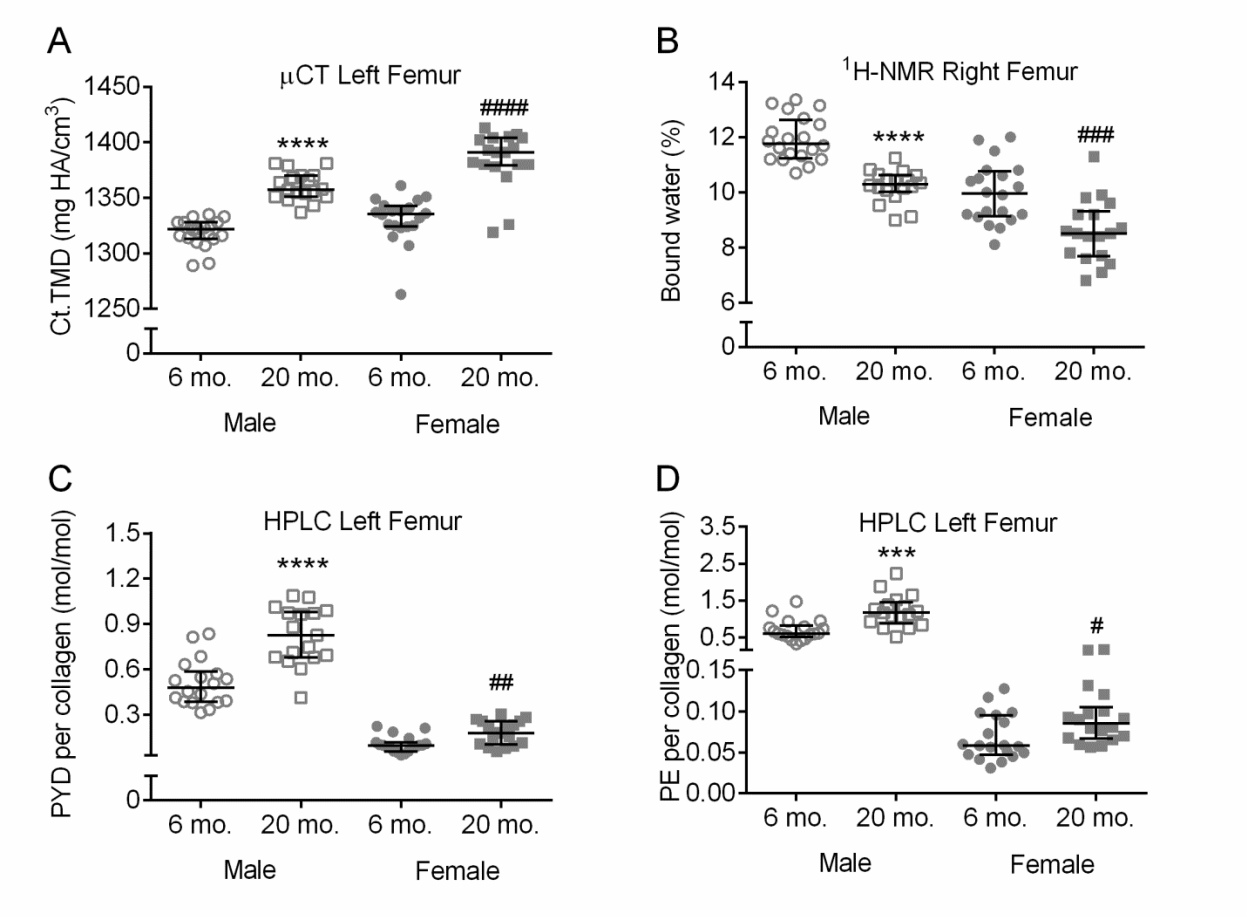

Figure 4.5 Matrix properties changed with age, as seen with higher Ct.TMD in older mice (A), lower bound water in older mice (B), and higher enzymatic (PYD) crosslinks (C) and non-enzymatic (PE) crosslinks (D). 6-mo mice are represented by circles and 20-mo. mice are represented by squares. Male mice are empty symbols and female mice are filled in symbols. Circles are 6-mo. and squares are 20-mo.

Both I_{1670}/I_{1610} and I_{1670}/I_{1640} were higher for 20-mo. than for 6-mo. female and male mice (Table 4.3). Interestingly, the so-called matrix maturity ratio I_{1670}/I_{1690} did not significantly differ with age for females but was significantly lower at 20-mo. that at 6-mo. for males (Table 4.3). The mature enzymatic crosslink PYD, as measured by HPLC was higher at 20-mo. than at 6-mo. (Figure 4.5C). Similarly, PE, a non-enzymatic crosslink, was higher in 20-mo. mice for both female and male BALB/c mice (Figure 4.5D). Lastly, bound water, as measured by ^{1}H-NMR was lower at 20-mo. compared to 6-mo. for both females and males (Figure 4.5B).

4.3.4 Multiple variable regressions

When using GLM in backwards, step-wise regression, to determine which matrix properties (Ct.TMD, PYD, PE) best explained the variance in material properties of the left femur, PYD concentration was the only significant predictor of toughness for male mice. Then, for female mice, PYD crosslinking was the only predictor of yield strength, while Ct.TMD was the primary explanatory variable of toughness (Table 4.3). For the right notched femur (Ct.TMD, bound water), in males, Ct.TMD explained each property when taking into account bound water while this was not the case with females (Table 4.3). When regressing individual variables by themselves, Ct.TMD, PYD and PE crosslinking each explained the variance in toughness for both males and females (Table 4.4). PYD crosslinking contributed to yield strength only in females even with only regressing one variable. Ct.TMD also significantly affected yield strength in both males and females when using a single variable regression (Table 4.4). Interestingly, for the right femur, bound water explained both $K_{c,initial}$ and cracking toughness for males and females whereas Ct.TMD only contributed to these material properties in males (Table 4.4). For the radius, Ct.TMD affected toughness only in males (Table 4.3).

Table 4.2 Raman spectroscopy

		Male				Female				
		6-mo.		20-mo.		6-mo.		20-mo.		
Property	Unit	n ≥ 11		n ≥ 11		n ≥ 19		n ≥ 18		
ν_1PO_4/Amide I		33.0	(31.6, 34.4)	38.1	(33.4, 42.0) *	42.1	(35.2, 45.7)	52.3	(46.6, 55.7)	####
ν_1PO_4/Proline		21.1	(19.7 25.0)	27.0	(26.0, 29.9) *	30.3	(16.0, 37.3)	43.8	(28.3, 56.4)	##
ν_1PO_4/Amide III		8.98	(6.99, 9.99)	12.44	(10.62, 14.22) **	7.71	(6.21, 9.22)	9.90	(8.91, 11.99)	##
ν_1PO_4/CH_2		8.78	(7.19, 9.42)	12.13	(9.69, 13.04) **	7.92	(6.37, 9.37)	10.20	(9.54, 12.15)	###
CO_3/ν_1PO_4		0.146	(0.142, 0.152)	0.157	(0.151, 0.161) **	0.141	(0.139, 0.146)	0.151	(0.147, 0.154)	####
Crystallinity		0.055	(0.054, 0.056)	0.057	(0.056, 0.058) **	0.056	(0.056, 0.057)	0.058	(0.058, 0.059)	####
I_{1670}/I_{1610}		3.62	(3.06, 4.64)	5.04	(3.58, 5.85) *	3.90	(3.00, 4.22)	4.61	(4.40, 4.99)	##
I_{1670}/I_{1640}		1.81	(1.71, 1.84)	1.92	(1.88, 1.98) **	1.81	(1.76, 1.91)	2.01	(1.86, 2.09)	##
I_{1670}/I_{1690}		2.20	(2.16, 2.43)	2.03	(2.01, 2.09) ***	2.04	(1.90, 2.23)	2.00	(1.73, 2.09)	

* indicate significant difference between 6-mo. and 20-mo. males, # indicate significant difference between 6-mo. and 20-mo. females

4.4 Discussion:

With advanced aging, the femurs of BALB/c mice became brittle having less ability to dissipate energy during fracture and less ability to resist crack growth by 20-mo. than at 6-mo., regardless of sex. Thus, in addition to the age-related loss in trabecular BV/TV or aBMD, BALB/c model of aging includes a deterioration in the material properties of cortical bone. Notably, the structural strength was either not different (femurs from males) between the age groups or higher at 20-mo. than at 6-mo. indicating perhaps a structural adaptation of diaphysis to compensate for the decrease in toughness and fracture toughness. Accompanying the deterioration in fracture resistance are a number of changes within the bone matrix: an increase in tissue mineral density, an increase in amount of carbonate in the mineral lattice, alterations in the secondary structure of type 1 collagen, an increase in both a enzymatic crosslink (PYD) and a non-enzymatic crosslink (PE), and a decrease in bound water. Except for the increase in TMD, all these changes occur in the cortical bone of humans with aging [39, 191, 192]. As such, the BALB/c strain, both females and males, can serve as a pre-clinical model of age-related changes in bone matrix fragility in addition to being a model of age-related loss in trabecular bone and deterioration in trabecular architecture.

While this is the first study to show that toughness and fracture toughness of mouse bone is lower at 20-mo. than at 6-mo., the age at which peak bone strength is being achieved, previous work by Willinghamm et al. comprehensively characterized changes in bone through skeletal maturity (2-mo., 4-mo., and 7-mo.) and with aging (7-mo., 12-mo., and 20-mo.) [142]. Consistent with this previous study, we also observed for both sexes higher Ct.TMD and higher I_{min} at 20-mo. compared to young adult mice (Figure 4.4 and Figure 4.5). As for the radius, both studies found that Ct.TMD and moment of inertia were also higher for old than for young adult

BALB/c mice, regardless of sex. Likewise, yield stress of radius mid-shaft did not vary between 6-mo. or 7-mo. and 20-mo. Perhaps due to a larger sample size (approximately double), we confirmed that the previously observed age-related trend in decreasing post-yield displacement of the diaphysis (femur and radius) is significant for both females and males [142].

There were few notable differences in the age-related changes in bone between male and female BALB/c mice. First of all, while body weight was lower in males at 20-mo., it did not significantly decrease for females, confirming previous observations [142]. While cortical thickness was lower in males at 20-mo. compared to 6 mo., it was higher in females (Figure 4.1). Based on the Willingham et al. study, cortical thickness for females peaks at 12 months as opposed to 7 months; which could be the reason for this sex-related discrepancy [142]. Similarly, while structural strength of the femur diaphysis was higher with age in females, it did not differ between the age groups for males (Table 4.1). The previous study found no difference in ultimate moment between 7-mo. and 20.-mo. for both sexes [142]. Perhaps due to these differences in changes of cortical area and thickness, stiffness and peak moment were higher for females at 20-mo., but did not differ for males (Table 4.1). For the radius, changes in thickness remained the same. Opposite of the Willingham study, while there were changes in yield properties for males in the radius (toughness, post-yield displacement, work to fracture); these were not significantly different among females for the radii (Figure 4.1 and Table 4.1). The age-related changes in bound water and Ct.TMD were consistent between males and females (Figure 4.5 and Table 4.3), and consistent in previously reported trends for water content and organic and ash content comparing 20-mo. to 7-mo. female and male mice [142].

There are of course limitations to the use of mice in studying cortical bone, namely the lack of extensive osteonal remodeling throughout the lifespan and hence the lack of cement line

as microstructural barrier to fracture. Nonetheless, age-related changes in the long bones of mice do not necessarily occur in aging rats. Previous work [176] observed that $K_{c,initial}$ increases with age in Fischer F344 male rats as opposed to the decrease with age in mice (Figure 4.4). Rats typically experience an increase in cortical porosity at the mid-shaft [176], while Ct.Po of the mid-shaft does not vary with age in mice (Figure 4.2) unless assessed at the distal and proximal ends of the diaphysis [30]. Much of the age-related increased in Ct.Po occurs near the endosteal surface [176]. In this study, BALB/c mice showed greater decreases in toughness than yield strength (Figure 4.3) as typically observed for human bone [205]. Similar to mice, rats have shown increases in BMD with aging [143], though other studies have found no difference [214]. Like this study, rats have also shown decreases in strength and toughness [143, 176].

There were multiple changes to the matrix that may lower the fracture resistance of bone. While in general material properties such as toughness are thought to be influenced by the organic matrix, degree of mineralization (ash fraction) is known to be inversely proportional to impact energy as observed from testing bones of different species with widely varying mineralization [215]. Thus, the age-related increase in Ct.TMD could have conferred lower toughness in the old mice. However, at odds with the paradigm of material strength being directly proportional to TMD or bone density [21], yield strength was lower for the old mice than for the young adult mice suggesting other matrix-related factors are influencing the material properties. For example, bound water has been observed to decrease with age in humans, and it correlates with fracture toughness [119] and ultimate strength [121] of human cortical bone. The age-related decrease in bound water (Figure 4.5) could have potentially reduce plasticity of the bone while also lower strength.

Other observed changes in the matrix likely also influence the age-related decrease in material properties. Multiple sub-peak ratios in the Amide I band were different between the age groups. Particularly, the ratio I_{1670}/I_{1640} was higher with age (Table 4.3). This sub-peak ratio negatively correlates with toughness of bovine cortical bone [179] and is affect by both thermal denaturation and mechanical damage [126, 179]. The so-called matrix maturity ratio was lower for old than for the young adult male mice, but did not significantly change between old and young adult female mice. Given that both enzymatic crosslinks and non-enzymatic crosslinks were higher with age (Fig. 4.5), irrespective of sex, our direct measurement of I_{1670}/I_{1690} is not likely an indicator of an age-related difference in crosslinking profile. Instead, Amide I sub-peak ratios are indicators of the secondary structure of collagen I [216], which can be affected by AGE accumulation [213], radiolysis of collagen I [216] and enzymatic crosslinking [68]. Thus, the higher sub-peak ratios I_{1670}/I_{1610} and I_{1670}/I_{1640} with age could indicative embrittling effect. Also, since bound water exists because of hydrogen bonding, increases in mineralization could displace bound water from the matrix [19]. Similarly, increases in collagen crosslinks could also confer less sites for hydrogen bonding. At least in soft tissue, collagen with fewer crosslinks binds more with water [217]. In effect, the age-related loss in material properties is likely multifactorial.

Various treatments have been used in aging mice and rats to treat age-related loss in fracture resistance. Bisphosphonates have been shown to increase Ct.TMD in the femur, trabecular BV/TV, and ultimate load [218, 219]. While these may increase bone strength, bisphosphonate treatment did not affect toughness or even reduced it. Using parathyroid hormone (PTH) in rats, Sato et al. showed increases BMD and increases in strength and toughness short term, but for long term use strength increased based on dose and toughness was

either the same or lower [220]. Fewer studies have looked at treatments with targets besides BMD. However, Farr et al. recently treated mice with a senolytic compound, which reduces senescent cells. Trabecular BV/TV was higher in treated groups, as was the peak force as calculated by μFEA, but the study did not examine material properties [221].

An inherent limitation of using mice when studying the age-related loss in fracture resistance is their lack of intracortical remodeling as occurs in large animals and in humans. When developing therapeutics, those related to bone formation rate are less effective due to this. However, therapeutics that target AGEs or matrix hydration may be able to be studied using rodent models. Raloxifene, a selective estrogen receptor modulator, is a potential therapeutic for targeting the matrix. Previous experiments have raloxifene treatment increases bound water, though the effects on material properties differ as to improving post-yield properties or not having an effect [60, 222]. A recent study using raloxifene after parathyroid hormone treatment has shown that it increased toughness and decreased AGEs in the trabecular bone [223]. Pyridoxamine, an AGE-inhibitor, could be potentially used, as it has been shown to decrease AGEs in bone with in vitro incubation [224] and in other tissues of treated rats [225, 226] and mice [131]. Overall, more investigation into therapeutics which target the bone matrix is needed.

4.5 Conclusions

Strength, toughness, and fracture toughness at the material levels are lower at 20-mo. than at 6-mo. for the BALB/c model of aging. This loss of fracture resistance may be the result of the multiple changes to cortical bone seen at the matrix level. While it is unclear which matrix-level change is the driving force for the loss of fracture resistance, the BALB/c mouse can be used as a preclinical model of aging for the development of therapeutics that target the matrix.

4.6 Acknowledgements

This work was funded in part by a training grant from NIDDK (DK101003) and by a grant from the National Institute of Arthritis and Musculoskeletal and Skin Diseases (AR067871).

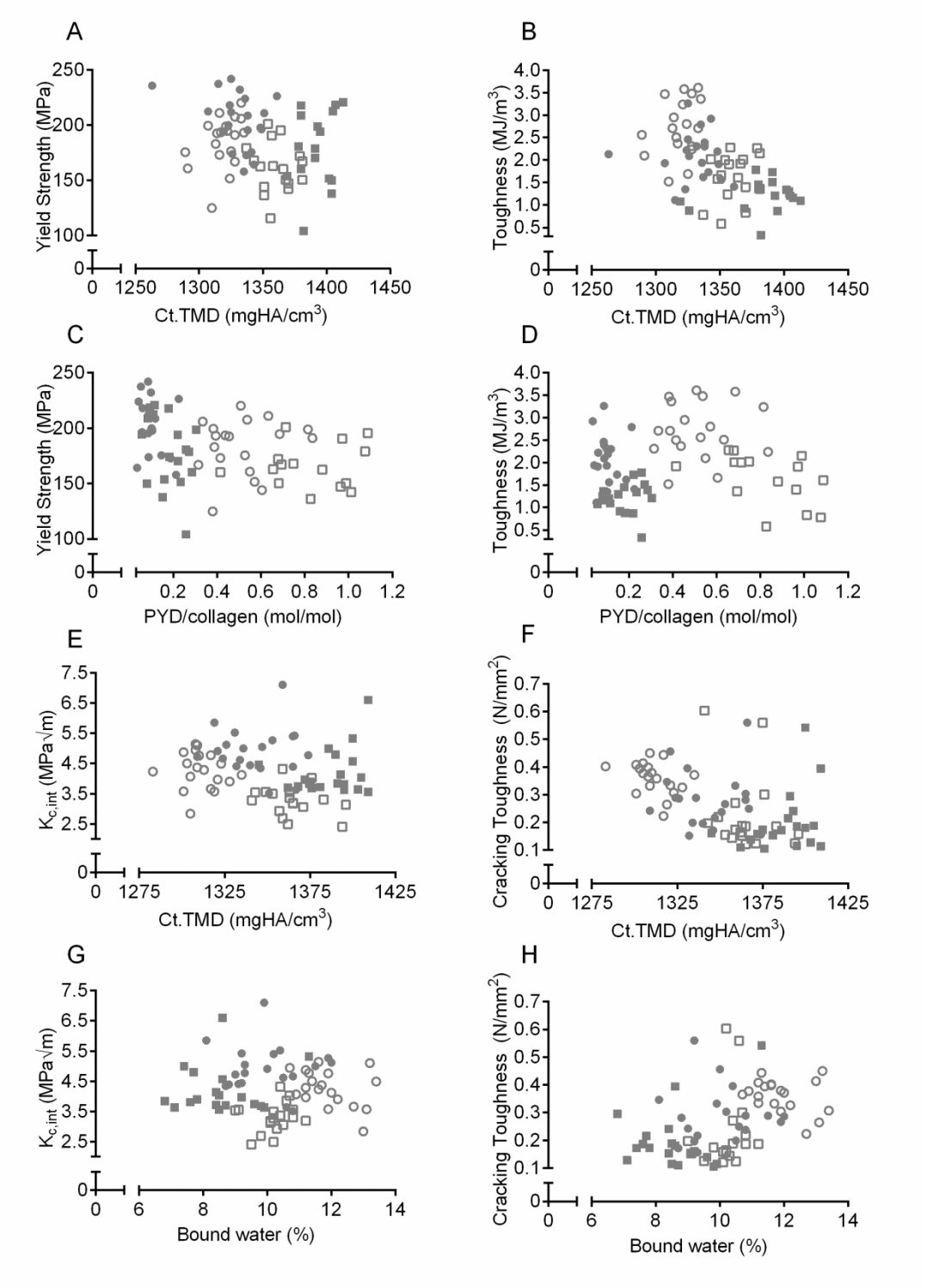

Figure 4.6 Scatter plots of fracture resistance and matrix parameters. Male mice are empty symbols and female mice are filled in symbols. Circles are 6-mo. and squares are 20-mo.

Table 4.3 General Linear Model Regression Analysis

Left Femur				Interactions			
Males		CtTMD	PYDpercol	PEpercol	CtTMD/PYD	CtTMD/PE	PYD/PE
yield strength	p	0.062	0.994	NS	NS	NS	NS
	β	-0.317	0.001				
toughness	p	0.107	**0.020**	NS	NS	NS	NS
	β	-0.267	-0.410				
Females							
yield strength	p	0.484	**0.041**	NS	NS	NS	NS
	β	-0.131	-0.395				
toughness	p	**0.003**	0.309	NS	NS	NS	NS
	β	-0.435	-0.162				

Right Femur				Interactions
Males		CtTMD	BW	CtTMD/BW
$K_{c,initial}$	p	**<0.0001**	0.778	NS
	β	-0.622	0.050	
cracking toughness	p	**0.002**	0.562	NS
	β	-0.534	0.094	
Females				
$K_{c,initial}$	p	0.325	0.275	NS
	β	-0.185	0.170	
cracking toughness	p	0.783	0.116	NS
	β	-0.059	0.300	

Bold and red values indicate when p was statistically significant, NS indicates not significant and removed

Table 4.4 Single Variable Regression

Left Femur				
Males		CtTMD	PYDpercol	PEpercol
yield strength	p	**0.026**	0.297	0.934
	β	-0.336	-0.176	0.015
toughness	p	**<0.0001**	**<0.0001**	**0.002**
	β	-0.491	-0.559	-0.467
Females				
yield strength	p	**0.018**	**0.008**	0.675
	β	-0.383	-0.459	-0.059
toughness	p	**<0.0001**	**0.022**	**0.044**
	β	-0.511	-0.372	-0.298
Right Femur				
Males		CtTMD	BW	
$K_{c,initial}$	p	**<0.0001**	**0.007**	
	β	-0.654	0.448	
cracking toughness	p	**<0.0001**	**0.003**	
	β	-0.594	0.436	
Females				
$K_{c,initial}$	p	0.082	**0.043**	
	β	-0.266	0.258	
cracking toughness	p	0.213	**0.012**	
	β	-0.200	0.328	
Right Radius				
Males		CtTMD		
yield strength	p	0.864		
	β	-0.032		
toughness	p	**0.034**		
	β	-0.289		
Females				
yield strength	p	0.269		
	β	-0.153		
toughness	p	0.396		
	β	-0.142		

Bold and red font indicates statistical significance

CHAPTER 5 POST-TRANSLATIONAL MODIFICATIONS OF MATRIX PROTEINS IN THE BALB/C AGING MOUSE MODEL

5.1 Introduction:

The ability of bone to resist fracture is dependent on its structure at multiple hierarchical scales of arrangement [22]. The extracellular matrix of bone contributes to fracture resistance by providing the scaffolding for mineralization to occur and by dissipating energy through multiple toughening mechanisms [28]. The mineral component primarily contributes to the strength of bone whereas the organic matrix primarily contributes to toughness, the ability of bone to dissipate energy during post-yield deformation [21]. Furthermore, the heterogeneous organization of the mineralized collagen fibrils impedes crack growth through deflections at lamellar interfaces. Aging increases fracture risk beyond what would be expected from the decrease in areal bone mineral density (aBMD), suggesting bone quality is being affected [7, 8]. The extracellular matrix may have a crucial role in bone quality [10].

Non-collagenous proteins (NCPs) of bone are thought to assist with mineral formation and act as ligands for cellular signaling. However, another role for them is more physical than biological in that NCPs likely contribute to the fracture resistance of bone. Existing at the interface between neighboring mineral crystals NCPs such as osteocalcin and osteopontin act as sacrificial bonds breaking when sufficient force is applied, thereby dissipating energy [77] as a nano-scale void forms between the mineral crystals [78]. Much of the work indicating that NCPs may influence the material properties of bone come from studies involving murine knock-out models [78, 80]. A double knock-out of osteopontin and osteocalcin had lower fracture toughness than controls [78] as did an osteopontin knock-out [227], but another study examining the radius found an osteopontin-osteocalcin knock-out mouse had a higher structural strength

[80]. One study suggested that the lower fracture resistance for the accelerated aging mouse model (α-klotho) was due to a loss in osteocalcin relative to wild-type mice [79]. In humans, one study indicated that there were likely not losses in proteoglycans in patients with osteoporosis, but there did seem to be changes in the organization of the non-collagenous matrix [228]. Additionally, another study indicated that there were lower amounts of α_2HS-glycoprotein, sialoprotein, and albumin in the bones of adults compared to children [229].

Type I collagen is the primary protein in bone, composing 90% of the organic matrix. The triple helix of this collagen consists of two α1 chains and one α2 chain. Collagen is crosslinked through lysine residues, on which hydroxylation occurs and then monosaccharides or disaccharides are added which enable crosslink formation [230]. Mutations in lysyl oxidase, which catalyzes reactions necessary for enzymatic crosslinking, have shown that collagen becomes less stable without enzymatic crosslinks. There is evidence that the collagen molecule changes with age. Danielsen et al. showed that as rats aged, the melting temperature (T_m) of collagen I decreased for bone. Similarly shrinkage temperature (T_s) decreased, a change that was not seen in collagen from skin [231]. Danielsen also showed that in human bone T_s decreased for older men, though not linearly, but that T_s was variable for women [232]. Others have reported that the temperature at which shrinkage starts to occur ($T_{s\text{-}up}$) and maximum rate of contraction of demineralized human bone decreases with age [207]. These are indicators that the collagen molecule becomes less stable with age. The post-translational modifications of collagen affect its structure and there is evidence that post-translational modifications of collagen are tissue-specific [233, 234].

While changes to fracture resistance may occur with enzymatic post-translational modifications to bone, there are also changes that affect bone that are not controlled

enzymatically. Advanced glycation end-products (AGEs) form non-enzymatically, and glycating bone with high concentrations of ribose can affect the material properties of bone. Specifically, these have been shown to negatively correlate with toughness of bone [196, 197, 199]. Furthermore, there is evidence that AGEs affect the ability of collagen to properly align and to be degraded [235]. AGEs in bone increase with age and thus may contribute to the age-related decrease in material properties. To date, most of the AGEs that have been measured are fluorescent. However, only a portion of AGEs that modify proteins are measured with these assays. More recently, carboxymethyl-lysine (CML) was shown to increase in bone with age using mass spectrometry and ELISA [236].

Mass spectrometry is a powerful tool with which to locate and quantitate specific post-translational modifications to proteins and has recently been applied to the analysis of extractable proteins from bone [237]. Groups have used it to analyze specific post-translational modifications that alter bone collagen in models of disease states [238, 239] or how post-translational modifications compare between bone and tendon [240]. Moreover, it has been used to compare bone proteins between the more mineralized interstitial tissue and the less mineralized osteonal tissue [241]. For NCPs, specific post-translational modifications have been studied for osteocalcin incubated with glucose and ribose in vitro [242] and sialoprotein isolated from murine pre-osteoblast cells in culture [243]. However, little information exists for how post-translational modifications to collagen and other non-collagenous proteins alter with age in bone.

To fully understand the age-related deterioration in bone matrix quality, important post-translational modifications to the bone matrix proteins need to be identified. Using protein extracts from bones of a previously analyzed mouse model of aging, we identified age-related

changes in non-collagenous proteins as well as site-specific post-translational modifications to extracellular matrix proteins including collagen I.

5.2 Materials and Methods

5.2.1 Animal care and tissue collection

As described in the previous chapter, long bones were harvested from 6-mo. and 20-mo. old male and female BALB/c mice. Upon removing the tibia from soft tissue, it was flash frozen in liquid nitrogen and subsequently stored -80 °C until analyzed.

5.2.2 Protein extraction from tibiae

A sub-set of the tibiae (n=6 mice/group) were thawed for protein extraction. The proximal and distal ends of the tibiae were removed and the tibiae were flushed. Tibiae were then frozen overnight at -80 °C. Flushed tibiae were subsequently powdered using a freezer/mill (6770, SPEX SamplePrep, Metuchen, NJ). Powdered samples were placed in a solution of 0.3 mL of 10 mM Tris HCl, 6 M guanidine hydrochloride, 50 mM EDTA and Halt's protease inhibitor cocktail. Proteins were extracted from the samples for 72 hours at 4 °C under rotation. Each sample was then centrifuged at 13,000 G for 15 minutes at 4 °C. The supernatant was collected and filtered using a 3 KDa centrifugal filtration unit (Amicon® Ultra-4, Merck Millipore Ltd, Burlington, MA). The supernatant was placed within the centrifugal filtration unit and the volume was increased to 4 mL using 10 mM Tris HCl. Samples were centrifuged at 4 °C at 4,000 RPM until the volume was approximately 100 µL. This was repeated two times through the same filter. The protein concentration of the samples was then measured using a Pierce™ BCA protein assay kit (Thermo Fisher Scientific, Waltham, MA).

5.2.3 Identification of post-translational modifications and protein sequences

Samples were digested with trypsin overnight at 37 °C. Protein sequence was analyzed by liquid chromatography-tandem mass spectrometry (LC-MS/MS). Peptides were loaded onto a capillary column and eluted as previously described [244] and subsequently analyzed with a LTQ Orbitrap Velos mass spectrometer with a nanoelectrospray ionization source. The peptides DRVYIHPF from angiotensin I, DRVYIHPFHL from angiotensin II, and RPPGFSP from bradykinin were injected as standards. The database SEQUEST was used for protein identification and results were assembled in Scaffold version 4.8.6. with a filtering criteria of 95% peptide probability. A ΔM of 58.0055 was used to identify carboxymethyl-lysine (CML), a ΔM of 15.9949 was used to identify hydroxylation (OH), a ΔM of 57.0215 was used to identify carbamidomethylation (CAM) on C, a ΔM of 178.0477 was used to identify galactosyl hydroxylysine (Gal), and a ΔM of 340.1006 was used to identify glucosylgalactosyl hydroxylysine (Gluc-gal). Results were manually confirmed with the program Xcalibur (version 2.1.0). The integrated area of the curve for a peptide peak was calculated. This value was then normalized to the area for the unmodified peptide or to the injected standard closest to the elution time if an unmodified version of the peptide was not found.

5.2.4 Statistical analysis

Differences between young and old mice were tested within each sex for significance using individual Mann-Whitney U tests (GraphPad software). Regression analysis was done using STATA with bootstrapping (500 replications) using fracture toughness variables, material properties and crosslinks as determined previously in the analysis of bone for BALB/c model of aging. Correlation analysis was separated for males and females, but 6-mo. and 20-mo. data were combined.

5.3 Results:

5.3.1 Non-collagenous proteins and type I collagen were detected in the extractions by the LC-MS/MS method

There were not differences in overall protein concentration between older and younger mice. For males, the protein concentration was 1.08±0.41 μg/μL for 6-mo. and 0.87±0.2 μg/μL for 20-mo. For females, the protein concentration was 0.55±0.08 μg/μL for 6-mo. and 0.61±0.08 μg/μL for 20-mo. Periostin was lower for older mice than for the young adult mice as indicated by multiple sequences for males, but this age-related change in periostin was not statistically significant for the analysis of protein extracts from the female bones (Table 5.1). The osteonectin peptide DEGNNLLTEK was lower for 20-mo. than for 6-mo. mice, irrespective of sex. Compared to 6-mo. mice, females at 20-mo. had lower values for a sequence for osteomodulin and decorin. Females at 20-mo. also had lower values than females at 6-mo. for two sequences of osteonectin. These may indicate differences in other non-collagenous proteins; however, we used a threshold of changes in at least three peptides to determine if protein concentration altered with age. For type I collagen α1, overall coverage was high (Figure 5.3). Peptides were detected from the N-terminal propeptide, N-terminal non-helical region, triple helical region, and C-terminal propeptide. Expectedly, most peptides were from the triple helical region since this is the most abundant protein.

5.3.2 CML was higher in older males and females

Carboxymethyl lysine (CML) was found to be higher for 20-mo. males and females than 6-mo. males and females on both biglycan and collagen α1 (Figure 5.1 and Figure 5.2). For biglycan, the sequence VGINDFCPMGFGVK^{CML} was detected by finding the MS1 m/z ion of 771.36 (Figure 5.1) and for collagen α1, the peptide SGEYWIDPNQGCNLDAIK^{CML} by

Table 5.1 Quantitation of non-collagenous proteins

Non-collagenous proteins		Males 6-mo.	Males 20-mo.	Males p value	Females 6-mo.	Females 20-mo.	Females p value
Periostin	GFEPGVTNILK	0.0325 ± 0.0069	0.0214 ± 0.0050	**0.015**	0.0258 ± 0.0066	0.0204 ± 0.0069	0.238
	DQGPNVC^{CAM}ALQQILGTK	0.0078 ± 0.0032	0.0043 ± 0.0018	**0.026**	0.0108 ± 0.0045	0.0064 ± 0.0019	0.132
	DLLTQPGDWTLFAPTNDAFK	0.0036 ± 0.0011	0.0021 ± 0.0009	**0.026**	0.0088 ± 0.0039	0.0061 ± 0.0019	0.238
	EGETVTEVIHGEPVIK	0.0118 ± 0.0026	0.0077 ± 0.0020	**0.015**	0.0137 ± 0.0047	0.0094 ± 0.0034	0.132
	VLTQIGTSIQDFLEAEDDLSSFR	0.0005 ± 0.0003	0.0002 ± 0.0001	**0.026**	0.0050 ± 0.0013	0.0045 ± 0.0014	0.474
Biglycan	IQAIELEDLLR	0.0395 ± 0.0136	0.0369 ± 0.0135	0.675	0.0424 ± 0.0092	0.0529 ± 0.0267	0.788
	VPAGLPDLK	0.0491 ± 0.0108	0.0542 ± 0.0105	0.474	0.0490 ± 0.0192	0.0615 ± 0.0341	0.675
	VVQC^{CAM}SDLGLK	0.0299 ± 0.0077	0.0286 ± 0.0045	0.675	0.0315 ± 0.0143	0.0361 ± 0.0213	0.675
Decorin	ISPEAFKPLVK	0.0523 ± 0.0230	0.0413 ± 0.0113	0.387	0.0507 ± 0.0451	0.0685 ± 0.0566	0.474
	ASYSAVSLYGNPVR	0.0112 ± 0.0073	0.0080 ± 0.0029	0.675	0.0050 ± 0.0025	0.0022 ± 0.0016	**0.041**
	ELHLDNNK	0.0154 ± 0.0060	0.0096 ± 0.0025	0.093	0.0104 ± 0.0054	0.0104 ± 0.0072	0.571
Osteocalcin	IYGITI	6.22 ± 1.20	6.06 ± 0.77	> 0.999	4.85 ± 2.15	4.28 ± 2.33	0.387
	TAYK	0.6185 ± 0.0844	0.5400 ± 0.0692	0.238	0.3752 ± 0.1902	0.3189 ± 0.1505	0.474
Osteopontin	ISHELESSSSEVN	0.1023 ± 0.0378	0.1124 ± 0.0298	0.675	0.1017 ± 0.0864	0.1056 ± 0.0442	0.675
	ESQESADQSDVIDSQASSK	0.0098 ± 0.0045	0.0069 ± 0.0015	0.180	0.0086 ± 0.0075	0.0095 ± 0.0070	0.474
	LYSLHPDPIATWLVPDPSQK	0.0772 ± 0.0360	0.1200 ± 0.0517	0.132	0.1226 ± 0.1097	0.1076 ± 0.0613	0.788
Osteonectin	DEGNNLLTEK	0.0312 ± 0.0070	0.0200 ± 0.0052	**0.026**	0.0321 ± 0.0169	0.0159 ± 0.0063	**0.026**
	LEAGDHPVELLAR	0.1105 ± 0.0281	0.1230 ± 0.0266	0.180	0.1174 ± 0.0586	0.0969 ± 0.0543	0.387
	TFDSSC^{CAM}HFFATK	0.0955 ± 0.0214	0.0877 ± 0.0244	0.474	0.0437 ± 0.0160	0.0119 ± 0.0089	**0.002**
	YIALEEWAGC^{CAM}FGIK	0.0031 ± 0.0010	0.0025 ± 0.0009	0.474	0.0036 ± 0.0014	0.0025 ± 0.0018	0.238
Osteomodulin	EC^{CAM}FC^{CAM}PTNFPTSMYC^{CAM}DNR	0.0044 ± 0.0016	0.0040 ± 0.0011	0.675	0.0025 ± 0.0008	0.0019 ± 0.0037	0.065
	LMQLNLC^{CAM}NNR	0.0108 ± 0.0030	0.0112 ± 0.0023	0.675	0.0097 ± 0.0048	0.0019 ± 0.0037	**0.026**
	LSNLQQLHLEHNNLEEFPFPLPK	0.0076 ± 0.0030	0.0061 ± 0.0021	0.474	0.0126 ± 0.0062	0.0092 ± 0.0046	0.180

Bold and red font indicates statistical significance. All sequences normalized to collagen α-1 sequence GEP^{OH}GATGVQGPP^{OH}GPAGEEGK

detecting the MS1 m/z ion of 1040.97 (Figure 5.2). The modification for K^{CML} was confirmed by detecting the MS2 m/z ion 205.1 for both sequences. Other MS2 ions were identified as well.

5.3.3 Hydroxylation sites were relatively stable with age

Overall, there were few hydroxylation sites that showed differences between the age groups. In males, the peptide $^{405}GFP^{OH}GADGVAGP^{OH}K$ was lower in 20-mo. compared to 6 mo. when normalizing to the sequence $^{405}GFP^{OH}GADGVAGPK$ (Figures 5.6-5.9). In contrast, $^{960}GFP^{OH}GLPGPSGEPGK$ was higher in 20-mo. than in 6-mo. males when normalized to the standard. A version of this sequence with two hydroxylation sites trended towards being lower in 20-mo. males, suggesting that the version with only one hydroxylation site increased as overall hydroxyproline amount decreased. Hydroxylation sites were not different between the age groups in the female bone extracts. As seen in Figures 5.6-5.9 hydroxylation sites across males and females were similar.

5.3.4 Lys^{254} for males and Lys^{266} for females had differing modifications

As illustrated in Figure 5.3, males and females differed in modifications to the lysine residues Lys^{254} and Lys^{266}. While Lys^{254} for males showed the presence of modifications for hydroxylation (OH), galactosyl hydroxylysine (Gal), and glucosylgalactosyl hydroxylysine (Gluc-gal), in females, only galactosyl hydroxylysine was found. However, for females, the modification for galactosyl hydroxylysine was also found on Lys^{266}. Hydroxylation was found on Lys^{266} for females as well. In contrast, in males, only hydroxylation was detected on Lys^{266}, it was not modified to galactosyl hydroxylysine.

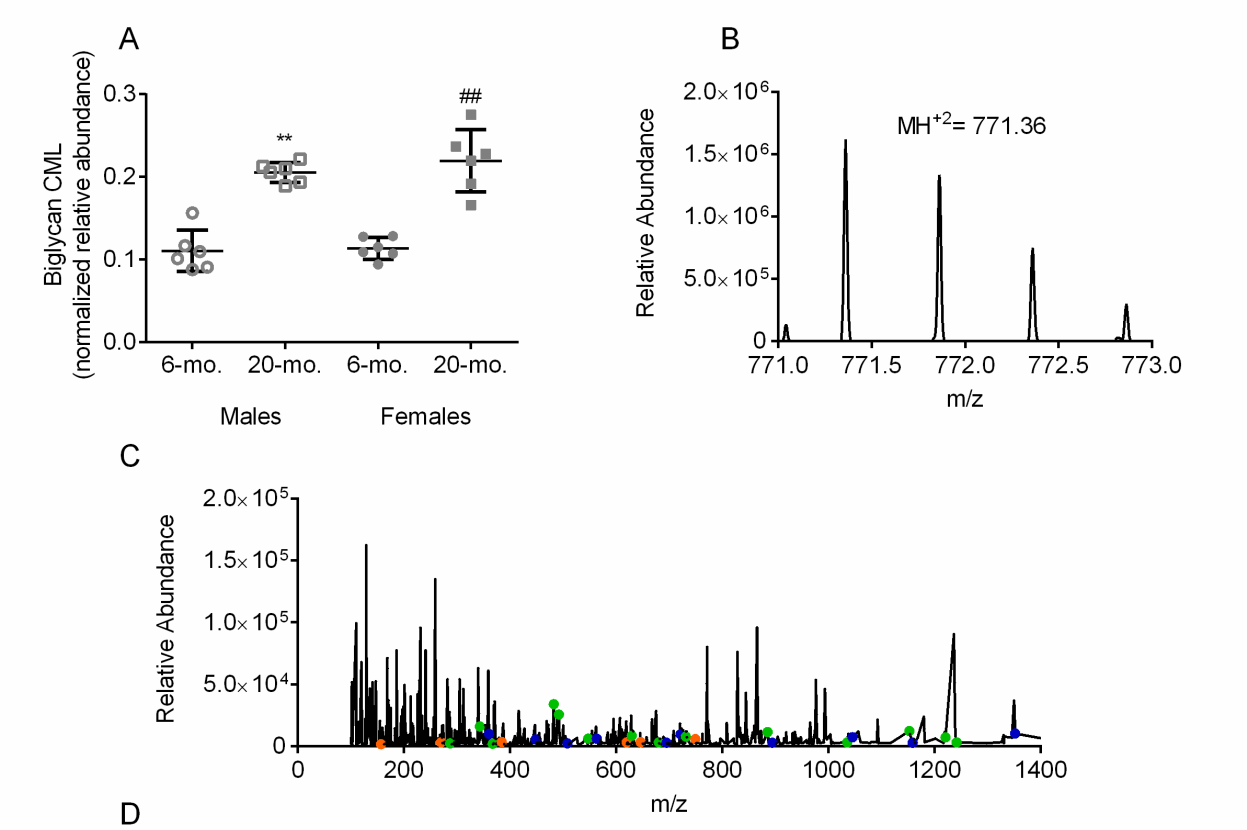

D

B	B Ions	B+2H	B-NH3	B-H2O	AA	Y Ions	Y+2H	Y-NH3	Y-H2O	Y
1	100.1				V	1,541.7	771.4	1,524.7	1,523.7	14
2	157.1				G	1,442.6	721.8	1,425.6	1,424.6	13
3	270.2				I	1,385.6	693.3	1,368.6	1,367.6	12
4	384.2		367.2		N	1,272.5	636.8	1,255.5	1,254.5	11
5	499.3		482.2	481.2	D	1,158.5	579.8	1,141.5	1,140.5	10
6	646.3	323.7	629.3	628.3	F	1,043.5	522.2	1,026.4		9
7	749.3	375.2	732.3	731.3	C	896.4	448.7	879.4		8
8	846.4	423.7	829.4	828.4	P	793.4	397.2	776.4		7
9	977.4	489.2	960.4	959.4	M	696.3	348.7	679.3		6
10	1,034.4	517.7	1,017.4	1,016.4	G	565.3		548.3		5
11	1,181.5	591.3	1,164.5	1,163.5	F	508.3		491.3		4
12	1,238.5	619.8	1,221.5	1,220.5	G	361.2		344.2		3
13	1,337.6	669.3	1,320.6	1,319.6	V	304.2		287.2		2
14	1,541.7	771.4	1,524.7	1,523.7	K+58	205.1		188.1		1

Figure 5.1 Quantitation and identification of CML-modified biglycan overall values normalized to unmodified peptide (A), MS1 spectra identifying the ion for the complete peptide (B), MS2 spectra identifying specific amino acid ions (C), the m/z of ions for this sequence calculated and highlighted in (D).

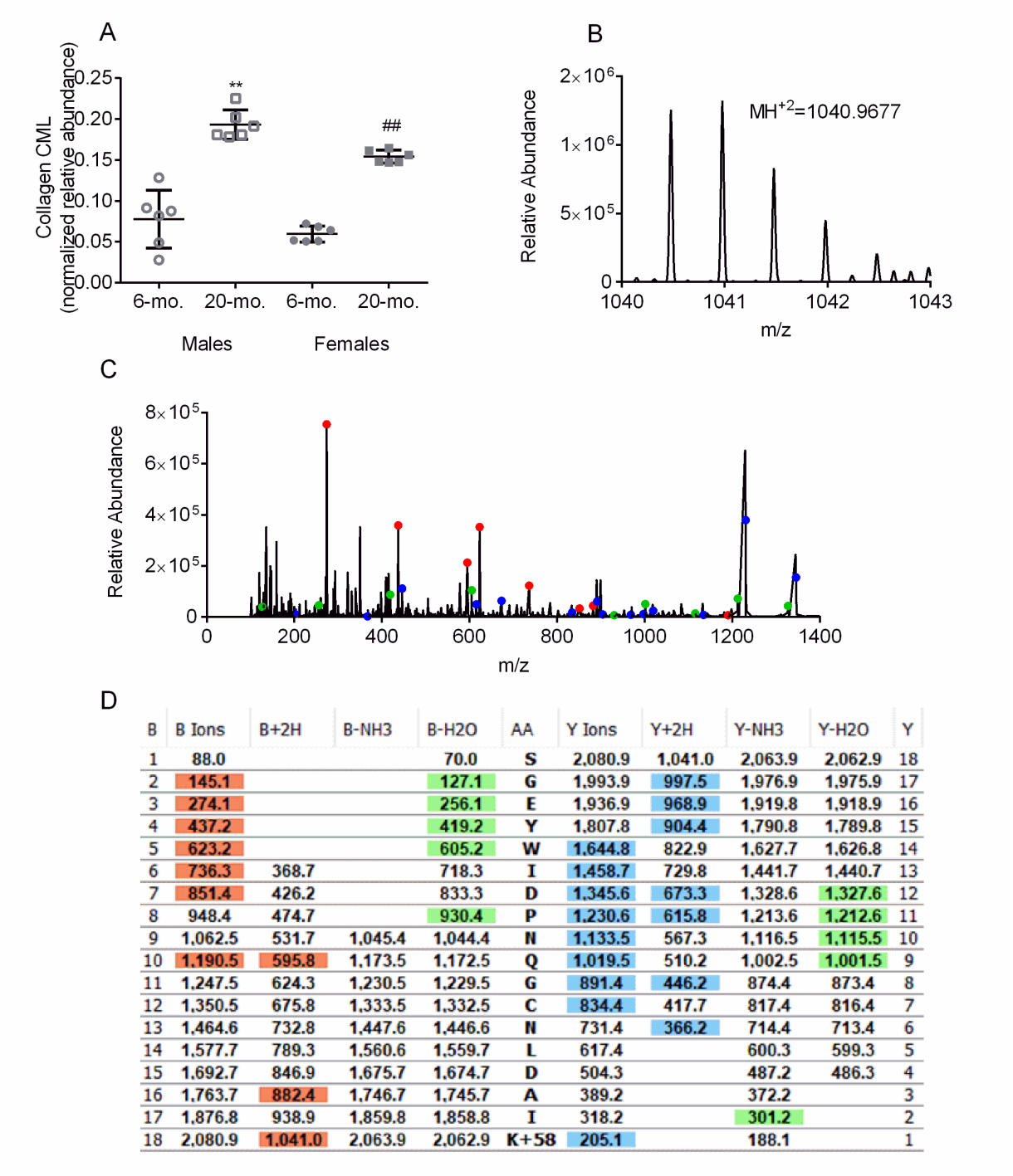

B	B Ions	B+2H	B-NH3	B-H2O	AA	Y Ions	Y+2H	Y-NH3	Y-H2O	Y
1	88.0			70.0	S	2,080.9	1,041.0	2,063.9	2,062.9	18
2	145.1			127.1	G	1,993.9	997.5	1,976.9	1,975.9	17
3	274.1			256.1	E	1,936.9	968.9	1,919.8	1,918.9	16
4	437.2			419.2	Y	1,807.8	904.4	1,790.8	1,789.8	15
5	623.2			605.2	W	1,644.8	822.9	1,627.7	1,626.8	14
6	736.3	368.7		718.3	I	1,458.7	729.8	1,441.7	1,440.7	13
7	851.4	426.2		833.3	D	1,345.6	673.3	1,328.6	1,327.6	12
8	948.4	474.7		930.4	P	1,230.6	615.8	1,213.6	1,212.6	11
9	1,062.5	531.7	1,045.4	1,044.4	N	1,133.5	567.3	1,116.5	1,115.5	10
10	1,190.5	595.8	1,173.5	1,172.5	Q	1,019.5	510.2	1,002.5	1,001.5	9
11	1,247.5	624.3	1,230.5	1,229.5	G	891.4	446.2	874.4	873.4	8
12	1,350.5	675.8	1,333.5	1,332.5	C	834.4	417.7	817.4	816.4	7
13	1,464.6	732.8	1,447.6	1,446.6	N	731.4	366.2	714.4	713.4	6
14	1,577.7	789.3	1,560.6	1,559.7	L	617.4		600.3	599.3	5
15	1,692.7	846.9	1,675.7	1,674.7	D	504.3		487.2	486.3	4
16	1,763.7	882.4	1,746.7	1,745.7	A	389.2		372.2		3
17	1,876.8	938.9	1,859.8	1,858.8	I	318.2		301.2		2
18	2,080.9	1,041.0	2,063.9	2,062.9	K+58	205.1		188.1		1

Figure 5.2 Quantitation and identification of CML-modified collagen α1, overall values normalized to unmodified peptide (A), MS1 spectra identifying the ion for the complete peptide (B), MS2 spectra identifying specific amino acid ions (C), the m/z as calculated and highlighted in (D).

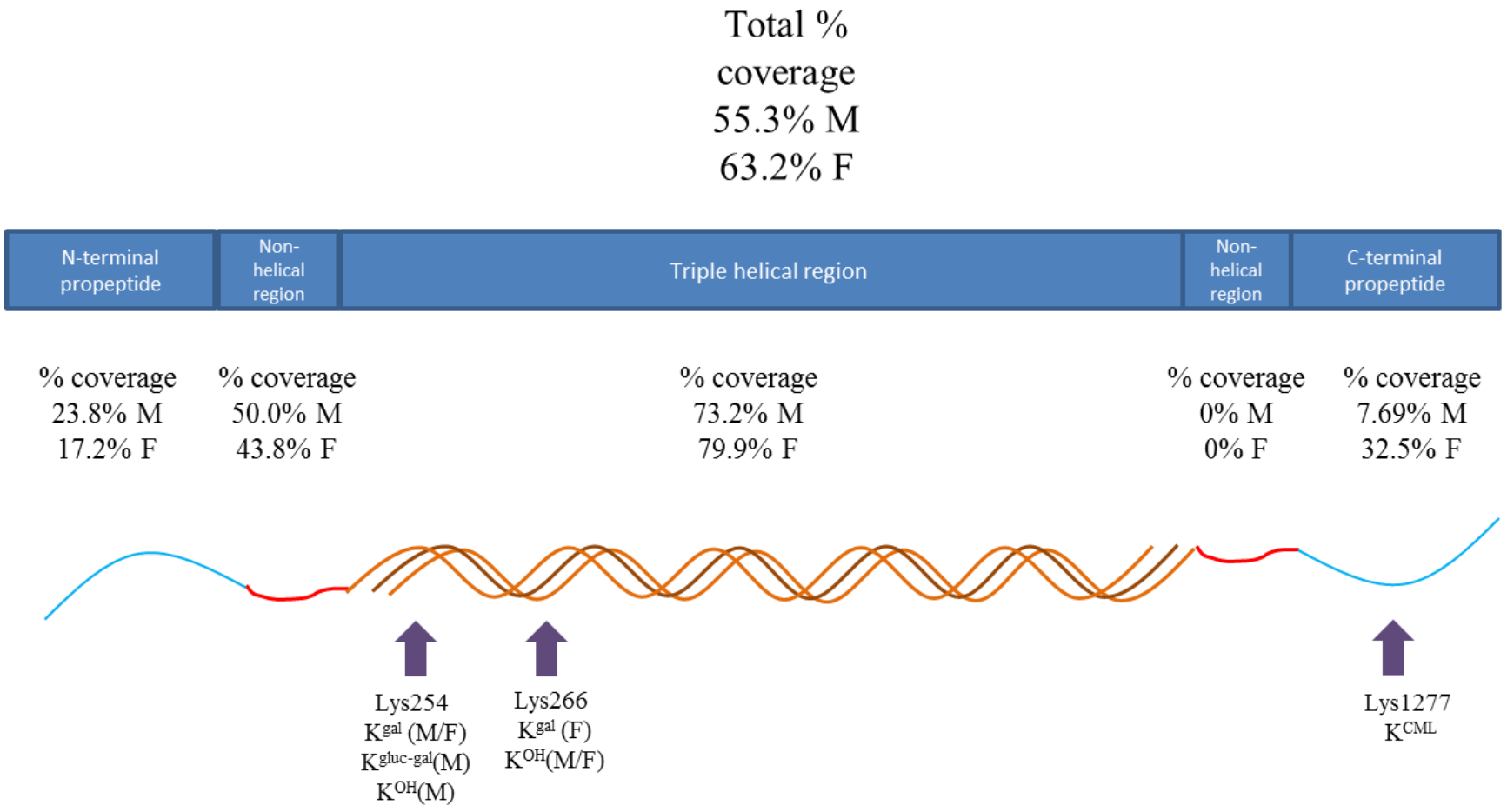

Figure 5.3 Location of specific post-translational modifications on collagen α1. The modifications for galactosyl-hydroxylysine (gal), glucosylgalactosyl-hydroxylysine (gluc-gal), hydroxylation (OH) and carboxymethyl-lysine (CML) are shown.

Table 5.2 Correlation analysis of post-translational modifications with aging bone material and matrix properties

		Males				Females			
		Periostin	Biglycan CML	Collagen CML	Lys254-Gal	Periostin	Biglycan CML	Collagen CML	Lys254-Gal
PYD/col	p	**<0.0001**	0.053	**0.011**	0.125	**0.035**	**<0.0001**	**0.018**	0.059
	β	-0.934	0.571	0.695	-0.403	-0.506	0.787	0.603	0.572
PE/col	p	0.247	**0.012**	0.128	**0.003**	0.636	0.926	0.753	0.353
	β	-0.437	0.585	0.544	-0.754	0.160	0.029	0.104	-0.230
Yield Strength	p	0.195	**<0.0001**	0.070	0.653	0.256	**0.026**	0.101	0.548
	β	0.447	-0.791	-0.532	0.187	0.381	-0.558	-0.438	-0.222
Toughness	p	0.059	**0.009**	**0.027**	0.133	0.264	**0.002**	**<0.0001**	0.488
	β	0.462	-0.690	-0.590	0.556	0.352	-0.708	-0.871	-0.242
$K_{c,initial}$	p	**<0.0001**	**<0.0001**	**<0.0001**	0.779	0.822	0.370	0.365	0.852
	β	0.799	-0.895	-0.948	-0.113	-0.071	-0.311	-0.284	0.056
Cracking Toughness	p	**<0.0001**	**<0.0001**	**<0.0001**	0.975	0.170	0.092	0.581	0.506
	β	0.836	-0.919	-0.946	0.012	0.396	-0.366	-0.171	-0.202
Bound water	p	0.152	**<0.0001**	**<0.0001**	0.998	**0.003**	**0.024**	0.145	**0.017**
	β	0.319	-0.823	-0.827	0.001	0.663	-0.542	-0.376	-0.641

Bold and red font indicates significance.

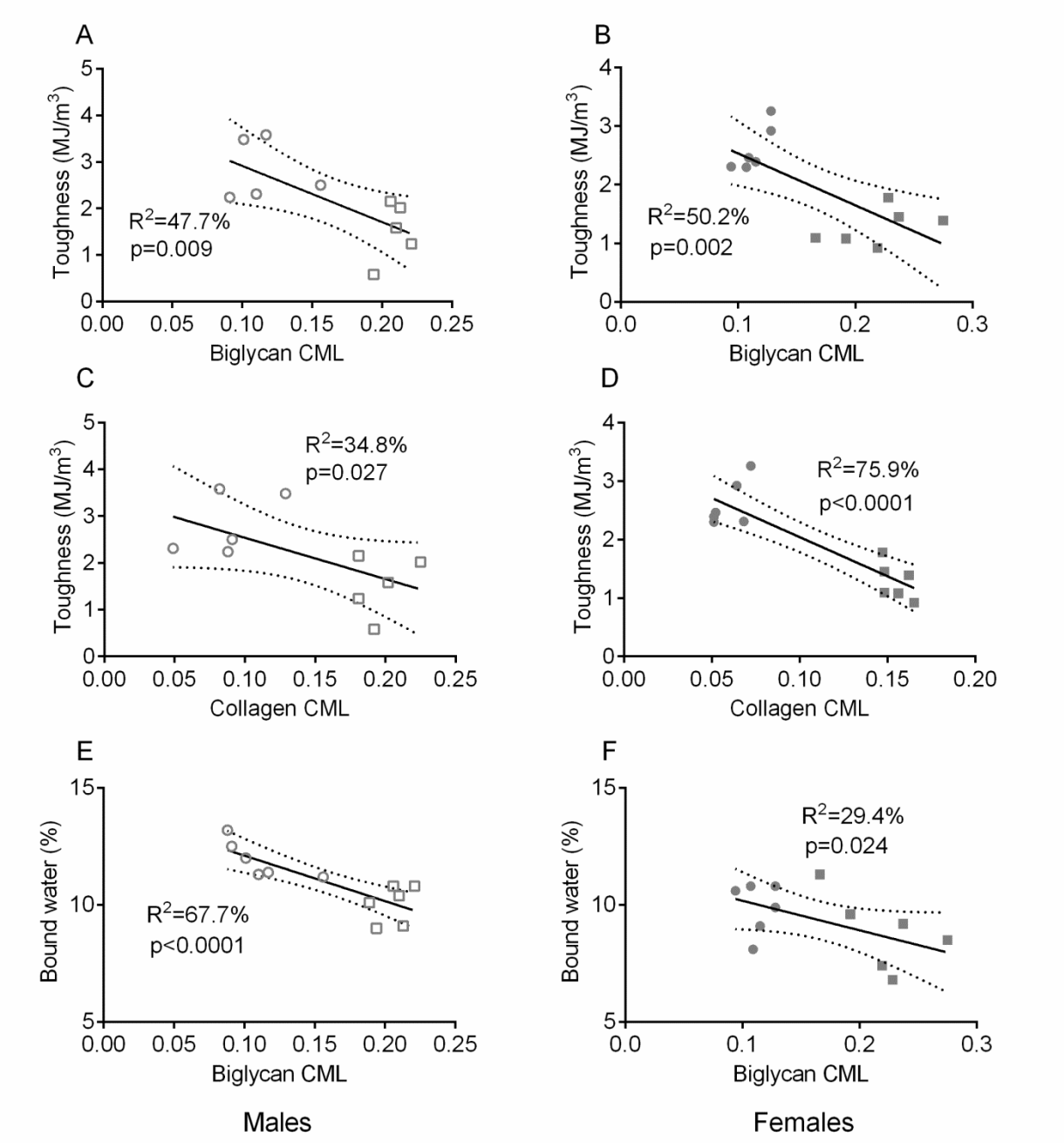

Figure 5.4 Correlation analysis of post-translational modifications for males and females aging bone material and matrix properties for toughness and CML modified biglycan (A&B), toughness and CML-modified collagen (C&D) and for bound water and CML-modified biglycan (E&F). Open symbols indicate males, closed symbols indicate females. Circles indicate 6-mo. and squares indicate 20-mo.

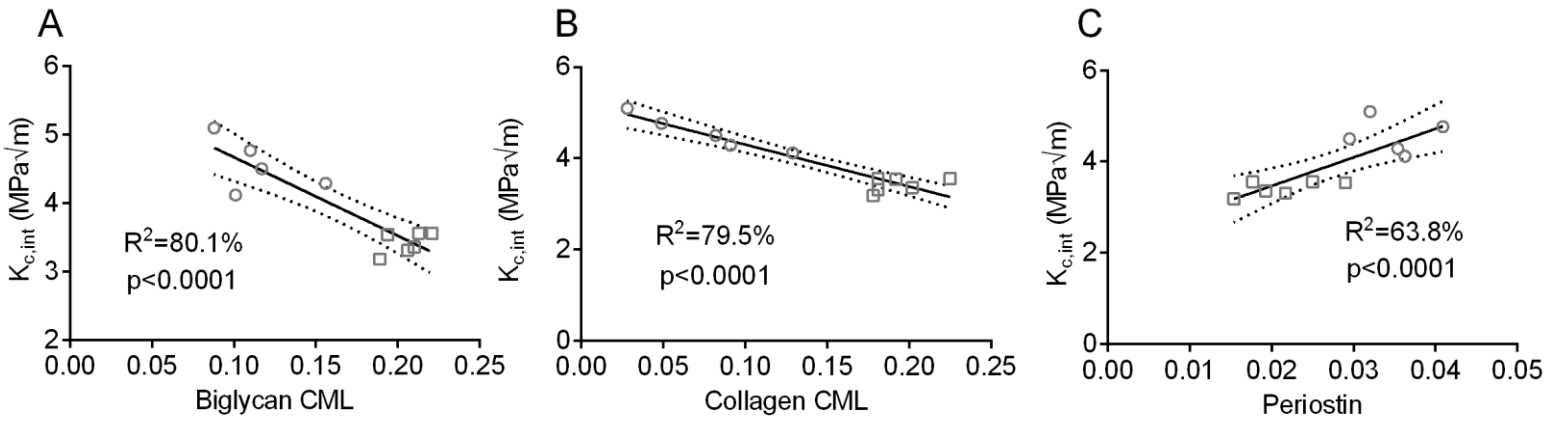

Figure 5.5 Correlation analysis of male values for CML-modified biglycan (A), CML-modified collagen (B) and periostin amount (C) with $K_{c,initial}$ for males. Circles indicate 6-mo. and squares indicate 20-mo.

5.3.5 Multiple material properties correlated with post-translational modifications to proteins

As seen in Table 5.2, there were multiple material properties of aging bone that could be explained by post-translational modifications of interest. Figure 5.4 contains graphs for correlations which were significant for both sexes. Notably, as levels of CML increased, toughness decreased. This held true for both CML modifications on collagen and those on biglycan. It should also be noted that bound water was lower as CML levels were higher. Strong correlations were observed for post-translational modifications and protein alterations and fracture toughness properties in males. As seen in Figure 5.5, $K_{c,initial}$ correlated positively with periostin and negatively with both CML on biglycan and collagen.

5.4 Discussion:

Overall, enzymatic post-translational modifications to collagen are stable in young compared to older mice. The modifications involved crosslink development and collagen stability are similar between young and old mice, suggesting that the differences in bone matrix quality between young and older mice is not related to changes in hydroxylation of proline or lysine residues in collagen. However, there were some changes in matrix proteins. While, there were not many differences in the amounts of non-collagenous proteins, multiple sequences for periostin were lower for older males than for young adult males. Any peptide sequence for other non-collagenous proteins that differed with age was lower in the older mice. Most notably, there are increases in AGEs which may result in a more brittle matrix and decreases in protein stability.

To start with, protein concentration from the samples was consistent across ages, indicating that the extraction protocol worked similarly well on young and old mice. The modifications were not biased based on extracting more from the different ages. Also, as seen in

Figure 5.3, the coverage of collagen was similar between males and females, with somewhat better coverage for females with total coverage of collagen being 55.3% and 63.2% for males and females. This is similar to the collagen coverage reported by Thomas et al of 42% [236]. Our method was able to detect multiple domains of the collagen molecule. The largest percentage of coverage was in the triple helical region, which is the largest part of the collagen molecule. Similarly, multiple sequences from different non-collagenous proteins were detected. This indicates that the extraction and LC-MS/MS protocol was able to detect multiple proteins from bone.

Non-collagenous proteins are thought to have an impact on bone mechanics, especially with regards to fracture toughness [139, 245]. There were no observed differences in osteocalcin or osteopontin levels with age. However, periostin in the bone matrix was significantly lower for older males, but it was not significantly lower for older females compared to young adult mice (Table 5.1). Periostin, known as a matricellular protein due to its role in cellular signaling [246], could also have an effect on material properties. In a knock-out mouse model, male mice without periostin had more cracks, fewer crosslinks, and lower hardness than control mice [247]. The knock-out mice had lower plastic energy when loaded compared to unloaded tibiae, and some groups had lower plastic energy than controls even without loading, though this was not consistent for groups or in a previous study [247, 248]. Presently, for male bones, there was a strong correlation between $K_{c,initial}$ and periostin (Figure 5.5). This suggests that periostin has could influence fracture toughness and may help prevent crack growth through crack bridging. However, periostin levels did not significantly explain $K_{c,initial}$ of female bone (Table 5.2), even though $K_{c,initial}$ was lower for 20-mo. than for 6-mo. female mice.

It is interesting to note the differences in glycosylation of lysine residues between males and females. Glycosylation of lysine residues is an important part for crosslink formation. While glycosylation of this specific residue has been detected before, Lys^{266} for females is different. Similarly, while the different stages of glycosylation (i.e., hydroxylysine, galactosyl-hydroxylysine and glucogalactosyl-hydroxylysine) were found for males on Lys^{254}, only galactosyl- hydroxylysine was detected for females at Lys^{254}. Alterations have previously been shown in disease models and have affected bone. Mutations in proteins that enable lysyl hydroxylation have reduced bone mass and increased bone fragility [239]; however, over-modification can cause fragility as well as seen in cases of osteogenesis imperfecta [249]. While there were no significant differences in the relative abundance of Lys^{254} alterations between young and older mice, it is important to note that this may not mean that there were not differences in crosslinks. Crosslinks form initially in an immature form and then in a series of reactions adapt into the mature form [230]. The pyridinoline (PYD) crosslink is a mature crosslink, and we have previously found this to be higher with age in this model. The ratio of immature to mature crosslinks may be differing in young and old mice, as opposed to differences in a specific lysine residue which forms these crosslinks.

Hydroxylation sites of proline and lysine are relatively consistent between young and old mice (Figures 5.6-5.9). Previous work has shown that prolyl hydroxylation is required for thermal stability and that under-hydroxylation decreases thermal stability [234]. Hydroxylation was lower for 20-mo. males on the sequence $^{405}GFP^{OH}GADGVAGP^{OH}K$, and the unmodified version of the peptide $^{960}GFP^{OH}GLP^{OH}GPSGEPGK$ was higher in older mice, suggesting that the modified version and thus hydroxylation was lower (Figures 5.6-5.9). Incidentally, these are both in the triple helical region of collagen. Males have shown differences in thermal stability

with age that were not seen in females, but this was in human samples [232]. Thermal stability may depend on factors besides hydroxylation sites. For instance, previous work has shown that an increase in AGEs prevents degradation, another measure of stability [235].

The increases in CML on both biglycan and collagen fit with previous findings that AGEs in bone increase with age [70, 196, 197]. As seen in Figure 5.2 and 5.3, the site of increased CML on collagen appears to be located on the C-terminal propeptide. This may mean that this increase is not related to changes in the structure of mature collagen or to its ability to form matrix; however, it could indicate an overall increase in AGEs in the matrix. Thomas et al. has previously detected CML on type I collagen in human bone using mass spectrometry. This modification was detected in the triple helix region, though this difference may be reflective of a different extraction protocol than the present method we used or analyzing humans as opposed to mice [236]. As with Thomas et al [236], there was a strong correlation between fracture toughness parameters and CML as seen in Table 5.2 and Figure 5.5 for males. Similarly, there were correlations with collagen CML levels and toughness for both males and females.

In addition to detecting CML on collagen, we were also able to detect CML on biglycan. Biglycan had higher CML values for old than for young adult mice, irrespective of sex. Using knock-out models, it has been shown that loss of biglycan lowers bone mass and density and may reduce yield energy [250]. Biglycan is also important for collagen fibril assembly, as knock-out mice have higher fibril diameters, more variability in the fibril diameter and less tight packing [251]. Indeed, biglycan and other proteoglycans are thought to have a role in fibrillogenesis, which may occur through binding to collagen [252]. Higher CML may alter biglycan's ability to interact with other proteins and its role in fibrillogenesis. To the best of the author's knowledge, the post-translational modification of CML has not been detected on

biglycan before. As with CML on collagen, CML levels on biglycan correlated strongly with fracture toughness parameters and with toughness. Interestingly, CML levels on biglycan also correlated with yield strength. Overall, CML had a negative impact on material properties and bound water. However, it should be noted that the sample size for correlation was small (n=12 across two age groups).

5.5 Conclusions

There were multiple post-translational modifications to the bone matrix proteins of the BALB/c mice which could affect the fracture resistance of bone. Notably, CML was higher with age on both biglycan and type I collagen in both sexes and could have an influence on material properties. There were few differences to enzymatic post-translational modifications with age. Mass spectrometry analysis of protein extracts from male bones indicated lower hydroxyproline at specific sites for older mice than for young adult mice, but this age-related change was not observed in females. Lastly, periostin was lower with age in males.

5.6 Acknowledgements

This work was funded in part by a training grant from NIDDK (DK101003), by a grant from the National Institute of Arthritis and Musculoskeletal and Skin Diseases (AR067871) and by the VA Office of Research and Development. The content is solely the responsibility of the authors and does not necessarily represent the official views of the National Institutes of Health or other funding agencies. I would also like to thank Dr. Paul Voziyan for all his help with the mass spectrometry analysis.

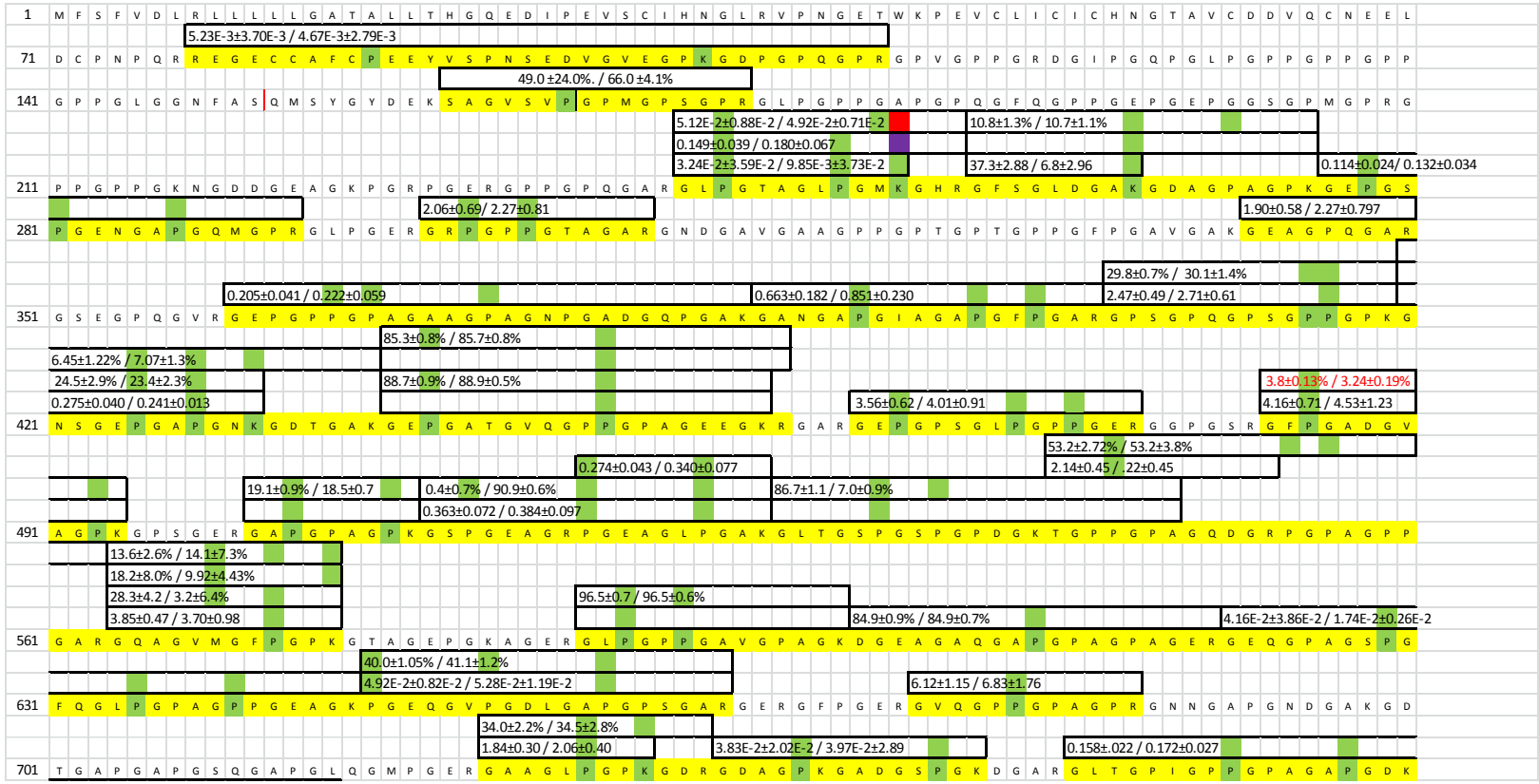

Figure 5.6 Post-translational modifications to partial sequence of collagen α-1 in males. Yellow indicates amino acid was detected, green indicates site for hydroxylation, red indicates site for galactosyl-hydroxylysine, purple indicates site for glucosylgalactosyl-hydroxylysine, and blue indicates site for carboxymethyl-lysine. Values are expressed as 6-mo. / 20-mo in the box above the detected sequence. If unmodified sequence was detected, peptide was expressed as percent modified. Otherwise, values are normalized to injected standards. Red font indicates significant difference.

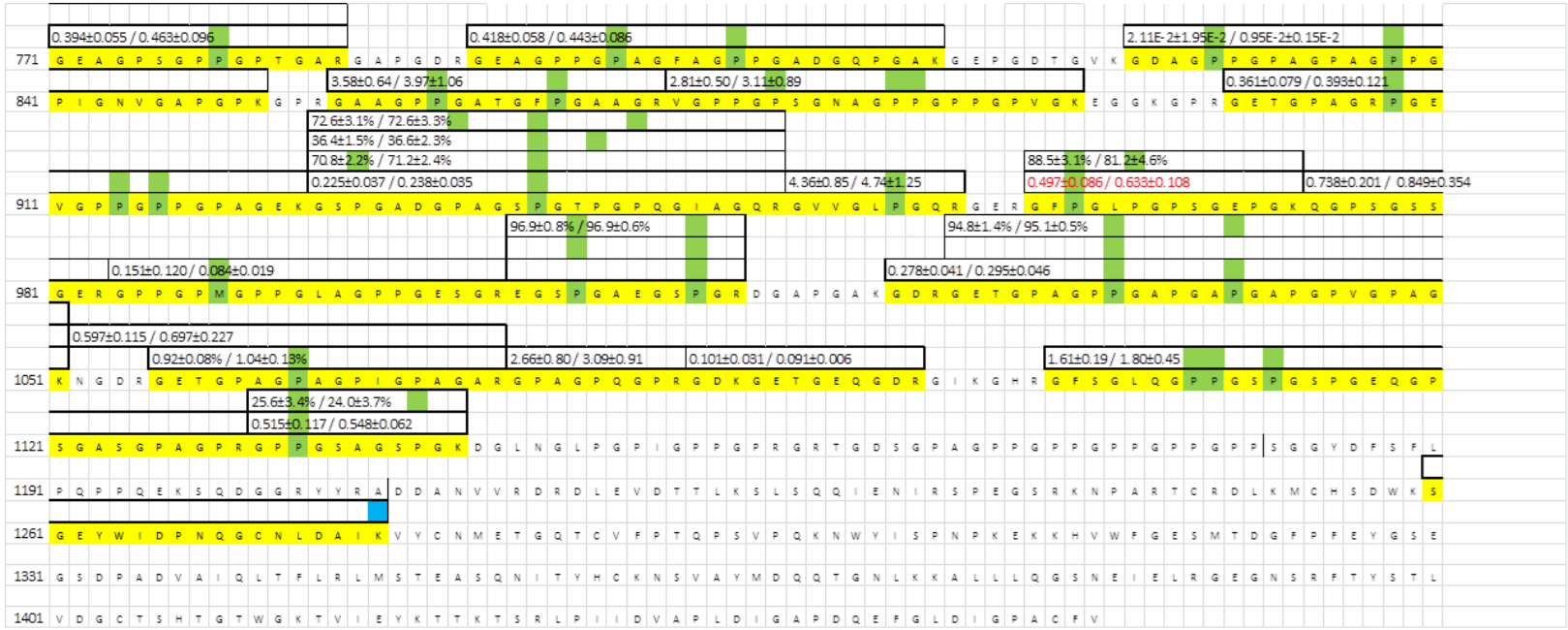

Figure 5.7 Post-translational modifications to partial sequence of collagen α-1 in males. Yellow indicates amino acid was detected, green indicates site for hydroxylation, red indicates site for galactosyl-hydroxylysine, purple indicates site for glucosylgalactosyl-hydroxylysine, and blue indicates site for carboxymethyl-lysine. Values are expressed as 6-mo. / 20-mo in the box above the detected sequence. If unmodified sequence was detected, peptide was expressed as percent modified. Otherwise, values are normalized to injected standards. Red font indicates significant difference.

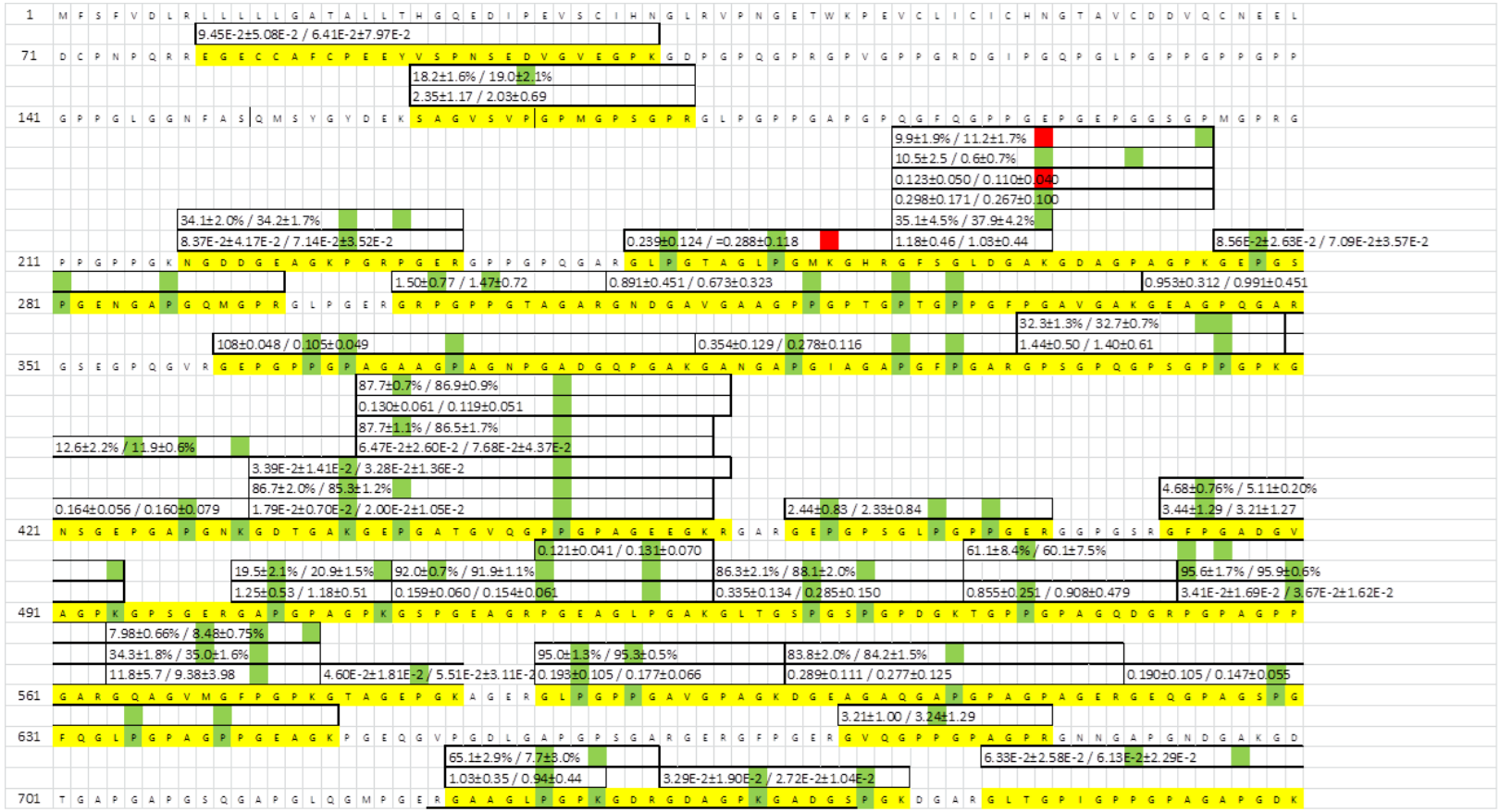

Figure 5.8 Post-translational modifications to partial sequence of collagen α-1 in females. Yellow indicates amino acid was detected, green indicates site for hydroxylation, red indicates site for galactosyl-lysine, purple indicates site for glucosylgalactosyl-lysine, and blue indicates site for carboxymethyl-lysine. Values are expressed as 6-mo. / 20-mo in the box above the detected sequence. If unmodified sequence was detected, peptide was expressed as percent modified. Otherwise, values are normalized to injected standards. Red font indicates significant difference.

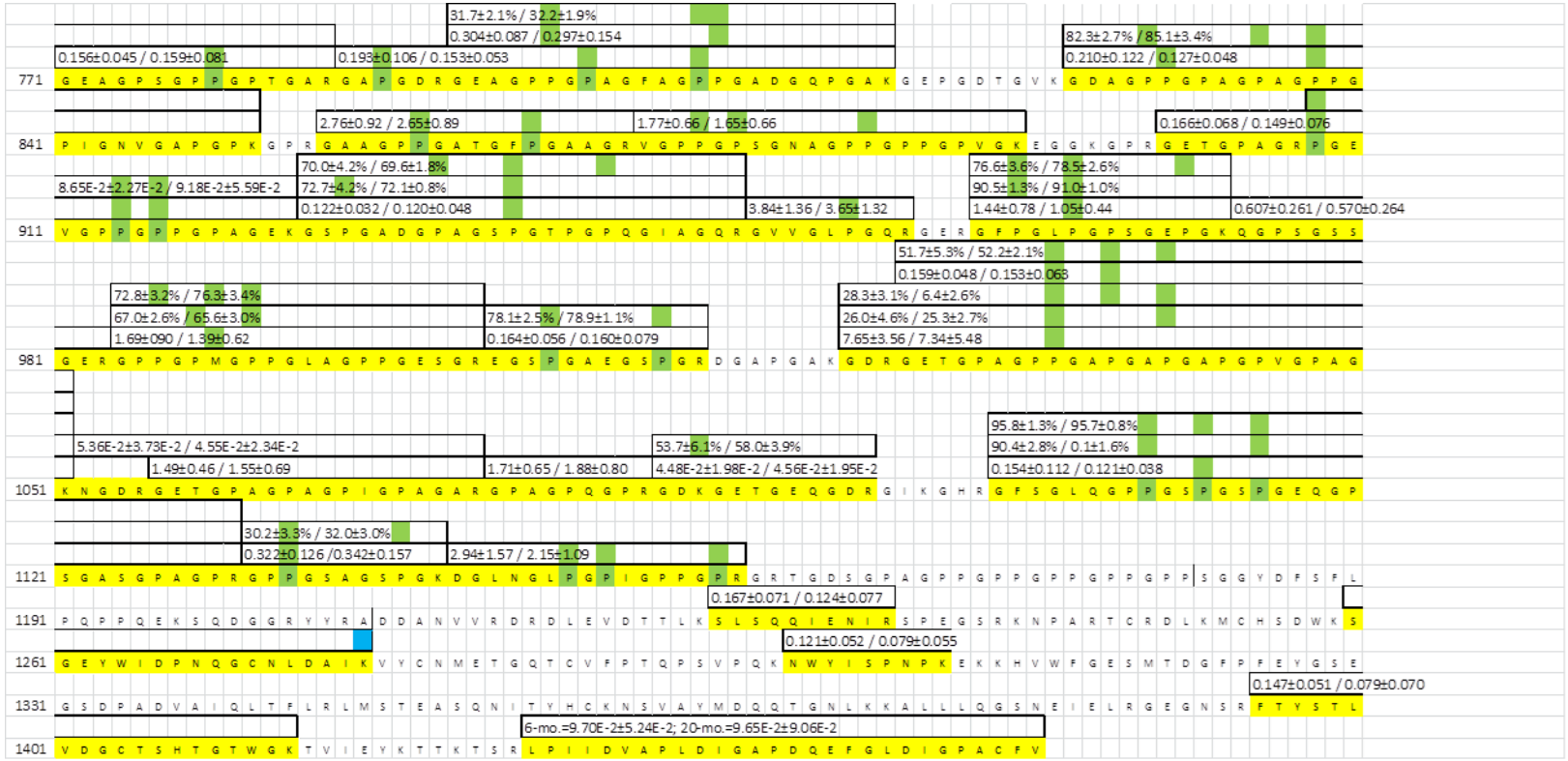

Figure 5.9 Post-translational modifications to partial sequence of collagen α-1 in females. Yellow indicates amino acid was detected, green indicates site for hydroxylation, red indicates site for galactosyl-hydroxylysine, purple indicates site for glucosylgalactosyl-hydroxylysine, and blue indicates site for carboxymethyl-lysine. Values are expressed as 6-mo. / 20-mo in the box above the detected sequence. If unmodified sequence was detected, peptide was expressed as percent modified. Otherwise, values are normalized to injected standards. Red font indicates significant differences

CHAPTER 6 CONCLUSIONS AND FUTURE WORK

6.1 Summary of Dissertation Findings

The extracellular matrix may contribute to the type 2 diabetes (T2D)- and age-related decreases in the fracture resistance of bone. This work has examined bone at multiple hierarchical levels organization from the whole-bone strength down to the nanostructure level composition and organization of collagen I. To start with, when examining a preclinical model of early-onset T2D, I found that the diabetic TallyHO mouse exhibits lower toughness than SWR/J controls. Bending strength was higher for diabetic mice at a younger age, but was no longer different as duration progressed. The ability of TallyHO bones to resist crack propagation showed no differences with age, though cracking toughness was lower with age in SWR/J mice but not in TallyHO mice. On the matrix level, the concentration of advanced glycaton end-products (AGEs) did not accumulate with an increase in the duration of T2D. However, enzymatic crosslink concentrations were higher with age in both strains. The TallyHO mice had higher mineral-matrix ratio and tissue mineral density which could be the cause of the lower toughness of the bones. However, Raman spectroscopy indicated there may have been alterations to the collagen helical structure as well. While there were some potential causes for lower toughness in TallyHO bones, a complicating factor for the model is that the control strain does not exhibit obesity and that there is much variability in the blood glucose levels of the TallyHO mice. Conversely, the BALB/c preclinical model for aging exhibited lower strength, toughness, and fracture toughness of the cortical bone with aging for both male and female mice. Enzymatic crosslinks and AGE crosslinks were higher in older mice. Similarly, mineral-to-matrix ratio and tissue mineral density were higher in the older mice than in the young adult mice. Using Raman spectroscopy analysis, differences in the Amide I band indicated that there may be age-related

changes in collagen I secondary structure. Analysis of bone by ^{1}H-NMR relaxometry showed that matrix-bound water was lower in older mice. Changes to the matrix continue to the protein level as measured by mass spectrometry. The relative amount of non-collagenous proteins, identified by mass spectrometry, did not generally vary with age. One exception was periostin, which was lower in older male mice, but did not vary between young adult and old female mice. Carboxymethyl-lysine (CML), an AGE adduct, was higher for both males and females on the non-collagenous protein biglycan and a propeptide region of collagen α1 chain. Overall, enzymatic collagen α1 modifications were consistent across ages, though hydroxylation was lower for a few specific sites with males and there were differences in lysine modifications between males and females. The levels of AGEs negatively correlated with toughness and bound water for the cortical bone of the BALB/c mice. Both with aging and T2D, there were differences in the matrix that could result in the lower fracture resistance observed for these models.

6.2 Major Conclusions

- Contrary to what would be expected from clinical studies of fracture risk in humans, the TallyHO model of T2D does not exhibit a progressive loss in fracture resistance with duration of the disease.
- There are differences in the bone matrix between the TallyHO mice and the non-diabetic SWR/J controls that could explain the low toughness phenotype of this diabetic mouse strain, namely higher mineralization density and higher Amide I sub-peak ratios indicative of lower helical order of the collagen I. However, this brittleness of the diabetic does not appear to be due to elevated AGEs, as would be expected for model of uncontrolled hyperglycemia.

- Fracture resistance is lower with age for the BALB/c mouse strain, as measured by yield strength, toughness, crack initiation toughness, and cracking toughness. This is consistent with what is observed for human bone with age.
- Multiple changes to the matrix occurred in the BALB/c preclinical model, including changes in mineralization, crosslinking, collagen structure, and bound water, making it an ideal preclinical model for therapeutics that target bone matrix quality.
- Non-fluorescent AGEs as measured by CML were higher in older mice and these higher levels of AGEs could explain the loss of toughness.
- Enzymatic PTMs to the bone matrix do not vary with age but non-enzymatic PTMs such as CML increase as mice age to 20 months

6.3 Future Directions

6.3.1 Validation of preclinical model of T2D

The TallyHO is an interesting model of T2D in that hyperglycemia is associated with obesity and has polygenic origin [174]. However, due to the lack of a littermate control and early onset obesity, it is difficult to separate out the effects of strain, body weight, and diabetic status. Mice could be treated with metformin, an antidiabetic drug that does not negatively affect bone [154], to reduce their glucose levels and thus limit one factor. TallyHO mice have been treated with metformin before. It has been shown to lower their glucose levels, though not to the level of the wild-type mice [253]. This study did not have information on bone phenotype. However, when MKR mice, another diabetic mouse model involving a mutation of the gene for insulin-like growth factor in the skeletal muscle, were given daily injections of metformin for 14 days, trabecular bone mineral density and trabecular bone volume (BV/TV) were higher than non-treated mice [254]. Additionally, while the TallyHO mice did not exhibit a progressive loss

in fracture resistance in our study, bones were analyzed at 16 weeks and 34 weeks. In humans, T2D increases fracture risk at ~10 years of duration [6]. Longer duration may be needed before progressive worsening is observed. However, results would still be affected by potential strain differences.

The KK-A^y/a mouse is another potential preclinical model for T2D. Like the TallyHO mouse, it is a polygenic model and it develops overt diabetes at approximately 8 weeks [170]. Unlike the TallyHO mice, these mice have a littermate control (a/a) which does not develop diabetes. Previous studies have shown altered bone phenotype, but so far, these studies have not utilized the proper a/a controls [171, 173]. One study has looked at the bones of KK-A^y/a mice compared to a/a mice, but this study did not assess the fracture resistance of the bones [184]. Interestingly, they did not observe a difference in pentosidine compared to controls at 20 weeks [184], but this is just one of many AGEs.

6.3.2 Determination of the effect of type 2 diabetes on the matrix of human bone

While preclinical models are important for research in order to determine treatment options, it is vital to relate this information back to what is seen clinically. Bone material strength index as measured through an impact micro-indentation method indicates that type 2 diabetics have compromised bone quality [47-49]. One group has measured pentosidine from samples from total hip arthroplasties, but did not find a difference [255]. More information is needed on the mechanical properties of bone and how this relates to the matrix in diabetic human samples.

We have been collecting cadaveric femurs from both diabetics and non-diabetics donors of varying ages. Similarly, we have been collecting the discarded femoral heads from total hip arthroplasties from both diabetic and non-diabetic patients. For future work, the structural and mechanical phenotype of these specimens will need to be characterized using μCT, tensile

testing of dog-bone specimens, and fracture toughness testing of notched specimens. Similarly, matrix information on the human samples will be collected using HPLC, Raman spectroscopy and ^{1}H-NMR.

6.3.3 Expansion of BALB/c mouse study

The study of BALB/c mice as a model of preclinical aging could be expanded on in multiple ways. Firstly, additional time points could be added at times such as 9, 12, and 16 months. This would help provide more insight as to the specific age when matrix characteristics peak and then decline. Such information would be useful to mechanistic studies with the goal of preventing specific changes in the matrix, thereby preventing the age-related decrease in mechanical properties. The bones of BALB/c mice have been studied at various points throughout their lifespans before; however, the material properties the bone and the matrix characteristics were not studied [142].

6.3.4 Treatment of preclinical model with therapeutics that target the matrix

Furthermore, as it was established that these mice could be a good preclinical model for the effects of therapeutics that target the matrix, the next step would be treating both male and female BALB/c mice with agents that may target the matrix and analyzing the bone phenotype. Two possibilities are raloxifene and pyridoxamine. Raloxifene may have a beneficial effect on bound water and yield properties [256]. It has previously had a beneficial effect on diabetic rats [129] and ovariectomized rabbits [223]. It has not been used so far in aging mice. Similarly, another option would be treating the mice with pyridoxamine, an AGE-inhibitor [257]. This may be particularly interesting given the BALB/c showed strong correlations between increases in AGEs and decreases in material properties. Diabetic mice treated with pyridoxamine showed lower levels of CML in their kidneys [131] and diabetic rats treated with pyridoxamine showed

lower levels of CML in skin and retinal tissue [225, 226]. Pyridoxamine improved material properties of bone measured with reference point indentation with in vitro incubation [224]; however, how pyridoxamine affects the bone of aging mice remains to be seen.

6.3.5 Determination of effect of post-translational modifications on the structure of bone matrix proteins

In order to truly understand the impact of the post-translational modifications, it would need to be observed whether or not these changes caused changes to overall structure. This would be done through molecular dynamic simulations, incorporating the changes that were observed with aging with regards to CML. Notably, it would be interesting to also see if there were changes with regards to males and females as far as structural changes to the collagen molecule that may occur through the differences in lysine glycosylation or if this solely has an effect on crosslinking. It would also be interesting to see if CML would alter the ability of biglycan to bind to collagen, as this may be important to its role in fibrillogenesis [252].

6.3.6 Further determination of relationship between post-translational modifications and bone material properties

For the post-translational modifications of matrix proteins, it is important to note that due to experimental constraints, the sample size was limited. That being said, it would be interesting, especially with regards to AGEs such as CML to see if correlations existed between these AGEs and material properties. For this assay, it would be ideal to switch to detecting CML using an ELISA assay, as recently demonstrated by Thomas et al. [236]. The exact relationship between post-translational modifications of proteins and material properties would need to be ascertained through a combination of molecular dynamic simulations and characterizing a wider range of samples using other assays. For instance, while not done here, it would be useful to determine

the melting behavior of collagen. This would give an idea if there were any differences with age that were not detected with mass spectrometry and if there were any differences between sexes.

6.3.7 Determination of post-translational modifications to bone matrix proteins of humans

As with the diabetic study, it will be important to relate what we found for post-translational modifications in murine bone to what occurs in human bone. We are currently analyzing bones from high fracture resistance and low fracture resistance groups to determine if there are differences in non-collagenous protein levels and post-translational modifications to bone matrix proteins.

REFERENCES

1. Burge, R., Dawson-Hughes, B., Solomon, DH, Wong, JB, King, A., Tosteson, A., *Incidence and Economic Burden of Osteoporosis-Related Fractures in the United States, 2005-2025*. Journal of Bone and Mineral Research, 2007. **22**(3): p. 465-475.

2. Center, J., Nguyen, TV, Schneider, D, Sambrook, PN, Eisman, JA, *Mortality after all major types of osteoporotic fracture in men and women: an observational study.* The Lancet, 1999. **353**: p. 878-882.

3. Gullberg, B., Johnell, O, Kanis, JA, *World-wide Projections for Hip Fracture*. Osteoporosis International, 1997. **7**: p. 407-413.

4. Oden, A., McCloskey, EV, Kanis, JA, Harvey, NC, Johansson, H, *Burden of high fracture probability worldwide: secular increases 2010-2040.* Osteoporosis International, 2015. **26**: p. 2243-2248.

5. Schwartz, A.V., Vittinghoff, E., Bauer, DC, Hillier, TA, Strotmeyer, ES, Ensrud, KE, Donaldson, Meghan G., Cauley, Jane A., Harris, Tamara B., Koster, Annemarie, Womack, Catherine R., Palermo, Lisa, Black, Dennis M., *Association of BMD and FRAX Score with Risk of Fracture in Older Adults with Type 2 Diabetes* JAMA, 2011. **305**(21): p. 2184-2192.

6. Majumdar, S.R., Leslie, William D., Lix, Lisa M., Morin, Suzanne N., Johansson, Helena, Oden, Anders, McCloskey, Eugene V., Kanis, John A., *Longer Duration of Diabetes Strongly Impacts Fracture Risk Assessment: The Manitoba BMD Cohort.* Journal of Clinical Endocrinology and Metabolism, 2016. **101**(11): p. 4489-4496.

7. Siris, E., Brenneman, SK, Barrett-Connor, E, Miller, PD, Sajjan, S, Berger, ML, Chen, YT, *The effect of age and bone mineral density on the absolute, excess, and relative risk of fracture in postmenopausal women aged 50-99: results from the National Osteoporosis Risk Assessment (NORA).* Osteoporosis International, 2006(17): p. 565-574.

8. Kanis, J., Johnell, O., Oden, A., Dawson, A., De Laet, C., Jonsson, B., *Ten Year Probabilities of Osteoporotic Fractures According to BMD and Diagnostic Thresholds.* Osteoporosis International, 2001(12): p. 989-995.

9. Hernandez, C.J., Keaveny, T.M, *A biomechanical perspective on bone quality*. Bone, 2006. **39**: p. 1173-1181.

10. Nyman, J.S., Makowski, A.J., *The Contribution of the Extracellular Matrix to the Fracture Resistance of Bone.* Current Osteoporosis Reports, 2010. **8**(2).

11. Rho, J.-Y., Kuhn-Spearing, Lisa, Zioupos, Peter, *Mechanical properties and the hierarchical structure of bone.* Medical Engineering and Physics, 1998. **20**: p. 92-102.

12. Burton, B., Gaspar, A, Josey, D, Tupy, J, Grynpas, MD, Willett, TL, *Bone embrittlement and collagen modifications due to high-dose gamma-irradiation sterilization.* Bone, 2014. **61**(C): p. 71-81.

13. Garnero, P., *The Role of Collagen Organization on the Properties of Bone.* Calcified Tissue International, 2015. **97**: p. 229-240.

14. Unal, M., Akkus, O, *Raman spectral classification of mineral- and collagen-bound water's associations to elastic and post-yield mechanical properties of cortical bone.* Bone, 2015. **81**(3): p. 15-26.

15. Saito, M., Marumo, K., *Collagen crosslinks as a determinant of bone quality: a possible explanation for bone fragility in aging, osteoporosis, and diabetes mellitus.* Osteoporosis International, 2010. **21**: p. 195-214.

16. Tang, S.Y., Zeenath, U., Vashishth, D., *Effects of non-enzymatic glycation on cancellous bone fragility*. Bone, 2007. **40**: p. 1144-1151.

17. Saito, M., Kida, Yoshikuni, Kato, Soki, Marumo, Keishi, *Diabetes, Collagen and Bone Quality*. Current Osteoporosis Reports, 2014. **12**: p. 181-188.

18. Poundarik, A.A., Wu, Ping-Cheng, Evis, Zafer, Sroga, Grazyna E., Ural, Ani, Rubin, Mishaela, Vashishth, Deepak, *A direct role of collagen glycation in bone fracture* Journal of the Mechanical Behavior of Biomedical Materials, 2015. **52**: p. 120-130.

19. Granke, M., Does, MD, Nyman, JS, *The role of water compartments in the material properties of cortical bone.* Calcified Tissue International, 2015. **97**(3): p. 292-307.

20. Morgan, S., Poundarik, AA, Vashishth, D, *Do Non-collagenous Proteins Affect Skeletal Mechanical Properties?* Calcified Tissue International, 2015. **97**: p. 281-291.

21. Unal, M., Creecy, A., Nyman, JS, *The Role of Matrix Composition in the Mechanical Behavior of Bone.* Current Osteoporosis Reports, 2018. **16**(3): p. 205-215.

22. Reznikov, N., Shahar, Ron, Weiner, Steve, *Bone hierarchical structure in three dimensions.* Acta Biomaterialia, 2014. **10**: p. 3815-3826.

23. *Bone Mechanics Handbook*. 2 ed, ed. S.C. Cowin. 2001: CRC Press LLC.

24. Bartel, D.L., Davy, Dwight T., Keaveny, Tony M., *Orthopaedic Biomechanics: Mechanics and Design in Musculoskeletal Systems*. 2006, Upper Saddle River, New Jersey: Peardson Prentice Hall.

25. Turner, C.H., Burr, D.B., *Basic Biomechanical Measurements of Bone: A Tutorial*. Bone, 1993. **14**: p. 595-608.

26. Boskey, A.L., Wright, T. M., Blank, R. D., *Collagen and Bone Strength.* Journal of Bone and Mineral Research, 1999. **14**(3): p. 330-336.

27. Burr, D., *The Contribution of the Organic Matrix to Bone's Material Properties.* Bone, 20002. **31**(1): p. 8-11.

28. Chavassieux, P., Seeman, E., Delmas, P.D., *Insights into Material and Structural Basis of Bone Fragility from Diseases Associated with Fractures: How Determinants of the Biomechanical Properties of Bone Are Compromised by Disease.* Endocrine Reviews, 2007. **28**(2): p. 151-164.

29. Fratzl, P., Gupta, H.S., Paschalis, E.P., Roschger, P., *Structure an mechanical quality of the collagen-mineral nano-composite in bone.* Journal of Material Chemistry, 2004. **14**: p. 2115-2123.

30. O'Brien, F.J., Taylor, David, Lee, T. Clive, *The effect of bone microstructure on the initiation and growth of microcracks.* Journal of Orthopaedic Research, 2005. **23**: p. 475-480.

31. Hernandez, C., van der Meulen, MCH, *Understanding Bone Strength Is Not Enough.* Journal of Bone and Mineral Research, 2017. **32**(6): p. 1157-1162.

32. Peterlik, H., Roschger, Paul, Klaushofer, Klaus, Fratzl, Peter, *From brittle to ductile fracture of bone.* Nature Materials, 2006. **5**: p. 52-54.

33. Nyman, J., Creecy, A, *Material Properties of Diabetic Bone*, in *Diabetic Bone Disease*, B. Lecka-Czernik, Fowlkes, J, Editor. 2016, Springer, Cham.

34. Nyman, J., Granke, M., Singleton, RC, Pharr, GM, *Tissue-Level Mechanical Properties of Bone Contributing to Fracture Risk.* Current Osteoporosis Reports, 2016. **14**(4): p. 138-150.

35. McCloskey, E., Oden, A, Harvey, NC, Leslie, WD, Hans, D, Johansson, H et al. , *A Meta-Analysis of Trabecular Bone Score in Fracture Risk Prediction and Its Relationship to FRAX.* Journal of Bone and Mineral Research, 2016. **31**(5): p. 940-948.

36. Siris, E., Chen, Y-T, Abbot, TA, Barrett-Connor, E, Miller, PH, Wehren, LE et al, *Bone mineral density thresholds for pharmacological intervention to prevent fractures.* Archives of Internal Medicine, 2004. **164**(10): p. 1108-1112.

37. Manhard, M., Nyman, JS, Does, MD, *Advances in imaging approaches to fracture risk evaluation.* Translational Research, 2017. **181**: p. 1-14.

38. Sundh, D., Nilsson, AG, Nilsson, M., Johansson, L., Mellstrom, D., Loretzon, M., *Increased cortical porosity in women with hip fracture.* Journal of Internal Medicine, 2017. **281**(5): p. 496-506.

39. Kral, R., Osima, M., Borgen, TT, Vestgaard, R., Richardsen, E., Bjornerem, A., *Increased cortical porosity and reduced cortical thickness of the proximal femur are associated with nonvertebral fracture independent of Fracture Risk Assessment Tool and Garvan estimates in postmenopausal women.* PLOSOne, 2017.

40. Liu, X., Stein, EM, Zhou, B., Zhang, CA, Nickolas, TL, Cohen, A., Thomas, V., McMahon, DJ, Cosman, F., Nieves, J., Shane, E., Guo XE, *Individual Trabecula Segmentation (ITS)-Based Morphological Analyses and Microfinite Element Analysis of HR-pQCT Images Discriminate Postmenopausal Fragility Fractures Independent of DXA Measurements.* Journal of Bone and Mineral Research, 2012. **27**(2): p. 263-272.

41. Diez-Perez, A., Bouxsein, ML, Eriksen, EF, Khosla, S., Nyman, JS, Papapoulos, S et al, *Technical note: Recommendations for a standard procedure to assess cortical bone at the tissue-level in vivo using impact microindentation.* Bone Reports, 2016. **5**: p. 181-185.

42. Allen, M., McNerny, EM, Organ, JM, Wallace, JM, *True Gold or Pyrite: A Review of Reference Point Indentation for Assessing Bone Mechanical Properties In Vivo.* Journal of Bone and Mineral Research, 2015. **30**(9): p. 1539-1550.

43. Malgo, F., Hamdry, NAT, Papaoulos, SE, Appelman-Dijkstra, NM, *Bone Material Strength as Measured by Microindentation In Vivo is Decreased in Patients With Fragility Fractures Independently of Bone Mineral Density.* Journal of Endocrinology & Metabolism, 2015. **100**(5): p. 2039-2045.

44. Sosa, D., Eriksen, EF, *Reduced Bone Material Strength is Associated with Increased Risk and Severity of Osteoporotic Fractures. An Impact Microindentation Study.* Calcified Tissue International, 2017(101): p. 34-42.

45. Rudang, R., Zoulakis, M, Sundh, D, Brisby, H, Diez-Perez, A, Johansson, L, et al, *Bone material strength is associated with areal BMD but not with prevalent fractures in older women.* Osteoporosis International, 2016. **27**(4): p. 1585-1592.

46. Rozental, T., Walley, KC, Demissie, S., Caksa, S, Martinez-Betancourt, A, Parker, AM et al, *Bone material strength index as measured by impact microindentation in postmenopausal women with distal radius and hip fractures.* Journal of Bone and Mineral Research, 2017: p. 1-22.

47. Farr, J., Drake, MT, Amin, S, Melotn, LJ, McCready, LLK, Khosla, S, *In vivo assessment of bone quality in postmenopausal women with type 2 diabetes* Journal of Bone and Mineral Research, 2014. **29**(4): p. 787-795.

48. Furst, J.R., Bandeira, Leonardo, C., Fan, Wen-Wei, Agarwal, Sanchita, Nishiyama, Kyle K., McMahon, Donald J., Dworakowski, Elzbieta, Jiang, Hongfeng, Silverberg, Shonni J., Rubin, Mishaela R., *Advanced Glycation Endproducts and Bone Material Strength in Type 2 Diabetes.* Journal of Clinical Endocrinology and Metabolism, 2016. **101**(6): p. 2502-2510.

49. Nilsson, A.G., Sundh, Daniel, Johansson, Lisa, Nilsson, Martin, Mellstrom, Dan, Rudang, Robert, Zoulakis, Michail, Wallander, Marit, Darelid, Anna, Lorentzon, Mattias, *Type 2 Diabetes Mellitus Is Associated With Better Bone Microarchitecture But Lower Bone Material Strength and Poorer Physical Function in Elderly Women: A Population-Based Study.* Journal of Bone and Mineral Research, 2017. **32**(5): p. 1062-1071.

50. Schwartz, A.V., *Epidemiology of fractures in type 2 diabetes.* Bone, 2016. **82**: p. 2-8.

51. Niebur, G., Feldstein, MJ, Yuen, JC, Chen, TJ, Keaveny, TM, *High-resolution finite element models with tissue strength assymetry accurate predict failure of trabecular bone.* Journal of Biomechanics, 2000. **33**(12): p. 1575-1583.

52. Koester, K., Ager, JW, Ritchie, RO, *The true toughness of human cortical bone measured with realistically short cracks.* Nature Materials, 2008. **7**(8): p. 672-677.

53. Hansen, U., Zioupos, P, Simpson, R, Currey, JD, Hynd, D, *The effect of strain rate on the mechanical properties of human cortical bone.* Journal of Biomechanical Engineering 2008. **130**(1).

54. Landrigan, M., Roeder, RK, *Systematic error in mechanical measures of damage during four-point bending fatigue of cortical bone.* Journal of Biomechanics, 2009. **42**(9): p. 1212-1217.

55. Yeni, Y., Shaffer, RR, Baker, KC, Dong, XN, Grimm, MJ, Les, CM, et al, *The effect of yield damage on the viscoelastic properties of cortical bone tissue as measured by dynamic mechanical analysis.* Journal of Biomedical Materials Research, 2007. **82**(3): p. 530-537.

56. Zimmermann, E., Busse, B, Ritchie, RO, *The fracture mechanics of human bone: influence of disease and treatment.* BoneKey Reports, 2015. **4**: p. 743.

57. Terajima, M., Perdivara, Irina, Sricholpech, Marnisa, Deguchi, Yoshizumi, Pleshko, Nancy, Tomer, Kenneth B., Yamauchi, Mitsuo, *Glycosylation and Cross-linking in Bone Type I Collagen.* Journal of Biological Chemistry, 2014. **289**(33): p. 22636-22647.

58. Gautieri, A., Vesentini, Simone, Redaelli, Alberto, Buehler, Markus J., *Hierarchical Structure and Nanomechanics of Collagen Microfibrils from the Atomistic Scale Up.* Nano Letters, 2011(11): p. 757-766.

59. Nair, A.K., Gautieri, Alfonso, Chang, Shu-Wei, Buehler, Markus J., *Molecular mechanics of mineralized collagen fibrils in bone.* Nature Communications, 2013. **4**(1724).

60. Gallant, M., Brown, DM, Hammond, M., Wallace, JM, Du, J., Deymier-Black, AC, Almer, JD, Stock, SR, Allen, MR, Burr, DB, *Bone cell-independent benefits of raloxifene on the skeleton: A novel mechanism for improving bone material properties.* Bone, 2014. **61**: p. 191-200.

61. Eyre, D., Weis, MA, *Bone collagen: new clues to its mineralization mechanism from recessive osteogenesis imperfecta.* Calcified Tissue International, 2013. **93**(4): p. 338-347.

62. Cabral, W.A., Perdivara, Irina, Weis, MaryAnn, Terajima, Masahiko, Blissett, Angela R., Chang, Weizhong, Perosky, Joseph E., Makareeva, Elena N., Mertz, Edward L., Leikin, Sergey, Tomer, Kenneth B., Kozloff, Kenneth M., Eyre, David R., Yamauchi, Mitsuo, Marini, Joan C., *Abnormal Type I Collagen Post-translational Modification and Crosslinking in a Cyclophilin B KO Mouse Model of Recessive Osteogenesis Imperfecta.* PLOS Genetics, 2014. **10**(6): p. e1004465.

63. Schrof, S., Varga, Peter, Hesse, Bernhard, Schone, Martin, Schutz, Roman, Masic, Admir, Raum, Kay, *Multimodal correlative investigation of the interplaying microarchitecture, chemical composition and mechanical properties of human cortical bone tissue reveals predominant role of fibrillar organization in determining microelastic tissue properties* Acta Biomaterialia, 2016. **44**: p. 51-64.

64. Granke, M., Gourrier, Aurelien, Rupin, Fabienne, Raum, Kay, Peyrin, Francoise, Burghammer, Manfred, Saied, Amena, Laugier, Pascal, *Microfibril Orientation Dominates the Microelastic Properties of Human Bone Tissue at the Lamellar Length Scale.* PLOSOne, 2013. **8**(3): p. e58043.

65. Jimenez-Palomar, I., Shipov, Anna, Shahar, Ron, Barber, Asa H., *Structural orientation depedent sub-lamellar bone mechanics.* Journal of the Mechanical Behavior of Biomedical Materials, 2015. **52**: p. 63-71.

66. Makowski, A.J., Uppuganti, S., Wadeer, S.A., Whitehead, J.M., Rowland, B.J., Granke, M., Mahadevan-Jansen, A., Yang, X., Nyman, J.S., *The loss of activating transcription factor 4 (ATF4) reduces bone toughness and fracture toughness.* Bone, 2014. **62**: p. 1-9.

67. Karunaratne, A., Xi, L., Bentley, L., Sykes, D., Boyde, A., Esapa, C.T., Terrill, N.J., Brown, S.D.M., Cox, R.D., Thakker, R.V., Gupta, H.S., *Multiscale alterations in bone matrix quality increased fragility in steroid induced osteoporosis.* Bone, 2016. **84**(15-24).

68. McNerny, E., Gong, B, Morris, MD, Kohn, DH, *Bone Fracture Toughness and Strength Correlate With Collagen Cross-Link Maturity in a Dose-Controlled Lathyrism Mouse Model.* Journal of Bone and Mineral Research, 2015. **30**(3): p. 446-455.

69. Berteau, J.-P., Gineyts, Evelyne, Pithioux, Martine, Baron, Cecile, Boivin, Georges, Lasaygues, Philippe, Chabrand, Patrick, Follet, Helene, *Ratio between mature and immature enzymatic cross-links correlates with post-yield cortical bone behavior: An insight into greenstick fractures of the child fibula*. Bone, 2015. **79**: p. 190-195.

70. Uppuganti, S., Granke, Mathilde, Makowski, Alexander J., Does, Mark D., Nyman, Jeffry S., *Age-related changes in the fracture resistance of male Fischer F344 rat bone.* Bone, 2016. **83**: p. 220-232.

71. Schmidt, F.N., Zimmermann, E.A., Campbell, G.M., Sroga, G.E., Puschel, K., Amling, M., Tang, S.Y., Vashishth, D., Busse, B., *Assessment of collagen quality associated with non-enzymatic cross-links in human bone using Fourier-transform infrared imaging.* Bone, 2017. **97**: p. 243-251.

72. Karim, L., Tang, SY, Sroga, GE, Vashishth, D, *Differences in non-enzymatic glycation and collagen cross-links between human cortical and cancellous bone*. Osteoporosis International, 2013. **24**(9): p. 2441-2447.

73. Willett, T., Sutty, S, Gaspar, A, Avery, N, Grynpas, M, *In vitro non-enzymatic ribation reduces post-yield strain accommodation in cortical bone.* Bone, 2013. **52**(6): p. 611-622.

74. Poundarik, A., Wu, PC, Evis, Z, Sroga, GE, Ural, A, Rubin, M, *A direct role of collagen glycation in bone fracture*. Journal of Mechanical Behavior of Biomedical Materials, 2015. **52**: p. 120-130.

75. Willems, N.M.B.K., Langenbach, Geerling E.J., Stoop, Reinout, den Toonder, Jaap M.J., Mulder, Lars, Zentner, Andrej, Everts, Vincent, *Higher number of pentosidine cross-links induced by ribose does not alter tissue stiffness of cancellous bone.* Materials Science and Engineering C, 2014. **42**: p. 15-21.

76. Rubin, M.R., Paschalis, Eleftherios P., Poundarik, Atharva, Sroga, Gyna E., McMahon, Donald J., Gamsjaeger, Sonja, Klaushofer, Klaus, Vashishth, Deepak, *Advanced Glycation Endproducts and Bone Material Properties in Type 1 Diabetic Mice.* PLOSOne, 2016. **11**(5).

77. Fantner, G.E., Hassenkam, Tue, Kindt, Johannes H., Weaver, James C., Birkedal, Henrik, Pechenik, Leonid, Cutroni, Jacqueline A., Cidade, Geraldo A. G., Stucky, Galen D., Morse, Daniel E., Hansma, Paul K. , *Sacrificial bonds and hidden length dissipate energy as mineralized fibrils separate during bone fracture.* Nature Materials 2005. **4**: p. 612-616.

78. Poundarik, A.A., Diab, T., Sroga, G.E., Ural, A., Boskey, A.L., Gundberg, C.M., Vashishth, D. , *Dilatational band formation in bone.* PNAS, 2012. **109**(47): p. 19178-19183.

79. Maruyama, N., Shibata, Yo, Mochizuki, Ayako, Yamada, Atsushi, Maki, Koutaro, Inoue, Tomio, Kamijo, Ryutaro, Miyazaki, Takashi, *Bone micro-fragility caused by the mimetic aging processes in a-klotho deficient mice: In situ nanoindentation assessment of dilatational bands.* Biomaterials, 2015. **47**: p. 62-71.

80. Bailey, S., Karsenty, Gerard, Gundberg, Caren, Vashishth, Deepak, *Osteocalcin and osteopontin influence bone morphology and mechanical properties.* Annals of the New York Academy of Sciences, 2017: p. 1-6.

81. Pasteris, J., Yoder, CH, Wopenka, B, *Molecular water in nominally unhydrated carbonated hydroxylapatitde: The key to a better understanding of bone mineral.* American Mineraologist. **99**(1): p. 16-27.

82. Stock, S., *The Mineral-Collagen Interface in Bone.* Springer US, 2015: p. 1-19.

83. Pasteris, J., *A mineraological view of apatitic biomaterials.* American Mineralogist, 2016. **101**(12): p. 2594-2610.

84. Currey, J., *The mechanical consequences of variation in the mineral content of bone.* Journal of Biomechanics, 1969. **2**(1): p. 1-11.

85. Bala, Y., Seeman, E., *Bone's Material Constituents and their Contribution to Bone Strength in Health, Disease, and Treatment.* 2015: p. 1-19.

86. Almer, J., Stock, SR, *Micromechanical response of mineral and collagen phases in bone.* Journal of Structural Biology, 2007. **157**(2): p. 365-370.

87. Deymier-Black, A., Yuan, F, Singhal, A, Almer, JD, Brinson, LC, Dunand, DC, *Evolution of load transfer between hydroxyapatite and collagen during creep deformation of bone.* Acta Biomaterialia, 2012. **8**(1): p. 253-261.

88. Donnelly, E., *Methods for assessing bone quality: a review.* Clinical Orthopaedics and Related Research, 2011. **469**(8): p. 2128-2138.

89. Paschalis, E., Gamsjaeger, S, Klaushofer, K, *Vibrational spectroscopic techniques to assess bone quality.* Osteoporosis International, 2017: p. 1-17.

90. Akkus, O., Adar, F, Schaffler, MB, *Age-related changes in physicochemical properties of mineral crystals are related to impaired mechanical function of cortical bone.* Bone, 2004. **34**(3): p. 443-453.

91. Donnelly, E., Chen, DX, Boskey, AL, Baker, SP, van der Meulen, MCH, *Contribution of mineral to bone structural behavior and tissue mechanical properties.* Calcified Tissue International, 2010. **87**(5): p. 450-460.

92. Zhang, R., Gong, H, Zhu, D Ma, R, Fang, J, Fan, Y, *Multi-level femoral morphology and mechanical properties of rats of different ages.* Bone, 2015. **76**: p. 76-87.

93. Roschger, P., Misof, B, Paschalis, E, Fratzl, P, Klaushofer, K, *Changes in the Degree of Mineralization iwth Osteoporosis and its Treatment.* Current Osteoporosis Reports, 2014. **12**(3): p. 338-350.

94. Vennins, S., Desyatova, A, Turner, JA, Watson, PA, Lappe, JM, Recker, RR et al, *Intrinsic material property differences in bone tissue from patients suffering low-trauma osteoporotic fractures, compared to matched non-fracturing women.* Bone, 2017. **97**(C): p. 233-242.

95. Lloyd, A., Gludovatz, B, Riedel, C, Luengo, EA, Saiyed, R, Marty, E, et al, *Atypical fracture with long-term bisphosphonate therapy is associated with altered cortical composition and reduced fracture resistance.* PNAS, 2017. **114**(33): p. 8722-8727.

96. Roschger, P., Fratzl-Zelman, N, Misof, BM, Glorieux, FH, Klaushofer, K, Rauch, F, *Evidence that abnormal high bone mineralization in growing children with osteogenesis imperfecta is not associated with specific collagen mutations.* Calcified Tissue International, 2008. **82**(4): p. 263-270.

97. Fratzl-Zelman, N., Schmidt, I, Roschger, P, Glorieux, FH, Klaushofer, K, Fratzl, P et al, *Mineral particle size in children with osteogenesis imperfecta type I is not increased independently of specific collagen mutations.* Bone, 2914. **60**: p. 122-128.

98. Imbert, L., Auregan, J-C, Pernelle, K, Hoc, T, *Mechanical and mineral properties of osteogenesis imperfecta human bones at the tissue level.* Bone, 2014. **65**: p. 18-24.

99. Vanleene, M., Porter, A, Guillot, P-V, Boyde, A, Oyen, M, Shefelbine, S, *Ultra-structural defects cause low bone matrix stiffness despite high mineralization in osteogenesis imperfecta mice.* Bone, 2012. **50**(6): p. 1317-1323.

100. Carriero, A., Zimmermann, E.A., Paluszny, A., Tang, S.Y., Bale, H., Busse, B., Alliston, T., Kazakia, G., Ritchie, R.O., Shefelbine, S.J., *How tough is Brittle Bone? Investigating Osteogenesis Imperfecta in Mouse Bone.* Journal of Bone and Mineral Research, 2014.

101. Fratzl-Zelman, N., Bachinger, HP, Vranka, JA, Roschger, P, Klaushofer, K, Rauch, F, *Bone matrix hypermineralization in prolyl-3 hydroxylase 1 deficient mice.* Bone, 2016. **85**: p. 15-22.

102. Vranka, J., Pokidysheva, E, Hayashi, L, Zientek, K, Mizuno, K, Ishikawa, Y et al, *Prolyl-3 hydroxylase 1 null mice display abnormalities in fibrillar collagen-rich tissues such as tendons, skin, and bones.* Journal of Biological Chemistry, 2010. **285**(22): p. 17253-17262.

103. Bousson, V., Bergot, C, Wu, Y, Jolivet, E, Zhou, LQ, Laredo, J-D, *Greater tissue mineralization heterogeneity in femoral neck cortex from hip-fractured females than controls. A microradiographic study.* Bone, 2011. **48**(6): p. 1252-1259.

104. Tamminen, I., Misof, Roschger, P, Mayranpaa, MK, Turunen, MJ, Isaksson, H et al, *Increased heterogeneity of bone matrix mineralization in pediatric patients prone to fractures: a biopsy study.* Journal of Bone and Mineral Research, 2014. **29**(5): p. 1110-1117.

105. Gourion-Arsiquaud, S., Lukashova, L, Power, J, Loveridge, N, Reeve, J, Boskey, AL, *Fourier transform infrared imaging of femoral neck bone: reduced heterogeneity of mineral-to-matrix and carbonate-to-phosphate and more variable crystallinity in treatment-naive fractures cases compared with fracture-free controls.* Journal of Bone and Mineral Research, 2013. **28**(1): p. 150-161.

106. Milovanovic, P., Rakocevic, Z, Djonic, D, Zivkovic, V, Hahn, M, Nikolic, S, et al, *Nano-structural, compositional and micro-architectectural signs of cortical bone fragility at the*

superolateral femoral neck in elderly hip fracture patients vs. healthy aged controls. Experimental Gerontology, 2014. **55**: p. 19-28.

107. Demirtas, A., Curran, E, Ural, A, *Assessment of the effect of reduced compositional heterogeneity on fracture resistance of human cortical bone using finite element modeling.* Bone, 2016. **91**: p. 92-101.

108. Granke, M., Makowski, AJ, Uppuganti, S, Nyman, JS, *Prevalent role of porosity and osteonal area over mineralization heterogeneity in the fracture toughness of human cortical bone.* Journal of Biomechanics, 2016. **49**(13): p. 2748-2755.

109. Torres, A., Matheny, JB, Keaveny, TM, Taylor, D, Rimnac, CM, Hernandez, CJ, *Material heterogeneity in cancellous bone promoted deformation recovery after mechanical failure.* PNAS, 2016.

110. Farlay, D., Panczer, G, Rey, C, Delmas, PD, Boivin, G, *Mineral maturity and crystallinity index are distinct characteristics of bone mineral.* Journal of Bone and Mineral Metabolism, 2013. **28**(4): p. 433-435.

111. Bala, Y., Farlay, D, Boivin, G, *Bone mineralization: from tissue to crystal in normal and pathological contexts.* Osteoporosis International, 2013. **24**(8): p. 2153-2166.

112. Bi, X., Patil, CA, Lynch, CC, Pharr, GM, Mahadevan-Jansen, A, Nyman, JS, *Raman and mechanical properties correlate at whole bone- and tissue-levels in a genetic mouse model.* Journal of Biomechanics, 2011. **44**(2): p. 297-303.

113. Yerramshetty, J., Akkus, O, *The associations between mineral crystallinity and the mechanical properties of human cortical bone.* Bone, 2008. **42**(3): p. 476-482.

114. Hanschin, R., Stern, WB, *X-ray diffraction studies on the lattice perfection of human bone apatite (Crista iliaca).* Bone, 1995. **16**(4 Suppl): p. 355S-363S.

115. Bala, Y., Depalle, B, Farlay, D, Douillard, T, Meille, S, Follet, H et al, *Bone micromechanical properties are compromised during long-term alendronate therapy independently of mineralization.* Journal of Bone and Mineral Research, 2012. **27**(4): p. 825-834.

116. Boskey, A., *Bone mineral crystal size.* Osteoporosis International, 2003. **Suppl 5**: p. S16-S20.

117. Pasteris, J., Wopenka, B, Valsami-Jones, E, *Bone and tooth mineralization: Why apatite?* Elements, 2008. **4**(2): p. 97-104.

118. Makowski, A., Granke, M, Ayala, OD, Uppuganti, S, Mahadevan-Jansen, A, Nyman, JS, *Applying Full Spectrum Analysis to a Raman Spectroscopic Assessment of Fracture Toughness of Human Cortical Bone.* Applied Spectroscopy, 2017. **84**(21).

119. Granke, M., Makowski, AJ, Uppuganti, S., Does, MD, Nyman, JS, *Identifying novel clinical surrogates to assess human bone fracture toughness.* Journal of Bone and Mineral Research, 2015. **30**(7): p. 1290-1300.

120. Manhard, M., Uppuganti, S, Granke, M, Gochberg, DF, Nyman, JS, Does, MD, *MRI-derived bound and pore water concentrations as predictors of fracture resistance.* Bone, 2016. **87**: p. 1-10.

121. Horch, R., Gochberg, DF, Nyman, JS, Does, MD, *Non-invasive Predictors of Human Cortical Bone Mechanical Properties: T2-Discriminated ^{1}H NMR Compared with High Resolution X-ray.* PLOSOne, 2011. **6**(1).

122. Bae, W., Chen, PC, Chung, CB, Masuda, K, D'Lima, D, Du, J, *Quantitative ultrashort echo time (UTE) MRI of human cortical bone: Correlation with porosity and bimechanical properties.* Journal of Bone and Mineral Research, 2012. **27**(4): p. 848-857.

123. Unal, M., Yang, S, Akkus, O, *Molecular spectroscopic identification of the water compartments in bone*. Bone, 2014. **67**: p. 228-236.

124. Bae, W., Patil, S, Biswas, R, Li, S, Chang, EY, Status, S et al. , *Magnetic resonance imaging assessed cortical porosity is highly correlated with uCT porosity*. Bone, 2014. **66C**: p. 56-61.

125. Wang, X., Xu, H, Huang, Y, Gu, S, Jiang, JX, *Coupling Effect of Water and Proteoglycans on the In Situ Toughness of Bone.* Journal of Bone and Mineral Research, 2016. **31**(5): p. 1026-1029.

126. Flanagan, C., Unal, M, Akkus, O, Rimnac, CM, *Raman spectral markers of collagen denaturation and hydration in human cortical bone tissue are affected by radiation sterilization and high cycle fatigue damage.* Journal of Mechanical Behavior of Biomedical Materials, 2017. **75**: p. 314-321.

127. Fajardo, R.J., Karim, Lamya, Calley, Virginia I, Bouxsein, Mary L, *A Review of Rodent Models of Type 2 Diabetic Skeletal Fragility.* Journal of Bone and Mineral Research, 2014. **29**(5): p. 1025-1040.

128. Prisby, R.D., Swift, Joshua M., Bloomfield, Susan A., Hogan, Harry A., Delp, Michael D., *Altered bone mass, geometry, and mechanical properties during the development and progression of type 2 diabetes in the Zucker diabetic fatty rat.* Journal of Endocrinology, 2008. **199**: p. 379-388.

129. Hill Gallant, K.M., Gallant, Maxime A., Brown, Drew M., Sato, Amy Y., Williams, Justin N., Burr, David B., *Raloxifene Prevents Skeletal Fragility in Adult Female Zucker Diabetic Sprague-Dawley Rats.* PLOSOne, 2014. **9**(9).

130. Reinwald, S., Peterson, Richard G., Allen, Matt R., Burr, David B., *Skeletal changes associated with the onset of type 2 diabetes in the ZDF and ZDSD rodent models.* Am J Physiol Endocrinol Metab, 2009. **296**: p. E765-E774.

131. Tanimoto, M., Gohda, Tomohito, Kaneko, Shigeru, Hagiwara, Shinji, Murakoshi, Maki, Aoki, Tatsuya, Yamada, Kaori, Ito, Takamichi, Matsumoto, Masakazu, Horikoshi, Satoshi, Tomino, Yasuhiko, *Effect of pyridoxamine (K-163), an inhibitor of advanced glycation end products, on type 2 diabetic nephropathy in KK-Ay/Ta mice.* Metabolism Clinical and Experimental, 2007. **56**: p. 160-167.

132. Williams, G., A., Callon, Karen E., Watson, Maureen, Costa, Jessica L, Ding, Yaoyao, Dickinson, Michelle, Wang, Yu, Naot, Dorit, Reid, Ian R., Cornish, Jillian, *Skeletal Phenotype of the Leptin Receptor-Deficient db/db Mouse.* Journal of Bone and Mineral Research, 2011.

133. Hamrick, M.W., Pennington, C., Newton, D., Xie, D., Isales, C., *Leptin deficiency produces contrasting phenotypes in bones of the limb and spine.* Bone, 2004. **34**: p. 376-383.

134. Lu, H., Li, Cai, *Leptin: a multifunctional hormone.* Cell Research, 2000. **10**: p. 81-92.

135. Ealey, K.N., Fonseca, Debbie, Archer, Michael C., Ward, Wendy E., *Bone abnormalities in adolescent leptin-deficient mice.* Regulatory Peptides, 2006. **136**: p. 9-13.

136. Devlin, M.J., Van Vliet, M., Motyl, K., Karim, L., Brooks, D.J., Louis, L., Conlon, C., Rosen, C.J., Bouxsein, M.L., *Early-Onset Type 2 Diabetes Impairs Skeletal Acquisition in the Male TALLYHO/JngJ Mouse.* Endocrinology, 2014. **155**(10): p. 3806-3816.

137. Jilka, R., *The Relevance of Mouse Models for Investigating Age-Related Bone Loss in Humans.* Journals of Geronotology: Biological Sciences, 2013: p. 1-9.

138. Halloran, B., Ferguson, VL, Simske, SJ, Burghardt, A, Venton, LL, Majumdar, S, *Changes in Bone Structure and Mass With Advancing Age in the Male C57BL/6J Mouse.* Journal of Bone and Mineral Research, 2002. **17**(6): p. 1044-1050.

139. Kiebzak, G., Smith, R., Gundberg, CC, Howe, JC, Sacktor, B., *Bone Status of Senescent Male Rats: Chemical, Morphometric, and Mechanical Analysis.* Journal of Bone and Mineral Research, 1988. **3**(1): p. 37-45.

140. Buie, H., Moore, CP, Boyd, SK, *Postpubertal Architectural Developmental Patterns Differ Between the L_3 Vertebrae and Proximal Tibia in Three Inbred Strains of Mice.* Journal of Bone and Mineral Research, 2008. **23**(12): p. 2048-2059.

141. Glatt, V., Canalis, E., Stadmeyer, L., Bouxsein, ML, *Age-Related Changes in Trabecular Architecture Differ in Female and Male C57BL/6J Mice.* Journal of Bone and Mineral Research, 2007. **22**(8): p. 1197-1207.

142. Willinghamm, M., Brodt, MD, Lee, KL, Stephens, AL, Ye, J., Silva, MJ, *Age-Related Changes in Bone Structure and Strength in Female and Male BALB/c Mice.* Calcified Tissue International, 2010(86): p. 470-483.

143. Bloomfield, S., Hogan, HA, Delp, MD, *Decreases in Bone Blood Flow and Bone Material Properties in Aging Fischer-344 Rats.* Clinical Orthopaedics and Related Research, 2002(396): p. 248-257.

144. Kuro-o, M., Matsumura, Y, Aizawa, H, Kawaguchi, H, Suga, T, Utsugi, T, Ohyama, Y, Kurabayashi, M, Kaname, T, Kume, E, Iwasaki, H, Iida, A, Shiraki-lida, T, Nishikawa, S, Nagai, R, Nabeshima, Y, *Mutation of the mouse klotho gene leads to a syndrome resembling ageing.* Nature, 1997. **390**: p. 45-51.

145. Nyman, J.S., *Chapter 68 - Age-Related Changes to Bone Structure and Quality in Rodent Models*, in *Conn's Handbook of Models for Human Aging (Second Edition)*, J.L. Ram and P.M. Conn, Editors. 2018, Academic Press. p. 919-936.

146. Almeida, M., Han, L, Martin-Millan, M, Plotkin, LI, Stewart, SA, Roberson, PK, Kousteni, S, O'Brien, CA, Bellido, T, Parfitt, AM, Weinstein, RS, Jilka, RL, Manolagas, SC, *Skeletal Involution by Age-associated Oxidative Stress and Its Acceleration by Loss of Sex Steroids.* Journal of Biological Chemistry, 2007. **282**(37): p. 27285-27297.

147. Creecy, A., Uppuganti, S., Unal, M., Bunn, RC, Voziyan, P., Nyman, JS, *Low bone toughness in the TallyHO model of juvenile type 2 diabetes does not worsen with age.* Bone, 2018. **110**: p. 204-214.

148. Heilmeier, U., Carpenter, DR, Patsch, JM, Harnish, R, Joseph, GB, Burghardt, AJ, Baum, T, Schwartz, AV, Lang, TF, Link, TM *Volumetric femoral BMD, bone geometry, and serum sclerostin levels differ between type 2 diabetic postmenopausal women with and without fragility fractures.* Osteoporosis International, 2015. **13**(1-11).

149. Janghorbani, M., Van Dam, Rob M., Willett, Walter C., Hu, Frank B., *Systematic Review of Type 1 and Type 2 Diabetes Mellitus and Risk of Fracture.* American Journal of Epidemiology, 2007. **166**(5): p. 495-505.

150. Melton, L.J., Leibson, Cynthia L, Achenbach, Sara J, Therneau, Terry M, Khosla, Sundeep, *Fracture Risk in Type 2 Diabetes: Update of a Population-Based Study.* Journal of Bone and Mineral Research, 2008. **23**(8): p. 1334-1342.

151. Wallander, M., Axelsson, Kristian F., Nilsson, Anna G., Lundh, Dan, Lorentzon, Mattias, *Type 2 Diabetes and Risk of Hip Fractures and Non-Skeletal Fall Injuries in the Elderly: A Study From the Fractures and Fall Injuries in the Elderley Cohort (FRAILCO).* Journal of Bone and Mineral Research, 2017. **32**(3): p. 449-460.

152. Schwartz, A.V., Vittinghoff, Eric, Sellmeyer, Deborah E., Feingold, Kenneth R., de Rekeneire, Nathalie, Strotmeyer, Elsa S., Shorr, Ronald I., Vinik, Aaron I., Odden, Michelle C., Park, Seok Won, Faulkner, Kimberly A., Harris, Tamara B., *Diabetes-related complications, glycemic control, and falls in older adults.* Diabetes Care, 2008. **31**(3): p. 391-396.

153. Shen, J., Nielson, Carrie M., Marshall, Lynn M., Lee, David C., Keaveny, Tony M., Orwoll, Eric S., *The association between BMI and QCT-derived proximal hip structure and strength in older men: a cross-sectional study.* Journal of Bone and Mineral Research, 2015. **30**(7): p. 1301-1308.

154. Shanbhogue, V., Michell, DM, Rosen, CJ, Bouxsein, ML, *Type 2 diabetes and the skeleton: new insights into sweet bones.* Lancet Diabetes Endocrinology, 2015.

155. *National Diabetes Statistics Report 2017: Estimates of Diabetes and Its Burden in the United States*. 2017, Centers for Disease Control and Prevention.

156. Dabelea, D., Mayer-Davis, Elizabeth J., Saydah, Sharon, Imperatore, Giuseppina, Linder, Barbara, Divers, Jasmin, Bell, Ronny, Badaru, Angela, Talton, Jennifer W., Crume, Tessa, Liese, Angela D., Merchant, Anwar T., Lawrence, Jean M., Reynolds, Kristi, Dolan, Lawrence, Liu, Lenna L., Hamman, Richard F., *Prevalence of Type 1 and Type 2 Diabetes Among Children and Adolescents From 2001 to 2009.* Journal of the American Medical Association, 2014. **311**(17): p. 1778-1786.

157. Reinehr, T., *Type 2 diabetes mellitus in children and adolescents.* World Journal of Diabetes, 2013. **4**(6): p. 270-281.

158. May, A.L., Kuklina, Elena V., Yoon, Paula W., *Prevalence of Cardiovascular Disease Risk Factors Among US Adolescents, 1999-2008.* Pediatrics, 2012. **129**(6): p. 1035-1042.

159. Skinner, A.C., Skelton, Joseph A., *Prevalence and Trends in Obesity and Severe Obesity Among Children in the United States, 1999-2012.* JAMA Pediatrics, 2014. **168**(6): p. 561-566.

160. Weber, D.R., Haynes, Kevin, Leonard, Mary B., Willi, Steven M., Denburg, Michelle R., *Type 1 Diabetes Is Associated with an Increased Risk of Fracture Across the Life Span: A Population-Based Cohort Study Using the Health Improvement Network (THIN).* Diabetes Care, 2015. **38**: p. 1913-1920.

161. Farr, J.N., Khosla, Sundeep, *Determinants of bone strength and quality in diabetes mellitus in humans.* Bone, 2015. **82**: p. 28-34.

162. Burghardt, A., Issever, AS, Schwartz, AV, Davis, KA, Masharani, U, Majumdar, S, et al, *High-resolution peripheral quantitative computed tomographic imaging of cortical and trabecular bone microarchitecture in patients with type 2 diabetes mellitus.* Journal of Clinical Endocrinology and Metabolism, 2010. **95**(11): p. 5045-5055.

163. Samelson, E.J., Demissie, Serkalem, Cupples, L Adrienne, Zhang, Xiaochun, Xu, Hanfei, Liu, Ching-Ti, Boyd, Steven K., McLean, Robert R., Broe, Kerry E., Kiel, Douglas P., Bouxsein, Mary L., *Diabetes and Deficits in Cortical Bone Density Microarchitecture, and Bone Size: Framingham HR-pQCT Study.* Journal of Bone and Mineral Research, 2017.

164. Yu, E., Putman, MS, Derrico, N, Abrishamanian-Garcia, G, Finkelstein, JS, Bouxsein, BL, *Defects in cortical microarchitecture among African-American women with type 2 diabetes.* Osteoporosis International, 2014(15): p. 1-7.

165. Paccou, J., Ward, KA, Jameson, KA, Dennison, EM, Cooper, C, Edwards MH, *Bone microarchitecture in men and women with diabetes: The importance of cortical porosity.* Calcified Tissue International, 2016. **98**(5): p. 465-473.

166. Patsch, J., Burghardt, AJ, Yap, SP, Baum, T, Schwartz, AV, Joseph, GB, Link, TM *Increased cortical porosity in type 2 diabetic postmenopausal women with fragility fractures* Journal of Bone and Mineral Research, 2013. **28**(2): p. 313-324.

167. Heilmeier, U., Cheng, K, Pasco, C, Parrish, R, Nirody, J, Patsch, JM et al., *Cortical bone laminar analysis reveals increased midcortical and periosteal porosity in type 2 diabetic postmenopausal women with history of fragility fractures compared to fracture-free diabetics.* Osteoporosis International, 2016. **27**(9): p. 2791-2802.

168. Goh, S.-Y., Cooper, Mark E., *The Role of Advanced Glycation End Products in Progression and Complications of Diabetes.* Journal of Clinical Endocrinology and Metabolism, 2008. **93**(4): p. 1143-1152.

169. Kawashima, Y., Fritton, J. Christopher, Yaka, Shoshana, Sol Epstein, Sol, Schaffler Mitchell B., Jepsen, Karl J., LeRoith, Derek, *Type 2 Diabetic Mice Demonstrate Slender Long Bones with Increased Fragility Secondary To Increased Osteoclastogenesis.* Bone, 2009. **44**(4): p. 648-655.

170. Iwatsuka, H., Shino, Akio, Suzuoki, Ziro, *General Survey of Diabetic Features of Yellow KK Mice.* Endocrinologia japonica, 1970. **17**(1): p. 23-35.

171. Takagi, S., Miura, Toshihiro, Yamashita, Takenori, Ando, Naoki, Nakao, Haruka, Ishihara, Eriko, Ishida, Torao, *Characteristics of Diabetic Osteopenia in KK-Ay Diabetic Mice.* Biological and Pharmaceutical Bulletin, 2012. **35**(3): p. 438-443.

172. Xu, F., Dong, Yonghui, Huang, Xin, Li, Mi, Qin, Liang, Ren, Ye, Guo, Fengjing, Chen, Animin, Huang, Shilong, *Decreased osteoclastogenesis, osteoblastogenesis and low bone mass in a mouse model of type 2 diabetes.* Molecular Medicine Reports, 2014(10): p. 1935-1941.

173. Fu, C., Zhang, Xiaolin, Ye, Fei, Yang, Jianhong, *High Insulin Levels in KK-Ay Diabetic Mice Cause Increased Cortical Bone Mass and Impaired Trabecular Micro-Structure.* International Journal of Molecular Sciences, 2015(16): p. 8213-8226.

174. Kim, J.H., Stewart, Taryn P., Soltani-Bejnood, Morvarid, Wang, Luan, Fortuna, Jennifer M., Mostafa, Ola A., Moustaid-Moussa, Naima, Shoieb, Ahmed M., McEntee, Michael F., Wang, Yun, Bechtel, Lawrence, Naggert, Jurgen K., *Phenotypic characterization of polygenic type 2 diabetes in TALLYHO/JngJ mice.* Journal of Endocrinology, 2006. **191**: p. 437-446.

175. Rhee, S.D., Sung, Y. Y., Lee, Y. S., Kim, J. Y., Jung, W. H., Kim, M. J., Lee, M. S., Lee, M. K., Yang, S. D., Cheon, H. G. , *Obesity of TallyHO/JngJ Mouse is Due to Increased Food Intake with Early Development of Leptin Resistance* Exp Clin Endocrinol Diabetes, 2011. **119**(4): p. 243-251.

176. Uppuganti, S., et. al., *Age-related Changes in the Fracture Resistance of Male Fischer F344 Rat.* Bone, 2016. **83**: p. 220-232.

177. Ritchie, R., Koester, KJ, Ionova, S, Yao, W, Lane, NE, Ager, JW, *Measurement of the toughness of bone: A tutorial with special reference to small animals.* Bone, 2008. **43**(5): p. 798-812.

178. Creecy, A., Uppuganti, Sasidhar, Merkel, Alyssa R., O'Neal, Dianne, Makowski, Alexander J., Granke, Mathilde, Voziyan, Paul, Nyman, Jeffry S., *Changes in the Fracture Resistance of Bone with the Progression of Type 2 Diabetes in the ZDSD Rat.* Calcified Tissue International, 2016. **99**(3): p. 289-301.

179. Unal, M., Jung, Hyungjin, Akkus, Ozan, *Novel Raman Spectroscopic Biomarkers Indicate That Postyield Damage Denatures Bone's Collagen.* Journal of Bone and Mineral Research, 2016. **31**(5): p. 1015-1025.

180. Fowlkes, J.L., Nyman, Jeffry S., Bunn, R. Clay, Cockrell, Gael E., Wahl, Elizabeth C., Rettiganti, Mallikarjuna R., Lumpkin Jr., Charles K., Thrailkill, Kathryn M., *Effects of long-term doxycycline on bone quality and strength in diabetic male DBA/2J mice.* Bone Reports, 2015. **1**: p. 16-19.

181. Leiter, E., *Selecting the "Right" Mouse Model for Metabolic Syndrome and Type 2 Diabetes Research,* in *Type 2 Diabetes,* C. Stocker, Editor. 2009, Humana Press.

182. Kim, J.H., Sen, Saunak, Avery, Cindy S., Simpson, Elizabeth, Chandler, Phillip, Nishina, Patsy M., Churchill, Gary A., Naggert, Jurgen K., *Genetic Analysis of a New Mouse Model for Non-Insulin-Dependent Diabetes.* Genomics, 2001. **74**: p. 273-286.

183. Kim, J.H., Saxton, A. M., *The TallyHO Mouse as a Model of Human Type 2 Diabetes*, in *Animal Models in Diabetes Research. Methods in Molecular Biology (Methods and Protocols)*, H. Joost, Al-Hasani, H., Schurmann, A., Editor. 2012, Humana Press: Totowa, NJ.

184. Hunt, H.B., Pearl, Jared C., Diaz, David R., King, Karen B., Donnelly, Eve, *Bone tissue collagen maturity and mineral content increase with sustained hyperglycemia in the KK-Ay murine model of type 2 diabetes.* Journal of Bone and Mineral Research, 2017.

185. Nyman, J.S., Even, Jesse L, Jo, Chan-Hee, Herbert, Erik G., Murry, Matthew R., Cockrell, Gael E., Wahl, Elizabeth C., Bunn, R. Clay, Lumpkin, Charles K., Fowlkes, John L., Thrailkill, Kathryn M., *Effect of Diabetes on the Fracture Resistance of Bone.* Clinical Reviews in Bone and Mineral Metabolism, 2013.

186. Won, H.Y., Lee, Jin-Ah, Park, Zong Sik, Song, Jin Sook, Kim, Hee Yun, Jang, Su-Min, Yoo, Sung-Eun, Rhee, Youmi, Hwang, Eun Sook, Bae, Myung Ae, *Prominent Bone Loss Mediated by RANKL and IL-17 Produced by CD4+ T Cells in TallyHO/JngJ Mice.* PLOSOne, 2011. **6**(3).

187. Currey, J.D., Brear, Kevin, Zioupos, Peter, *The Effects of Ageing and Changes in Mineral Content in Degrading the Toughness of Human Femora.* Journal of Biomechanics, 1996. **29**(2): p. 257-260.

188. Zioupos, P., Currey, John D., Casinos, Adria, *Exploring the Effects of Hyperminerlisation in Bone Tissue by Using an Extreme Biological Example.* Connective Tissue Research, 2000. **41**(3): p. 229-248.

189. Currey, J.D., Zioupos, Peter, Davies, Peter, Casinos, Adria, *Mechanical properties of nacre and highly mineralized bone.* Proceedings of the Royal Society of London B, 2017. **268**: p. 107-111.

190. Saito, M., Fujii, K, Mori, Y, Marumo, K, *Role of collagen enzymatic and glycation induced cross-links as a determinant of bone quality in spontaneously diabetic WBN/Kob rats.* Osteoporosis International, 2006. **17**: p. 1514-1523.

191. Milovanovic, P., Adamu, U., Simon, MJK, Rolvien, T., Djuric, M., Amling, M., Busse, B., *Age- and Sex-Specific Bone Structure Patterns Portend Bone Fragility in Radii and Tibiae in Relation to Osteodensitometry: A High-Resolution Peripheral Quantitative Tomography Study in 385 Individuals.* Journals of Gerontology: Medical Sciences, 2015. **70**(10): p. 1269-1275.

192. Macdonald, H., Nishiyama, KK, Kang, Jian, Hanley, DA, Boyd, SK, *Age-Related Patterns of Trabecular and Cortical Bone Loss Differ Between Sexes and Skeletal Sites: A Population-Based HR-pQCT Study.* Journal of Bone and Mineral Research, 2011. **26**(1): p. 50-62.

193. Andreasen, C., Delaisse, JM, van der Eerden, BCJ, van Leeuwen JPTM, Ding, M., Andersen, TL, *Understanding Age-Induced Cortical Porosity in Women: The Accumulation and Coalescence of Eroded Cavities Upon Existing Intracortical Canals Is the Main Contributor.* Journal of Bone and Mineral Research, 2017.

194. Nirody, J., Cheng, KP, Parrish, RM, Burghardt, AJ, Majumdar, S., Link, TM, Kazakia, GJ, *Spatial distribution of intracortical porosity varies across age and sex.* Bone, 2015(75): p. 88-95.

195. Fields, A., Keaveny, TM, *Trabecular Architecture and Vertebral Fragility in Osteoporosis.* Current Osteoporosis Reports, 2012. **10**: p. 132-140.

196. Wang, X., Shen, X., Li, X., Agrawal, C. Mauli, *Age-related Changes in the Collagen Network and Toughness of Bone.* Bone, 2002. **31**(1): p. 1-7.

197. Nyman, J., Roy, A, Tyler, JH, Acuna, RL, Gayle, HJ, Wang, X, *Age-related factors affecting the postyield energy dissipation of human cortical bone.* Journal of Orthopaedic Research, 2007. **25**(5): p. 646-655.

198. Odetti, P., Rossi, S., Monacelli, F., Poggi, A., Cirnigliaro, M., Federici, M., Federici, A., *Advanced Glycation End Products and Bone Loss during Aging.* Annals of the New York Academy of Sciences, 2005. **1043**(1): p. 710-717.

199. Zimmermann, E.A., Schaible, Eric, Bale, Hrishikesh, Barth, Holly D., Tang, Simon Y., Reichert, Peter, Busse, Bjoern, Alliston, Tamara, Ritchie, Robert O. , *Age-related changes in the plasticity and toughness of human cortical bone at multiple length scales.* PNAS, 2011. **108**(35): p. 14416-144421.

200. Hansen, S., Hauge, EM, Jensen, JB, Brixen, K., *Differing Effects of PTH 1-34, PTH 1-84, and Zoledronic Acid on Bone Microarchitecture and Estimated Strength in Postmenopausal Women With Osteoporosis: An 18-Month Open-Labeled Observational Study Using HR-pQCT.* Journal of Bone and Mineral Research, 2013. **28**(4): p. 736-745.

201. Burghardt, A., Kazakia, GJ, Sode, M., de Papp, AE, Link, TM, Majumdar, S., *A Longitudinal HR-pQCT Study of Alendronate Treatment in Postmenopausal Women With Low Bone Density: Relations Among Density, Cortical and Trabecular Microarchitecture, Biomechanics, and Bone Turnover.* Journal of Bone and Mineral Research, 2010. **25**(12): p. 2558-25571.

202. Tsai, J., Uihlein, AV, Burnett-Bowie, SM, Neer, RM, Zhu, Y., Derrico, N., Lee, H., Bouxsein, ML, Leder, BZ, *Comparative Effects of Teriparatide, Denosumab, and Combination Therapy on Peripheral Compartmental Bone Density, Microarchitecture, and Estimated Strength: the DATA-HRpQCT Study.* Journal of Bone and Mineral Research, 2015. **30**(1): p. 39-45.

203. Keaveny, T., Crittenden, DB, Bolognese, MA, Genant, HK, Engelke, K., Oliveri, B., Brown, JP, Langdahl, BL, Yan, C., Grauer, A., Libanati, C., *Greater Gains in Spine and Hip Strength for Romosozumab Compared With Teriparatide in Postmenopausal Women With Low Bone Mass.* Journal of Bone and Mineral Research, 2017. **32**(9): p. 1956-1962.

204. Seref-Ferlengez, Z., Kennedy, OD, Schaffler, MB, *Bone microdamage, remodeling and bone fragility: how much damage is too much damage?* BoneKey Reports, 2015. **4**(644).

205. Burstein, A., Reilly, DT, Martens, M., *Aging of Bone Tissue: Mechanical Properties.* Journal of Bone and Joint Surgery, 1976. **58**: p. 82-86.

206. McCalden, R., McGeough, JA, Barker, MB, Court-Brown, CM, *Age-Related Changes in the Tensile Properties of Cortical Bone: The Relative Importance of Changes in Porosity, Mineralization, and Microstructure.* Journal of Bone and Joint Surgery, 1993. **75**(8): p. 1193-1205.

207. Zioupos, P., Currey, JD, Hammer, AJ, *The role of collagen in the declining mechanical properties of aging human cortical bone.* Journal of Biomedical Materials Research, 1999. **45**: p. 108-116.

208. Diab, T., Sit, S., Kim, D., Rho, J., Vashishth, D, *Age-dependent fatigue behaviour of human cortical bone.* European Journal of Morphology, 2005. **42**(1/2): p. 53-59.

209. Riggs, B., Melton, LJ, Robb, RA, Camp, JJ, Atkinson, EJ, Peterson, JM, Rouleau, PA, McCollough, CH, Bouxsein, ML, Khosla, S., *Population-Based Study of Age and Sex Differences in Bone Volumetric Density, Size, Geometry, and Structure at Different Skeletal Sites.* Journal of Bone and Mineral Research, 2004. **19**(12): p. 1945-1954.

210. Silva, M., Jepsen, KJ, *Age-Related Changes in Whole-Bone Structure and Strength*, in *Skeletal Aging and Osteoporosis. Studies in Mechanobiology, Tissue Engineering and Biomaterials*, M. Silva, Editor. 2012, Springer: Berlin, Heidelberg.

211. Ferguson, V., Ayers, RA, Bateman, TA, Simske, SJ, *Bone development and age-related bone loss in male C57BL/6J mice.* Bone, 2003. **33**: p. 387-398.

212. Rachner, T., Khosla, S., Hofbauer, LC, *Osteoporosis: now and the future.* The Lancet, 2011. **377**: p. 1276-1287.

213. Unal, M., Uppuganti, S, Leverant, CJ, Creecy, A, Granke, M, Voziyan, P, Nyman, JS, *Assessing Glycation-mediated Changes in Human Cortical Bone with Raman Spectroscopy.* Journal of Biophotonics, 2018.

214. Benedict, M., Adiyaman, S., Ayers, DC, Thomas, FD, Calore, JD, Dhar, V., Richman, RA, *Dissociation of Bone Mineral Density From Age-Related Decreases in Insulin-like Growth Factor-I and Its Binding Proteins in the Male Rat.* Journals of Geronotology: Biological Sciences, 1994. **49**(5): p. B224-B230.

215. Currey, J., *Effects of differences in mineralization on the mechanical properties of bone.* Philosophical Transactions of the Royal Society B, 1984. **304**(1121): p. 509-518.

216. Mandair, G.S., Morris, Michael D., *Contributions of Raman spectroscopy to the understanding of bone strength.* BoneKey Reports, 2015. **4**.

217. Kopp, J., Bonnet, M., Renou, JP, *Effect of Collagen Crosslinking on Collagen-Water Interactions (A DSC Investigation).* Matrix, 1989. **9**: p. 443-450.

218. Aref, M., McNerny, EMB, Brown, D., Jepsen, KJ, Allen, MR, *Zoledronate treatment has different effects in mouse strains with contrasting baseline bone mechanical phenotypes.* Osteoporosis International, 2016: p. 3637-3643.

219. Shahnazari, M., Yao, W., Dai, W., Wang, B., Ionova-Martin, SS, Ritchie, RO, Heeren, D., Burghardt, AJ, Nicolella, DP, Kimiecik, MG, Lane, NE, *Higher doses of bisphosphonates further improve bone mass, architecture, and strength but not the tissue material properties in aged rats.* Bone, 2010. **46**: p. 1267-1274.

220. Sato, M., Vahle, J., Schmidt, A., Westmore, M., Smith, S, Rowley, E., Ma, LY, *Abnormal Bone Architecture and Biomechanical Properties with Near-Lifetime Treatment of Rats with PTH.* Endocrinology, 2002. **143**(9): p. 3230-3242.

221. Farr, J., Xu, M., Weivoda, MM, Monroe, DG, Fraser, DG, Onken, JL, Negley, BA, Sfeir, JG, Ogrodnik, MB, Hachfeld, CM, LeBrasseur, NK, Drake, MT, Pignolo, RJ, Pirtskhalava, T.,

Tchkonia, T., Oursler, MJ, Kirkland, JL, Khosla, S., *Targeting cellular senescence prevents age-related bone loss in mice.* Nature Medicine, 2017. **23**(9): p. 1072-1079.

222. Allen, M., McNerny, E., Aref, M., Organ, JM, Newman, CL, McGowan, B., Jang, T., Burr, DB, Brown, DM, Hammond, M., Territo, PR, Lin, C., Persohn, S., Jiang, L., Riley, AA, McCarthy, BP, Hutchins, GD, Wallace, JM, *Effects of combination treatment with alendronate and raloxifene on skeletal properties in a beagle dog model.* PLOSOne, 2017.

223. Kimura, S., Saito, M., Kida, Y., Seki, A., Isaka, Y., Marumo, K., *Effects of raloxifene and alendronate on non-enzymatic collagen cross-links and bone strength in overiectomized rabbits in sequential treatments after daily human parathyroid hormone (1-34) administration.* Osteoporosis International, 2017. **28**: p. 1109-1119.

224. Abar, O., Dharmar, S., Tang, SY, *The effect of aminoguanidine (AG) and pyridoxamine (PM) on ageing human cortical bone.* Bone and Joint Research, 2018. **7**(1): p. 105-110.

225. Alderson, N., Chachich, ME, Youssef, NN, Beattie, RJ, Nachtigal, M, Thorpe, SR, Baynes, JW, *The AGE inhibitor pyridoxamine inhibits lipemia and development of renal and vascular disease in Zucker obese rats.* Kidney International, 2003. **63**: p. 2123-2133.

226. Stitt, A., Gardiner, TA, Alderson, NL, Canning, P, Frizzell, N, Duffy, N, Boyle, C, Januszewski, AS, Chachich, M, Baynes, JW, Thorpe, SR, *The AGE Inhibitor Pyridoxamine Inhibits Development of Retinopathy in Experimental Diabetes.* Diabetes, 2002. **51**: p. 2826-2832.

227. Thurner, P., Chen, CG, Ionova-Martin, S., Sun, L, Harman, A., Porter, A., Ager JW, Ritchie, RO, Alliston, T., *Osteopontin Deficiency Increases Bone Fragility but Preserves Bone Mass.* Bone, 2010. **46**(6): p. 1564-1573.

228. Ferris, B., Kelnerman, L, Dodds, RA, Bitensky, L. Chayan, J., *Altered Organization of Non-Collagenous Bone Matrix in Osteoporosis.* Bone, 1987. **8**: p. 285-288.

229. Dickson, I., Bagga, MK, *Changes with Age in the Non-Collagenous Proteins of Human Bone.* Connective Tissue Research, 1985. **14**(1): p. 77-85.

230. Yamauchi, M., Sricholpech, M., *Lysine post-translational modifications of collagen.* Essays in Biochemistry, 2012. **52**: p. 113-133.

231. Danielsen, C., *Age-related thermal stability and susceptibility to proteolysis of rat bone collagen.* Biochemical Journal, 1990. **272**: p. 697-701.

232. Danielsen, C., Mosekilde, L., Bollerslev, J., Mosekilde, L., *Thermal Stability of Cortical Bone Collagen in Relation to Age in Normal Individuals and in Individuals with Osteopetrosis.* Bone, 1994. **15**(1): p. 91-96.

233. Shoulders, M.D., Raines, Ronald T., *Collagen Structure and Stability.* Annual Reviews Biochemistry, 2009. **78**: p. 929-958.

234. Notbohm, H., Mosler, S., Bodo, M., Yang, C., Lehmann, H., Batge, B., Muller, PK, *Comparative Study of the Thermostability of Collagen I of Skin and Bone: Influence of Posttranslational Hydroxylation of Prolyl and Lysyl Residues.* Journal of Protein Chemistry, 1992. **11**(6): p. 635-643.

235. Panwar, P., Lamour, G., Mackenzie, NCW, Yang, H., Ko, F., Li, H., Bromme, D., *Changes in Structural-Mechanical Properties and Degradability of Collagen during Aging-associated Modifications.* Journal of Biological Chemistry, 2015. **290**(38): p. 23291-23306.

236. Thomas, C., Cleland, TP, Sroga, GE, Vashishth, D., *Accumulation of carboxymethyl-lysine (CML) in human cortical bone.* Bone, 2018. **110**: p. 128-133.

237. Jiang, X., Ye, M., Jiang, X., Liu, G., Feng, S., Cui, L., Zou, H., *Method Development of Efficient Protein Extraction in Bone Tissue for Proteome Analysis.* Journal of Proteome Research, 2007(6): p. 2287-2294.

238. Cabral, W.A., Chang, Weizhong, Barnes, Aileen, M., Weis, Mary Ann, Scott, Melissa A., Leikin, Sergey Makareeva, Elena, Kuznetsova, Natalia, Rosenbaum, Kenneth N., Tifft, Cynthia J., Bulas, Dorothy I., Kozma, Chahira, Smith, Peter A., Eyre, David R., Marini, Joan C., *Prolyl 3-hydroxylase 1 deficiency causes a recessive metabolic bone disorder resembling lethal/severe osteogenesis imperfecta.* Nature Genetics, 2008. **39**(3): p. 359-365.

239. Heard, M., Besio, R., Weis, M., Rai, J., Hudson, DM, Dimori, M., Zimmerman, SM, Kamykowski, JA, Hogue, WR, Swain, FL, Burdine, MS, Mackintosh, SG, Tackett, AJ, Suva, LJ, Eyre, DR, Morello, R., *Sc65-Null Mice Provide Evidence for a Novel Endoplasmic Reticulum Complex Regulating Collagen Lysyl Hydroxylation.* PLOS Genetics, 2016.

240. Hudson, D., Garibov, M., Dixon, DR, Popowics, T., Eyre, DR, *Distinct post-translational features of type I collagen are conserved in mouse and human periodontal ligament.* Journal of Periodontal Research, 2017. **52**: p. 1042-1049.

241. Sroga, G., Karim, L., Colon, W., Vashishth, D., *Biochemical Characterization of Major Bone-Matrix Proteins Using Nanoscale-Size Bone Samples and Proteomics Methodology.* Molecular and Cellular Proteomics, 2011. **10**(9): p. 1-12.

242. Thomas, C., Cleland, TP, Zhang, S., Gundberg, CM, Vashishth, D., *Identification and characterization of glycation adducts on osteocalcin.* Analytical Biochemistry, 2017(525): p. 46-53.

243. Xu, L., Zhang, Z., Sun, X., Wang, J., Xu, W., Shi, L., Lu, J., Tang, J., Liu, J. Su, X., *Glycosylation status of bone sialoprotein and its role in mineralization.* Experimental Cell Research, 2017(360): p. 413-420.

244. Brown, K.L., Darris, Carl, Rose, Kristie Lindsey, Sanchez, Otto A., Madu, Hartman, Avance, Josh, Brooks, Nickolas, Zhang, Ming-Zhi, Fogo, Agnes, Harris, Raymond, Hudson, Billy G., Voziyan, Paul, *Hypohalous Acids Contribute to Renal Extracellular Matrix Damage in Experimental Diabetes.* Diabetes, 2015.

245. Danielsen, C., Mosekilde, L., Svenstrup, B., *Cortical Bone Mass, Composition, and Mechanical Properties in Female Rats in Relation to Age, Long-Term Ovariectomy, and Estrogen Substitution.* Calcified Tissue International, 1993. **52**: p. 26-33.

246. Bonnet, N., Garnero, P., Ferrari, S., *Periostin action in bone.* Molecular and Cellular Endocrinology, 2016. **432**: p. 75-82.

247. Bonnet, N., Gineyts, E., Ammann, P., Conway, SJ, Garnero, P., Ferrari, S., *Periostin Deficiency Increases Bone Damage and Impairs Injury Response to Fatigue Loading in Adult Mice.* PLOSOne, 2013. **8**(10): p. 1-15.

248. Bonnet, N., Standley, KN, Bianchi, EN, Stadelmann, V., Foti, M., Conway, SJ, Ferrari, SL, *The Matricellular Protein Periostin Is Required for Sost Inhibition and the Anabolic Response to Mechanical Loading and Physical Activity.* Journal of Biological Chemistry, 2009. **284**(51): p. 35939-35950.

249. Kirsch, E., Krieg, T., Remberger, K., Fendel, H., Bruckner, P., Muller, PK, *Disorder of collagen metabolism in a patient with osteogenesis imperfecta (lethal type): increased degree of hydroxylation of lysine in collagen types I and III.* European Journal of Clinical Investigation, 1981. **11**: p. 39-47.

250. Xu, T., Bianco, P., Fisher, LW, Longenecker, G., Smith, E., Goldstein, S., Bonadio, J., Boskey, A., Heegaard, A., Sommer, B., Satomura, K., Dominguez, P., Zhao, C., Kulkarni, AB, Robey, PG, Young, MF, *Targeted disruption of the biglycan gene leads to an osteoporosis-like phenotype in mice.* Nature Genetics, 1998. **20**: p. 78-82.

251. Corsi, A., Xu, T., Chen, XD, Boyde, A., Liang, J., Mankani, M., Sommer, B., Iozzo, RV, Eichstetter, I., Robey, PG,Bianco, P., Young, MF, *Phenotypic Effects of Biglycan Deficiency Are Linked to Collagen Fibril Abnormalities, Are Synergized by Decorin Deficiency, and Mimic Ehlers-Danlos-Like Changes in Bone and Other Connective Tissues.* Journal of Bone and Mineral Research, 2002. **17**(7): p. 1180-1189.

252. Ameye, L., Young, MF, *Mice deficient in small leucine-rich proteoglycans: novel in vivo models for osteoporosis, osteoarthritis, Ehlers-Danlos syndrome, muscular dystrophy, and corneal diseases.* Glycobiology, 2002. **12**(9): p. 107R-116R.

253. Neschen, S., Scheerer, M., Seelig, A., Huypens, P., Schultheiss, J., Wu, M., Wurst, W., Rathkolb, B., Suhre, K., Wolf, E., Beckers, J., Hrabe de Angelis, M., *Metformin Supports the Antidiabetic Effect of a Sodium Glucose Cotransporter 2 Inhibitor by Suppressing Endogenous Glucose Production in Diabetic Mice.* Diabetes, 2015. **64**: p. 284-290.

254. Li, X., Guo, Y., Yan, W., Snyder, MP, Li, X., *Metformin Improves Diabetic Bone Health by Re-Balancing Catabolism and Nitrogen Disposal.* PLOSOne, 2015. **10**(12).

255. Pritchard, J., Papaioannou, A., Schwarcz, HP, Adachi, JD, DeBeer, J., Winemaker, M., Avram, V., Willett, T., *A Comparison of Collagen Crosslink Content in Bone Specimens from Elective Total Hip Arthroplasty Patients with and without Type 2 Diabetes.* Journal of Bone Reports and Recommendations, 2016. **2**(3).

256. Gallant, M.A., Brown, Drew M., Hammond, Max, Wallace, Joseph M., Du, Jiang, Deymier-Black Alix C., Almer, Jonathan D., Stock, Stuart R., Allen, Matthew R., Burr, David B. , *Bone cell-independent benefits of raloxifene on the skeleton: A novel mechanism for improving bone material properties.* Bone, 2014. **61**: p. 191-200.

257. Voziyan, P.A., Hudson, B.G., *Pyridoxamine as a multifunctional pharmaceutical: targeting pathogenic glycation and oxidative damage.* Cellular and Molecular Life Sciences, 2005. **62**: p. 1671-1681.